Universidad Autónoma de Madrid

Facultad de Ciencias

Departamento de Geología y Geoquímica

Towards the reconstruction of flood histories: luminescence dating of palaeoflood deposits

Tesis doctoral

Alicia Medialdea Utande

Madrid, Diciembre 2012

Universidad Autónoma de Madrid.

Facultad de Ciencias

Departamento de Geología y Geoquímica

Towards the reconstruction of flood histories: luminescence dating of palaeoflood deposits.

Tesis Doctoral presentada por Alicia Medialdea Utande para la obtención del título de Doctora por la Universidad Autónoma de Madrid.

Dr. Gerardo Benito Ferrández
Museo Nacional de Ciencias Naturales, CSIC.
Director

Dra. Kristina J. Thomsen
Centre for Nuclear Technologies
Technical University of Denmark
Codirectora

Dr. Jerónimo López Martínez
Universidad Autónoma de Madrid
Tutor

Madrid, Diciembre 2012

Contents

Resumen

La datación absoluta de depósitos de paleocrecidas juega un papel clave en el entendimiento de las crecidas fluviales, consideradas uno de los principales peligros naturales relacionados con el clima y que causa importantes daños en la actividad humana.

El reto que supone datar de forma precisa estos eventos ha favorecido la mejora de los procesos de medida y análisis en la datación por OSL, convirtiéndola en una técnica altamente fiable en la datación de procesos cuaternarios. Esta Tesis se ha centrado en la aplicación de la técnica a situaciones en que ésta se puede ver limitada como es el caso de los depósitos fluviales recientes, potencialmente afectados por blanqueamiento parcial y en los que cualquier factor extrínseco puede suponer una estimación errónea de la edad.

Para este trabajo se han tomado muestras de cuatro ríos de la Península Ibérica con el fin de abarcar un amplio tipo de depósitos. Se ha empleado una secuencia compuesta por ocho muestras del río Guadalentín con edades asignadas basadas en registros históricos y dataciones de radiocarbono, para comparar el comportamiento de estadística robusta, el modelo CAM, el modelo MAM y la aproximación IEU en el análisis de medidas sobre granos individuales y sobre alícuotas multigrano pequeñas. Se han aplicado transformaciones para poder aplicar los modelos CAM y MAM a estas muestras recientes que presentan valores negativos de dosis en sus distribuciones. La incertidumbre causada por únicamente factores intrínsecos se ha determinado mediante experimentos de recuperación de dosis llevados a cabo sobre muestras irradiadas con una fuente gamma. Se ha estudiado el efecto de la incertidumbre asociada en los resultados obtenidos por CAM y MAM. Se ha demostrado la idoneidad de las medidas realizadas sobre alícuotas pequeñas en combinación con la aproximación IEU para la determinación de la edad. Las conclusiones obtenidas con el estudio de estas muestras de edad conocida se han implementado para la datación del resto de muestras tomadas de los otros tres ríos: Rambla de la Viuda (mediterráneo), Huebra y Duero (atlánticos).

Se ha propuesto el método idóneo en cada caso específico, evitando el efecto de la contaminación por feldespato, el blanqueamiento parcial del sedimento y la mezcla de granos con distintas dosis, que se pueden encontrar en suelos desarrollados y en suelos retrabajados con fines agrícolas.

Abstract

The accurate dating of paleoflood deposits plays a key role in the understanding of river flooding events, which are one of the main natural hazards related to climate, causing severe damage on mankind's life.

The challenge of accurate dating these events has motivated developments in the measuring and analysing processes applied to OSL dating that are making this technique highly reliable to assess chronologies for Quaternary processes. This Thesis has focused on the application of the technique in cases in which it can be hampered. This is the case of fluvial young sediments which are likely to suffer from incomplete bleaching and for which any extrinsic factor could lead to a dramatic misestimate of the burial age.

Samples from four rivers of the Iberian Peninsula have been used for this study to provide wide variety sediments. A sequence of eight modern (40-1000 a) flash flood deposits, potentially incomplete bleached, from Guadalentin River with available age control from historical records and radiocarbon dating, has been used to compare the behaviour of robust statistics, CAM, MAM and IEU models on distribution from single grain and multi-grain aliquots measurements. Modifications were made to use the CAM and MAM models on dose distributions containing zero and near zero values. The assessment of the over-dispersion has been based on dose recovery test carried out on gamma irradiated samples. The effect of the over-dispersion value assessed on the behaviour of MAM and IEU age models was studied. The suitability of small aliquots in combination with IEU approach for the accurate estimation of the ages was also tested finding good agreement with the known values. Achieved conclusions have been applied to date the samples from the remaining three rivers: Rambla de la Viuda (Mediterranean), Huebra and Duero Rivers (Atlantic).

The most suitable methods for each specific case avoiding the effect of feldspar contamination, incomplete bleaching of grains and mixture of grains population found in developed soils and reworked deposits for agricultural purposes, has been proposed.

Agradecimientos

Agradecer por escrito a todos aquellos que me han ayudado durante el tiempo dedicado a esta tesis supondría otros cuantos meses de escritura así que comienzo pidiendo disculpas por la brevedad de estos agradecimientos y la inevitable omisión de algunos de los que habéis estado cerca.

Gracias al CSIC por financiar esta investigación a través del proyecto intramural 200430E595.

Quisiera agradecer a mi director Gerardo Benito por…por todo, tanto en la parte profesional como en la personal. Por haber estado aquí desde que esta tesis era tan solo una vaga idea. Por haberla hecho posible. Te debo mucho.

I would like to change to English to thank all those that have helped me far from home. I would like to thank my "forced" supervisor Kristina Thomsen. Thank you for your always open door. Thank you very much for showing me the wonders of luminescence but most of all, for making me think and not letting me whine.

Thank you very much to Andrew Murray for welcoming me at NLL. For the revealing comments on luminescence and crucial help in these last two years.

Quisiera agradecer a mi tutor, Jerónimo López, por su paciente apoyo a lo largo de estos años y al departamento de Geología y Geoquímica por darme la oportunidad de presentar esta Tesis.

A María José por tu cariño y toda tu ayuda.

A Pablo Corella por dar sin pedir nada a cambio.

A Virgilio Correcher por ponerlo siempre fácil. Porque tu buena disposición que ha sido decisiva en estos últimos años. Por los buenos consejos incluso aquellos de toque eclesiástico.

Special thanks to Christine Thiel, for the meeting of our growth life curves. For our fruitful conversations on jellyfish reproduction and the

conclusions on luminescence that those have brought. For all we have shared and all still to be shared.

Thank you very much to Jan-Pieter for sharing the warmth and affection of your family.

Thank you to Naomi Porat for guiding me on my first steps in this field and giving me the great advice of going to Risø. Looking forward the collaborations that future may bring!

Thank you very much to Vichy Hansen, Mette Adrian and Joy Mayland. Thank you to the Risø crew for your help and sharing with me the great atmosphere along the corridor.

A mis queridas amigas Beatriz y Rosa por estar siempre cerca a pesar de las circunstancias. Por poder teneros conmigo allá donde esté.

A Leticia Miguens, por tu firme amistad que no has vendido a ningún precio. Por ser una auténtica química y enseñarme la importancia de las buenas prácticas de laboratorio. Por haberte encontrado en el camino.

A Ana Isabel Ortega y todos los compañeros del Cenieh que entendieron mis decisiones.

A Isabel Carazo por seguir aquí.

A todos los amigos que os habéis mantenido cerca a pesar de la distancia.

Finalmente me gustaría dar las gracias a los que más las merecen y menos las reciben…mi familia.

1.

Introduction

1.1. **Overview**

Palaeoflood deposits have been used for reconstructing the magnitude and frequency of past floods (Baker *et al*., 2002) to support studies on flood hazard assessment as well as understanding the linkages between climate, land-use, flood frequency and channel morphology. Palaeoflood studies typically lead to four phases of analysis: (1) documentation and assessment of flood evidence; (2) determination of paleoflood ages; (3) estimation of flow magnitude, typically peak discharge, associated with flood evidence; and (4) incorporation of paleoflood data into the flood frequency analysis. Dating of sedimentary flood units and intervening deposits is a key task supporting analysis of temporal flood behaviour and recurrence. Dating methods applied in paleoflood hydrology can be divided into three categories (Jacobson *et al*., 2003): numerical, relative, and hybrid-correlated. Development of a time-scale sequence of paleofloods requires in most cases a combination of methods mostly relying on multiple numerical ages at individual sites from flood-sediment layers and interbedded and bounding deposits such as colluvium and soils. Numerical dating supports chronologies which are mainly established by deposit stratigraphy and site-to-site correlations based on deposit characteristics and sequences.

Numerical dating methods aim to establish the timing of individual floods, typically by radiocarbon and Optically Stimulated Luminescence (OSL). Radiocarbon dating is the most common absolute dating tool employed in paleohydrologic work (e.g. Baker *et al*.,

1985). Organic materials such as wood, charcoal, seeds and leaf fragments are entrained by floods and commonly deposited in conjunction with clastic sediment in slackwater sequences. Organic materials most likely to provide high fidelity constraints on flood ages are those not likely to have persisted for a long period of time before deposition, such as seeds, fine organic detritus, and twigs. Commonly, however, radiocarbon dating is performed on charcoal contained within flood deposits, which can persist for hundreds or thousands of years prior to incorporation within a flood deposit (Blong and Gillespie, 1978). For most studies, it is assumed that radiocarbon ages from detrital material within flood deposits closely approximates the flood date, although the most conservative assumption is that the radiometric date provides a maximum limiting age for the enclosing deposit. Moreover, the 5730 year half-life of ^{14}C and the variations in the calibration curve prevents radiocarbon dating of deposits older than 40,000 years. Also, radiocarbon dating suffers from significant uncertainty for the period 1650 to 1950 AD due to the amounts of fossil fuel burning and introduction of variable amounts of ^{14}C into the atmosphere during the industrial revolution.

Optical Stimulated Luminescence (OSL) dating is becoming more popular among palaeohydrologists because this dating technique directly measures the burial time of deposits, specifically quartz and feldspar grains contained within the deposit. In OSL dating the time when the sediment was last exposed to light ("bleached") is determined. For the purposes of dating flood deposit sequences, the general assumption is that the sediment was last exposed to light during transport prior to deposition. Luminescence dating might be limited if the sediment to be measured has been heterogeneously exposed to light prior to be buried and shielded from daylight. In these cases, the measurement of multi-grain aliquots would derive in over-estimation of the burial dose and thus, over-estimation of the age. Developments in the OSL technique during the last 15 years has enabled the reduction of the sample size to individual quartz and feldspar grains (e.g. Duller and Murray, 2000; Bøtter-Jensen *et al*., 2000), from which the heterogeneity within the grain population can be analyzed. This involves the use of statistical methods and the so-called minimum age models to estimate the true burial dose thus the analysis become more complex.

Moreover, new analytical protocols have specially improved the application of OSL dating (Murray and Wintle, 2000, Wintle and Murray, 2006), resulting in numerical ages known to 5-10%, even for young deposits (<300 yrs) (e.g. Ballarini *et al*., 2003, Duller, 2004, Arnold *et al*., 2009). Despite these recent improvements, the technique can be hampered in situations (1) in which quartz is not present in the deposits, and (2) where the transported sediment was not sufficiently bleached by exposure to light, either because of high turbidity levels, transport occurring at night or insufficient exposure time. Radiocarbon dating has been the most common absolute dating tool employed in paleohydrologic work (e.g. Baker et al., 1985). But under appropriate conditions, OSL dating can be an important tool, especially for deposits (1) containing little or no organic materials, (2) older than the range of radiocarbon dating (>40,000 years), or (3) younger than 300 years old so that radiocarbon dating cannot yield precise results. These advantages are increasingly making luminescence dating the preferred technique for Quaternary chronological studies.

This research focuses on applying and testing the reliability of OSL dating of palaeoflood sediments for a variety of sedimentary environments and a diversity of catchment lithological and hydrological characteristics.

1.2. **Objectives**

This research focuses on applying and testing the reliability of equivalent dose determination methods and age models for OSL dating of palaeoflood sediments, with particular emphasis on historical and modern flood deposits. More specifically, this study is aimed to determine the experimental and statistical procedures best suited for OSL dating the diversity of palaeoflood depositional environments.

This study seeks to add information and analysis about the performance of the estimation of the burial dose of flood sediments comparing OSL ages obtained from single grains and small multi-grain aliquots with other independent age control from historical records and radiocarbon analysis. As part of the lithological and hydrological diversity of the Iberian Peninsula, the study of palaeoflood sites at Mediterranean and

Atlantic rivers provide a wide perspective of luminescence dating problems within different settings. The focus is on applying luminescence dating to the particular characteristics of palaeoflood sediments testing different sample size, experimental procedures and statistical approaches to obtain the most robust luminescence results for this case. A final objective is to confirm that the achieve conclusions are suitable of being applied to different environments and for a wider age range.

This work focuses on reaching the following specific objectives:

- Compare the results obtained when measuring the samples using single grains and when using small multi-grain aliquots.
- Test the performance of different minimum age models on single grains dose distributions of samples from different lithological and hydrological settings, finding the best options for each case, focusing on the behaviour of models on young samples which dose distributions contain negative and zero values.
- Analyze the performance of minimum age models applied on dose distributions from multi-grain aliquot measurements.
- Confirm the reproducibility of the methods achieving the best results for the young flash-flood deposits from a Mediterranean catchment when applied to different environments and wider age range.
- Propose new guidelines on OSL data analysis towards the dating of palaeoflood sediments according to age and lithological contexts within the Iberian Peninsula.

1.3. Organisation of the dissertation

This dissertation is organised into five chapters. Following this introductory chapter, Chapter 2 focuses on describing the basic principles of luminescence dating and the statistical analysis applied to differentiate well-bleached grains from incompletely bleached ones. The aim is to give the reader an understanding of the pros and cons of the luminescence experimental procedure (single grain versus multi-grain aliquots, basic descriptive statistics to more sophisticated age models) applied to palaeoflood

deposits. Chapter 3 focuses on the application of these procedures to young and recent palaeoflood deposits. In this chapter the most appropriate dose estimation method is identified. Alternative treatments of the data is proposed for applying the original CAM and MAM models on distributions containing negative and zero values, frequently found among young samples.

Chapter 4 presents the age estimates of different type of sediments from different environments based on the conclusions derived from chapter 3. Their suitability for the dating of a number of sites with different characteristics and wider age range will be confirmed by comparison with independent age control and stratigraphic information.

Chapter 5 provides a summary of the concluding remarks together with recommendations of this study and discussion about how they fit into the body of research on luminescence dating of slackwater palaeoflood deposits. The dissertation concludes with a discussion of where research is still needed for the luminescence dating of recent and young palaeoflood sediments and for the case of the studied regions (Atlantic and Mediterranean river basins).

2.

Basic concepts in luminescence dating

2.1. **Principles of luminescence dating**

The luminescence signal from natural crystals released by thermal stimulation (thermoluminescence, TL), or by optical stimulation (optically stimulated luminescence, OSL) can be used to determine when a sediment was last exposed to sunlight (i.e. the burial time) (Figure 2.1).

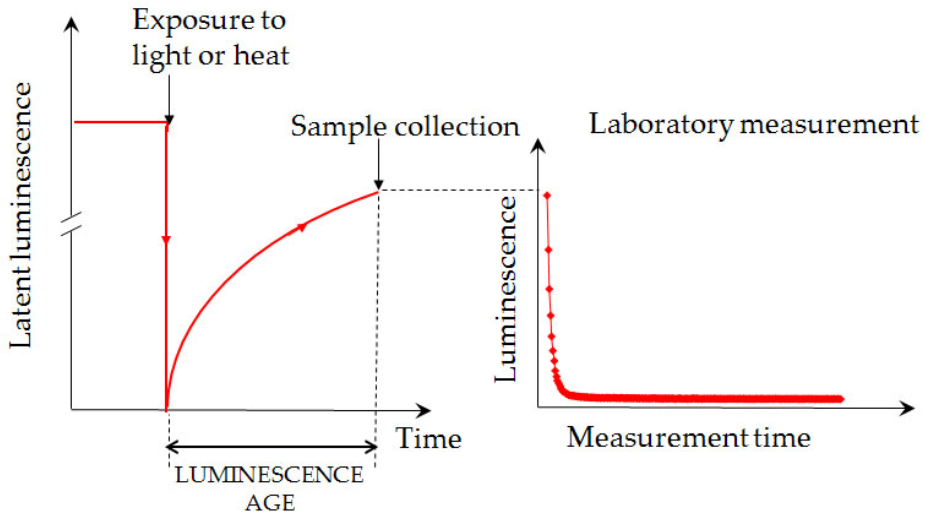

Figure 2.1. Basic principle of luminescence dating. When mineral grains (mainly quartz and feldspar) are exposed to light or heat, their luminescence signal falls to negligible levels (i. e. the luminescence signal resets). Once the grains are buried and shielded from light they start receiving ionizing radiation from their environment and their luminescence signal builds up. The luminescent emission can be forced by stimulation the grains with heat or light. On the figure, an optical luminescence decay curve is shown.

Luminescence dating is based on the ability of minerals to store charge (electrons and holes) released from the exposure to ionizing radiation in the crystal lattice. Today OSL dating is mainly based on measurements of quartz and feldspar; minerals which both can be classified as insulators; this means that electrons would need high energy (~ 3 – 10 eV) to overcome the distance between the valence band and the conduction band, the forbidden band gap. Defects in the crystal lattice, like impurities and missing atoms, act as traps at energy levels within the forbidden band gap. When ionizing radiation interacts with the luminescent material a redistribution of charge (electrons and holes) within the crystal lattice takes place and the fraction of free electrons and holes which does not recombine instantaneously is trapped in these defect sites, located at a depth E below the conduction band (Figure 2.2 (a) and (b)).

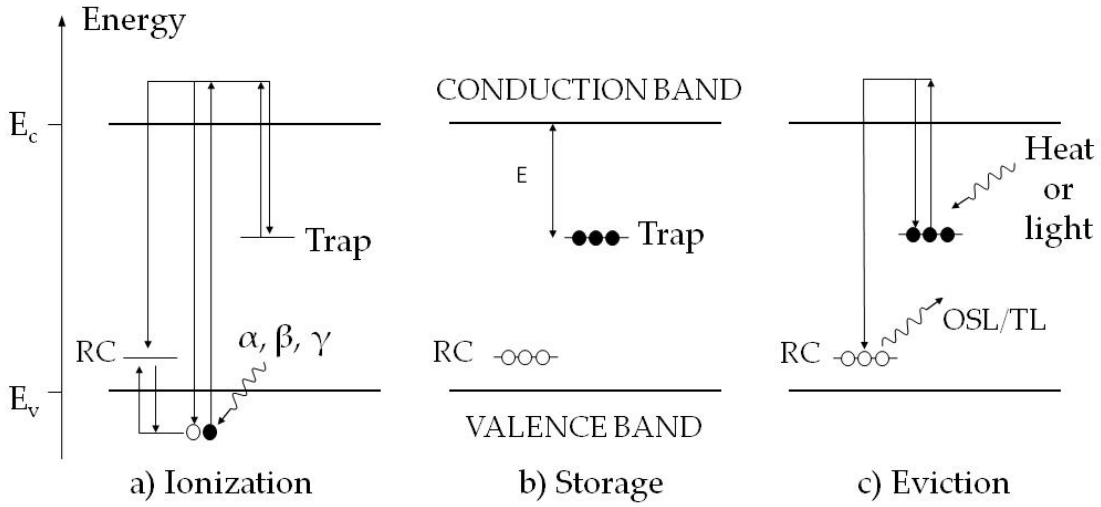

Figure 2.2. (a) As a consequence of ionizing radiation, charge moves to the recombination centres and to traps; (b) if electrons do not have enough energy to jump to the conduction band, then they are stored in the traps; (c) once the electrons receive external energy (optical stimulation) electrons are evicted and luminescence emission occurs. E_c and E_v are the conduction band edge and valance band edge, respectively. RC indicates a recombination centre. Traps are located at a depth E below the conduction band.

These traps are located in certain positions below the conduction band, having a specific energy and lifetime. The amount of trapped charge is uniquely determined by the time the crystal has been receiving radiation once buried.

Stimulation of specific energy may cause luminescence. When energy greater than that between the trap and the conduction band is applied, then electrons escape to the conduction band. Part of them may be retrapped and a small fraction of the remaining electrons recombine with the trapped holes at the recombination centres, RC; the majority dissipate as heat. Some of this recombination processes are radiative resulting in the emission of luminescence (Figure 2.2(c)).

Daylight has enough energy to empty these metastable levels of energy thus the crystal only accumulates in the traps charge derived from ionizing radiation once it is buried and kept away from light. In the laboratory, the OSL signal is reset by optical stimulation with an appropriate wavelength. For quartz, blue (~ 470 nm) or green (~ 530 nm) stimulation is employed. The natural luminescence signal, (i.e. the signal corresponding to the dose that a sample has received during its burial time) is measured this way and the equivalent dose is determined.

The dose per unit time the mineral receives in nature (i.e. dose rate) is the integration of all ionizing radiation from all sources including the decay of radioactive nuclides found in its vicinity and the cosmic rays corrected for the burial depth. Water content of the environment also takes part in the final dose rate received as it causes attenuation of the radiation.

The age of a certain material can then be estimated from the relation

$$Age\ [ka] = \frac{Equivalent\ dose,\ \ D_e\ [Gy]}{Dose\ rate\ [Gy/ka]}$$

where Gy denotes the unit of dose, Gray, equivalent to 1 Joule of absorbed energy per kg of matter, and ka is one thousand years.

2.2. **Luminescence signal**

In most OSL dating applications the sample is stimulated with a constant light intensity (continuous wave stimulation, CW) and the luminescence emission is measured simultaneously using a photomultiplier tube. The OSL signal is observed to decrease with stimulation time, due to detrapping of captured electrons and subsequent radiative recombinations at recombination centres. In the simplest model, considering one trap type and one recombination centre, it can be shown that the OSL signal decays exponentially in the absence of significant retrapping. However, in nature most materials will contain more than a single trap type (different trap types are characterized by different optical cross sections) and thus the observed OSL curve is usually a sum of decreasing exponentials, where each exponential represents a specific trap type. The quartz OSL signal is generally made up of three different exponentials generally named the fast, the medium and the slow component (Smith and Rhodes, 1994; Bailey *et al*., 1997; Singarayer and Bailey, 2003; Jain *et al*., 2003). It has been suggested that retrapping of charge is responsible for the non-exponential decay deriving in the slow and medium components (Bailey *et al*., 1997). The fast component has the largest optical cross-section (i.e. the probability for electrons being evicted from the trap is the greatest) and thus, it is the most readily reset by exposure to light and therefore the most relevant component to optical dating. In addition, only traps with a lifetime significantly greater than the burial time can be used for dating. The lifetime of the fast component is 10^8 years and thus, stable enough for Quaternary applications. It has been reported that the separation slower components of the decay signal -in order to maximize the contribution of the fast component-, results in more accurate dose estimates as its signal behaviour is more reproducible than those from slow or medium components (Choi *et al*., 2003; Jain *et al*., 2005). Both slow and medium components have been shown to easily lead to underestimation of the age (Wintle and Murray, 2006). In addition, the fast component is expected to be better bleached than the rest of the components thus its isolation and basing the dose estimate on this part of the signal is likely to provide the most accurate burial dose (e.g. Jain *et al*., 2003).

The subtraction of the early background, EBG, is usually expected to minimise any effects of slower components, which may suffer from incomplete bleaching, on the net signal (Cunningham and Wallinga, 2010). The same authors suggested that the net signal most dominated by the fast OSL component can be obtained when the background integral immediately follows the initial signal and is approximately 2.5 times its length. The effect of the chosen background summation limits has been analyzed in this study.

2.3. Equivalent dose measurement: SAR protocol

The equivalent dose is that derived from laboratory measurements and is equivalent to the total dose the sample has been exposed to in nature after burial. It is determined by interpolating the measured natural OSL signal onto a laboratory dose response curve, showing a pattern of OSL signal to dose of ionizing radiation. Individual points on the dose response curve are determined by measuring the OSL signals induced by laboratory irradiations given by a calibrated beta source. Several individual aliquots are measured, each one providing a D_e value.

Many samples show significant sensitivity changes along the measuring procedure, leading to inaccurate D_e estimates. The single-aliquot regenerative-dose (SAR) protocol (Murray and Wintle, 2000) has been accepted to provide the most accurate D_e estimates because it is designed to correct such sensitivity changes. SAR uses additional OSL measurements at a constant dose established as reference value, termed "test dose", to trace and correct possible changes in luminescence sensitivity that might occur along the measuring cycle, due mainly to thermal treatments. If sensitivity change occurs, along the measuring sequence, then the dose response curve cannot be trusted to determine the equivalent dose accurately since it would not only be affected by the controlled variation in dose but the effect would also affect the curve and thus, would affect the determined D_e. Inset in Figure 2.3 shows the sensitivity changes along the cycles in a measuring sequence for heated quartz (circles) and sedimentary quartz (squares) when applying in each cycle a constant chosen dose. It can be observed that

although the given dose is kept constant, the sensitivity changes along the cycles; increasing slowly linearly for the sedimentary quartz and following an exponentially saturating increase in the case of heated quartz. Using the test dose in each cycle makes it possible to track sensitivity changes and correct the dose response curve to subtract the effect of these changes in sensitivity. The relation between the regenerative dose response and the test dose response is shown in Figure 2.3., where their approximately linear relation can be observed.

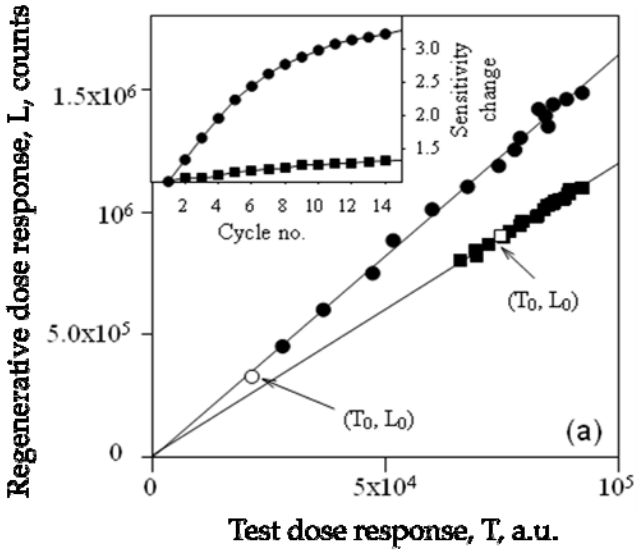

Figure 2.3. Sensitivity changes along the cycles in a measuring sequence for heated quartz (circles) and sedimentary quartz (squares) when applying in each cycle a constant chosen dose (i.e. test dose). Sensitivity increases slowly linearly for the sedimentary quartz and following an exponentially saturating increase in the case of heated quartz. The inset shows the response over the cycles without correction for sensitivity changes (taken from Wintle and Murray, 2006).

The first step in the SAR protocol is to preheat the sample to a given temperature, usually in the range 180-300°C to empty shallow traps causing the equal redistribution of charge similar to the effect in a natural environment. The preheating sensitise all signals to the same degree so both, natural and regenerative signals are given the same treatment (Murray and Wintle, 2003; Ankjaergaard *et al*., 2006). Then the first OSL signal, corresponding to the natural dose, L_0, is measured. Subsequently, aliquots are

subjected to the test dose, followed by a cutheat. For the measurements done in this study, a cutheat temperature lower than the preheat temperature has been used to guarantee that no new alterations are induced. The reference OSL signal, T_0, derived from the test dose is then measured (Figure 2.4).

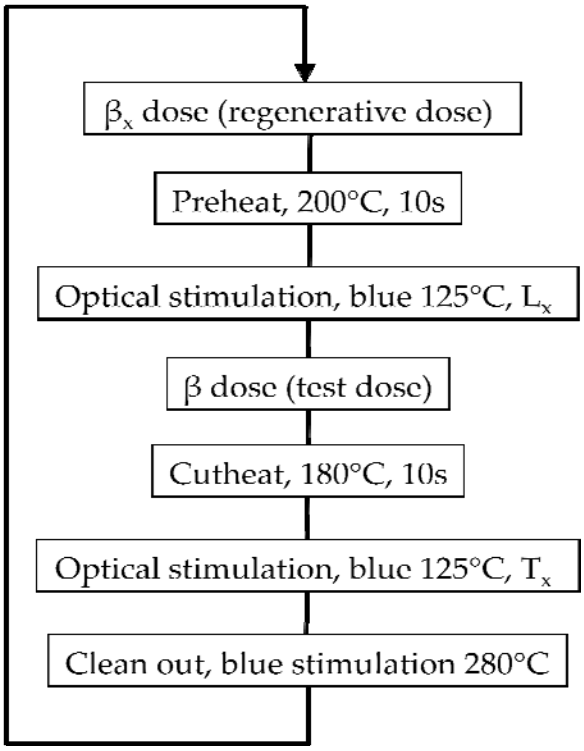

Figure 2.4. Single-aliquot regenerative-dose (SAR) protocol. Typically this cycle is repeated using three regeneration points, a zero (recuperation) and a recycling point (usually the second regeneration). For the first cycle, x=0, the first step (regenerative dose) is not given, thus, the signal measured during the first optical stimulation corresponds to the natural dose.

The cycle is repeated typically using three regeneration points, a zero dose point (recuperation) and a recycling point (usually repeating the second regeneration dose value). The difference from cycle to cycle in a measuring sequence is the given regenerative dose, β_x, which is not given in the first cycles and it is varied in the following cycles. A clean out with optical stimulation at higher temperature than that used for the measurements is used to eliminate any possible residual signal.

The repeated cycles of dosing and heating involved in the measuring process may sensitize the samples. A series of test are suggested to be carried out routinely to evaluate the effect of different independent intrinsic factors on the behaviour of the sample.

In order to trust the defined dose response curve for the determination of the D_e it is important to assure that the dose points can be repeated accurately. For this purpose a regeneration dose is repeated (recycling point) to confirm that the protocol has corrected adequately for sensitivity changes. The recycling ratio is given by the ratio of these two sensitivity corrected signals. If sensitivity changes are successfully corrected by SAR then this ratio should be unity. Also recuperation of the signal is tested by giving a zero dose regeneration point in order to detect if there is negligible signal when no dose is given, even after the possible effects caused by previous irradiation, preheating and stimulation processes. The recuperation is typically calculated as the ratio of the sensitivity corrected recuperation point and natural sensitivity corrected signal following the relation:

$$Recuperation\ (\%) = \frac{L_0/T_0}{L_{NAT}/T_{NAT}}\ x\ 100$$

It is advisable to carry out a dose recovery test to check how accurately a laboratory given dose can be recovered (Wintle and Murray, 2006). For that, a number of sample aliquots are bleached, either under solar simulator, daylight or using built-in stimulation sources. After bleaching the aliquots a known dose is given, which will play the role of the natural dose. Then a normal SAR protocol is measured and the "artificial natural dose" is interpolated onto the dose response curve to determine the equivalent dose. The ratio of the measured dose to the given dose is known as the dose recovery ratio. If this ratio is within 10% of unity or within two standard errors of unity the protocol is assumed to be applicable to the sample.

2.4. **Annual dose rate**

The natural dose rate consists of contributions from alpha, beta, gamma and cosmic radiation. These contributions arise from internal radionuclides, usually negligible in quartz but significant in potassium feldspar, external radionuclides (e.g. Uranium and Thorium) and usually a small contribution from cosmic radiation (Prescott and Hutton, 1994). During chemical treatment to isolate quartz grains, a solution of HF is used which etches the outer layer (~10 μm) of quartz grains thus, eliminating the area affected by alpha radiation. The concentration of ^{40}K and daughters of the decay chains of ^{238}U and ^{232}Th have to be measured (e.g. by neutron activation analysis, gamma spectrometry, low-level gamma spectrometry at the sampling point).

The annual dose rate is calculated under the assumption that the rate of energy absorption is equal to the rate of energy emission per unit mass. Moreover, it is assumed that the radiation is uniform within the matrix and that the absorption coefficients of the constituents are uniform, this means the soil/sediment is homogeneous over a distance greater than the particle range (Aitken, 1985).

In general, the dose rate during burial is assumed to be constant. However, this assumption is not always valid (e.g. Zander *et al.*, 2007); e.g. soil heterogeneity, water content change during burial. Although, such changes may influence the luminescence age significantly a constant average value is assumed for each independent sample based on the water content and saturation measurements. Corrections on the dose rate according to the water content estimated for the burial time are important since water significantly attenuates the radiation. Once the dose rate range is restricted, the main challenge in the dating process lays on the determination of the equivalent dose.

2.5. Analytical facilities

In this section various analytical facilities used during this work are described.

2.5.1. Luminescence readers

OSL measurements were made using automated Risø TL/OSL DA-20 luminescence readers (Bøtter-Jensen *et al.*, 2010, Figure 2.5)

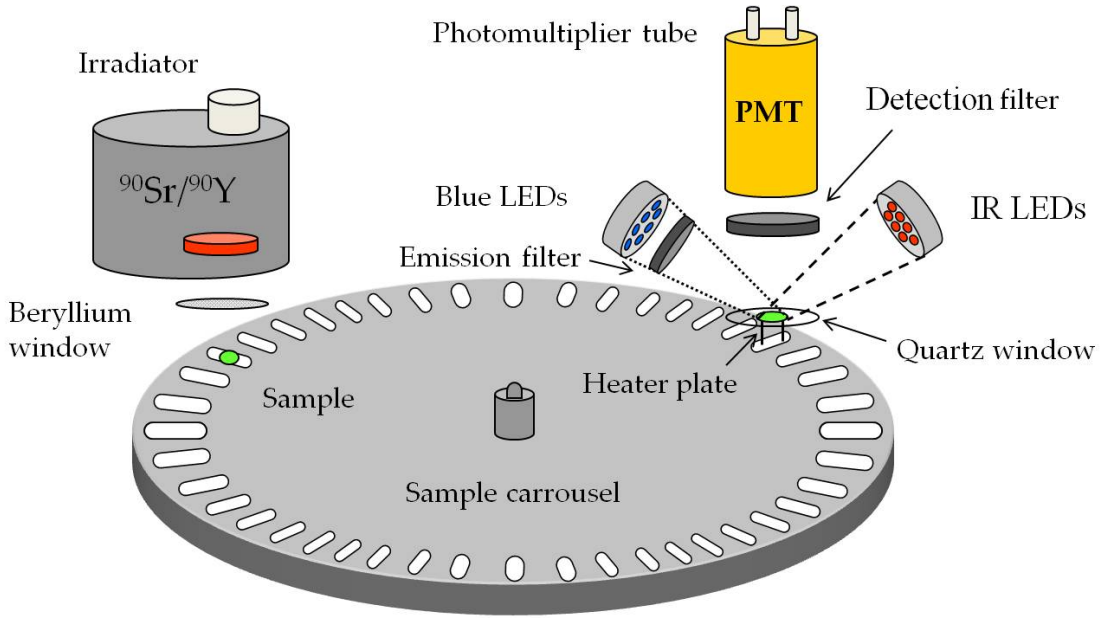

Figure 2.5. Schematic drawing of the most important components in the Risø TL/OSL luminescence readers (taken from Thomsen, 2004).

These readers are equipped with different optical stimulation sources, a light detection system, an irradiation source, a heater and a single grain attachment:

i. A blue (470 ± 30 nm) light emitting diode array providing a stimulation power of ~80 mW/cm^2 at the sample position was used for multi-grain aliquot stimulation. Samples were mounted in a monolayer on 9.7 mm diameter stainless steel discs using silicon oil.

ii. Luminescence was detected using a bialkali EMI 9235QB photomultiplier tube. A set of filters is commonly used to shield the PMT from scattered stimulation light and to define the spectral detection window. For the measurement in this study, light was detected through a 7.5 mm Hoya U-340 filter which has a peak transmission around 340 nm.

iii. A heater specially design to provide a very good heat transmission to the sample. Samples can be heated up to 700°C at linear heating rates from 0.1 to 10 K/s. To minimise thermal time lag between sample and the heating plate, heating rates above 5 K/s should be avoided.

iv. Single grain measurements were undertaken using the Risø single grain attachment (Duller *et al*., 1999; Bøtter-Jensen *et al*., 2000). In this case optical stimulation was achieved using a green (532 nm) Nd:YVO_4 laser providing a power density of ~50 W/cm^2. Single grains were loaded into aluminium discs containing 100 grain holes, each with a depth and diameter of 300 μm Figure 2.6.

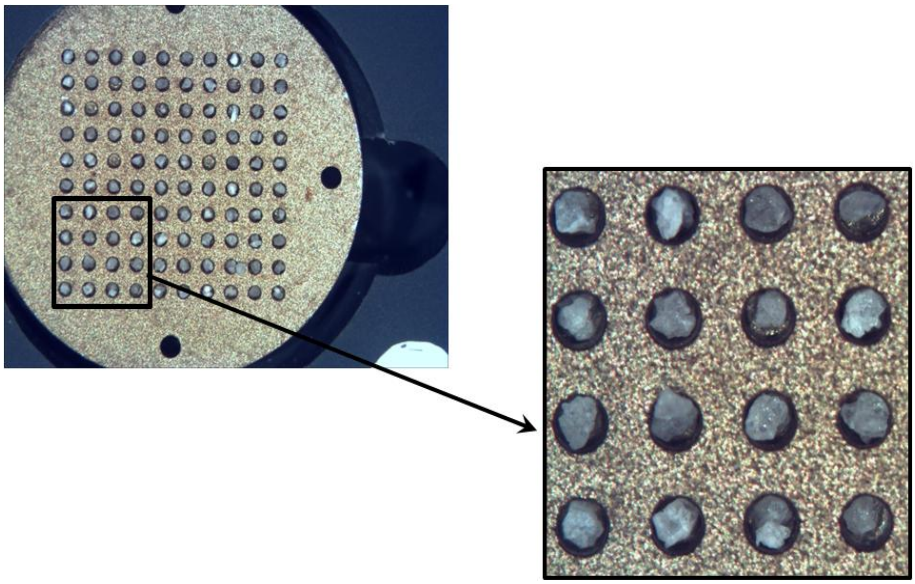

Figure 2.6. A picture of a standard single grain disc containing 100 grain holes with a depth and diameter of 300 μm. Also shown is a close up of the single grain disc. The disc has been loaded with 180-250 μm quartz grains.

2.5.2. Built-in beta source

A calibrated $^{90}Sr/^{90}Y$ beta source built in the reader is used for the artificial beta irradiations (providing dose rates in quartz mounted on stainless steel discs of 0.04 to 0.11 Gy/s).

It has been reported (Spooner *et al.*, 2000; Thomsen *et al.*, 2005; Ballarini *et al.*, 2006; Lapp *et al.*, 2012) that the laboratory dose rate from the in-built beta source can be inhomogeneous across the sample area. The sources manufacturing process was modified in 2000 to reduce the radiation hazard during manufacturing. Sources manufactured before 2000 had a quite homogeneous radiation field but the manufacturing process was modified to improve workers' safety. The dose rate inhomogeneity of sources manufactured between 2000 and 2010 has been found to be highly variable because the new production method as radioactive material was melted in a free cavity for the manufacturing and radioactive material could be located in any position within the cavity. Sources manufactured after 2010 provide a more spatially uniform dose rates as they made by placing pellets of radioactive material symmetrically distributed depression in the source backing material prior to melting (Lapp et al., 2012,Figure 2.7). Although symmetric, the radioactive field presents a spatial variation due to the position of the radioactive material within the backing material geometry.

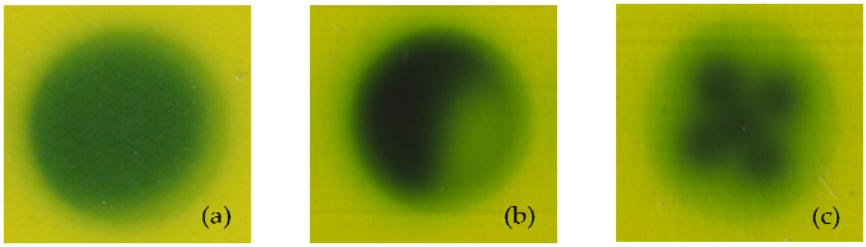

Figure 2.7. Beta source radioactive field corresponding to sources manufactured (a) before 2000 (≈40 mCi, ≈10 s); (b) between 2000 and 2010 (≈80 mCi, ≈5 s); (c) after 2010 (≈40 mCi, ≈10 s). These images are direct exposures of GAF Chromic film to the corresponding beta source. The uniformity is improved considerably when the source is backed away (as it is in the reader where there is a distance of ~5 mm between source and sample).

Beta dose rate non-uniformity has a negligible effect when measuring small aliquots in which the sample is centred on the disc and it can be assumed that the entire area of the sample is receiving the same dose but could contribute significantly to the observe variability in single grain dose distributions, because the laboratory given dose vary from grain to grain (Figure 2.8). This dose anisotropy demands corrections as it may have a significant effect on the D_e estimates. As a result of individual manufacturing the radiation field is different for each source so it must be corrected independently.

Two different beta sources were used for the single grain measurements presented here. One of them, source ID155, was manufactured before 2000 and is thus expected to have a relatively uniform distribution of radioactive material while ID195 was manufactured in 2006 and thus it is expected to have a broader spatial variation (Lapp *et al.*, 2012).

In order to map the uniformity of the sources GAF Chromic film (i.e. radiation sensitive film commonly used for dosimetry) is placed on the sample position and irradiated with known doses. The exposed film is scanned with a colour scanner and stored as a bitmap file. Mapping the beta source following the approach of Lapp *et al*. (2012) showed that the effective dose rate varied spatially by up to 5% and 13% for the sources ID155 and ID195, respectively. Lapp *et al*. (2012) have developed software that makes it possible to correct for this dose rate inhomogeneity automatically using this dose-rate map (Figure 2.8).

The corresponding correction matrix was used in all cases prior to any calculation with the measured data.

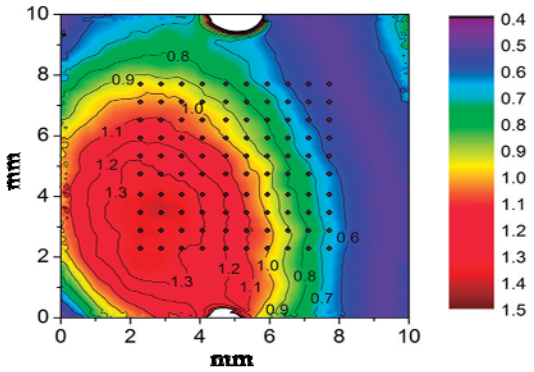

Figure 2.8. Dose rate correction matrix. The 10 x 10 dot pattern shows the position of the single grain holes (Lapp et al., 2012).

2.5.3. Gamma irradiation

For gamma irradiation a ^{137}Cs (662 keV) collimated point gamma source (providing a dose rate in quartz of ~ μ30 Gy/s) has been used. Samples were place in a special container to guarantee electronic equilibrium avoiding the sample to be within the build up region (Figure 2.9). Tubular glass containers with a 1.8 mm wall thickness and 2.6 mm internal spacing were used for holding the samples during gamma irradiation, as they fulfill the electronic equilibrium requirement. Glass was chosen for having a density similar to quartz grains.

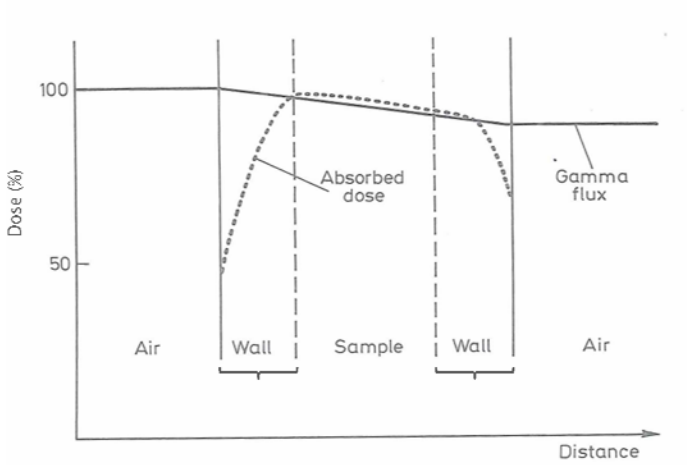

Figure 2.9. Schematic drawing of the energy deposition by a gamma source when irradiating a sample located in a container. The dose builds up in a distance comparable with the range of the most energetic secondary electrons (~ 1 mm).

2.6. Sources of variability in the dose distributions

The dose distributions from the measured (single grain or multi-grain) aliquots contain a number of D_e values and their corresponding uncertainties. From these distributions, the burial dose is estimated. For this study dose distributions are shown by plotting the OSL response from the natural test dose as a function of the measured dose. D_e corresponding to an intense test dose signal show very narrow error bars giving more precise values than those from dim signal which usually have much wider error bars.

The dose distributions from the samples studied here have different shapes. Those from Guadalentin and Rambla de la Viuda appear to be positively skewed with a minimum dose edge and a tail of bigger doses. More than 20% of the D_e values are not contained in the main peak (centred on the minimum dose edge) possibly indicating the presence of incomplete bleaching. Dose distributions from samples from Guadalentin are centred at the minimum doses and have a tail of higher doses. Distributions from Huebra and Duero appear to have less contribution of incompletely bleached grains showing a much more symmetric distribution possibly centred on the true burial dose and missing the tail of higher doses than can be observed in the dose distributions from Guadalentin River.

2.6.1. Thermal transfer

From naturally or artificially bleached samples no luminescence signal is expected but in contrast, a detectable signal is often found. As a consequence of preheating, thermal transfer of charge from shallow light insensitive traps to deeper light sensitive ones might arise. Due to thermal treatment, electrons located at shallow light insensitive traps but sensitive to heat may jump to the conduction band and fall into different traps. If the electrons move to heat sensitive traps, then a TL signal might be emitted but this will not have any effect on the OSL signal. Problems might arise if electrons from the light insensitive trap jump to the conduction band, as a consequence of preheating, and from there to a light sensitive trap. This could result in a luminescence signal which would not have been produced with the original charge distribution

(Figure 2.10). If such a signal is produced it will contribute to the OSL signal. This contribution is usually very small, negligible when the doses measured are high enough, but when measuring low doses (i.e. young sample) it could be a significant fraction of the signal of interest (Rhodes, 2000) thus resulting in dose over-estimation. Several authors have analysed the variation of thermal transfer on artificially bleached samples using different temperatures (e.g. Madsen and Murray, 2009; Pagonis *et al.*, 2007). The use of a lower temperature preheat may mitigate the effect of D_e overestimation (Rhodes, 2000). The possible effect of thermal transfer has been studied in detail for the samples presented in this work as its effect could be significant for the age estimates.

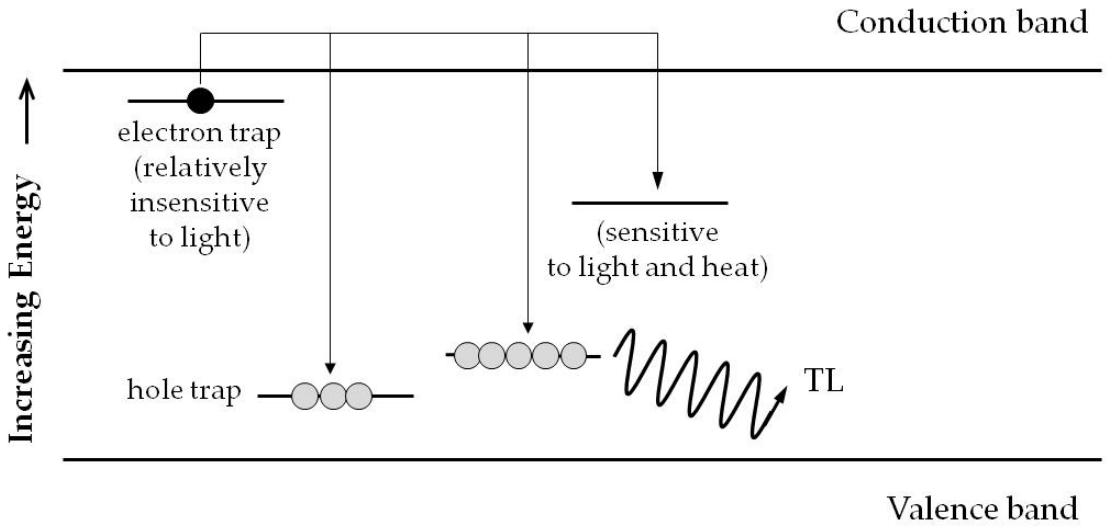

Figure 2.10. Thermal transfer of charge from shallow insensitive traps to deeper sensitive traps as a consequence of preheating. When applying a thermal treatment, electrons located at light insensitive traps might move to hole traps or to heat sensitive traps. In this case, a TL signal might be observed during heating with no effect when measuring OSL. But, if electrons move to light sensitive traps, then a signal which would not have been caused with the original charge distribution might occur, contributing to the measured OSL.

2.6.2. Partial bleaching and single grain

In conventional optical dating methods the OSL signal of multiple grains is measured simultaneously. Multi-grain aliquots are comprised of a number of grains usually loaded on a disc or cup where they are positioned by using silicon spray oil. The

number of grains in each aliquot depends on the grain size and the surface cover by the sample.

The OSL dating based on the luminescence signal of certain sediment assumes that the exposure to sunlight of all grains prior to burial is sufficient to reset thee latent OSL signal. The main consequence of failure to meet this assumption is an overestimation of the burial age.

The likelihood of a sample to be completely bleached depends on the exposure time and spectral composition prior to burial. OSL dating has been successfully used to date aeolian and costal dune sediments (e.g. Stokes and Rhodes, 1989; Stokes, 1992; Berger, 1995; Duller, 1996) which typically have extended exposures to light prior to deposition (Lancaster, 2008; Roberts, 2008). In fluvial environments, as those studied in this work, it is possible that the light reaching the sediment is strongly attenuated by water and flow turbidity as well as for transport duration and distance. This situation could result in incomplete bleaching of the sediment, i.e. the sediment is buried already carrying an OSL signal (Rhodes and Pownall, 1994; Olley *et al*., 1998). In such cases, samples may contain a mixture of grains with different degrees of bleaching. The typical heterogeneous bleaching of grains from fluvially-transported sediments means that aliquots containing a larger number of grains are more likely to include grains with a significant residual dose. These would contribute to the OSL signal and thus resulting in an overestimation of the burial dose. The greater the number of grains that are measured simultaneously, this is the number of grains on each aliquot, the less the variation in the D_e will be observed (Olley *et al*., 1999; Wallinga, 2002).

New instrumentation developments (Duller *et al*., 1999; Duller and Murray, 2000) and methods (Murray and Wintle, 2000) have allowed reducing the sample size for OSL measurements to a single grain. Measurements on single grains allow the identification of grains with a residual signal as a consequence of not being completely reset so that the well bleached fraction can be selected and used for the age determination (e.g. Murray and Roberts, 1997; Galbraith *et al*., 1999; Olley *et al*., 1999). However, determination of burial dose based on single-grain OSL measurements is difficult not

only because of incomplete resetting of the OSL signal but also due to other sources of scatter in optical dating. These sources include: (a) measurement uncertainty related to weak and noisy OSL signals of individual grains, (b) heterogeneous radiation exposure due to mixed radionuclide distributions and therefore heterogeneous grain exposure to dose rates in the natural environment, (c) inappropriate luminescence properties of some grains that may prevent equivalent dose determination using standard single aliquot regenerative dose (SAR) procedures and, d) instrument reproducibility.

Although using single grains gives the possibility of measuring a bigger number of aliquots (single grains in this case) per unit time, the procedure involves a tedious sample loading and a complex analysis of the data. In addition, it has to be taken into account that generally only a small percentage of grains have detectable luminescence signal so a larger number of single grains than multi-grain aliquots have to be measured to obtain the same number of D_e values. Thus, the entire process to estimate a burial dose involves longer time than that when multi-grain aliquots are used. For these reasons, single grain measurement should not be considered a routine procedure but only an option in specific type of problematic sediments (i.e. those affected by partial bleaching). In addition, the analysis of single grain data involves statistical approaches in order to determine the well-bleached fraction so the D_e estimation is not a straight forward process. A number of statistical approaches have been presented in the last years to do so (e.g. Galbraith *et al*. 1999; Lepper and McKeever, 2002; Thomsen *et al*., 2007; Arnold *et al*., 2009) reaching good agreement with expected values but involving a complex analysis of the uncertainties that may lead to significant changes in their results.

Although single grain measurement was presented as the "right" way to identify the well-bleached fraction in a sample and select only the grains deriving to the true burial dose, the limitations of the technique have put the limits to the, in theory, perfect procedure. The suitability of multi-grain aliquots to date incomplete bleached samples is under discussion with contradictory conclusions presented (Rhodes, 2000; Arnold and Roberts, 2009) and it has also being studied here in detail.

2.7. **Method of analysis**

The quartz grain size fraction used was the 180-250 μm. This fraction was chosen because it has been shown to be better bleached than smaller grain sizes (e.g. Truelsen and Wallinga, 2003). Samples were measured using the SAR protocol (Murray and Wintle, 2000) giving three to five regeneration doses, a 0 dose point to check recuperation of the signal after the measurement using the largest regeneration dose and a recycling of the second regeneration dose. In this study, the protocol employed a preheat temperature of 200°C for 10 s and a cut-heat of 180°C at a heating rate of 5°C/s for all measurements, unless otherwise stated.

The OSL measurement were carried out at 125°C to avoid retrapping of charge in the trap corresponding to the 110°C TL peak (Murray and Wintle, 1998). Unless otherwise stated multi-grain measurements were carried out using 2 mm aliquots containing ~30 grains each. The OSL signals from multi-grain aliquots are based on the summation of the first 0.64 s of stimulation corrected for background derived from the following 0.64 s in order to eliminate the contribution of other components of smaller optical cross-section (Early BackGround subtraction, EBG, e.g. Cunningham and Wallinga, 2010). As explained in section 2.2, the OSL decay curve is assumed to be the sum of several OSL components where the fast component (i.e. the component with the largest cross-section) is the preferred component for dating as it is most likely to be well-bleached, is geologically stable over millions of years and is less susceptible to thermal transfer (Wintle and Murray, 2006).

Single grain OSL signals are derived from the summation of the first 0.1 s of stimulation corrected with the last 0.2 s for background (i.e. Late BackGround subtraction, LBG). Using EBG on single grain measurements reduced the number of accepted grains by ~10% without changing the dose estimate or over-dispersion significantly (see section 3.5.1.1 for further details) – this may reflect variable effective stimulation power arising from reflection and scatter from grain surfaces (Thomsen *et al*., 2012).

Poisson statistics were assumed to estimate the uncertainty of the background-corrected signal, s_n, given by

$$s_n^2 = Y_n + \frac{B_m}{k^2}$$

where Y_n is the integrated signal of the first n channels, B_m is the integrated signal of the last m channels and $k = m/n$ (Galbraith, 2002). Estimates of uncertainty s_n associated to individual dose estimates D_N are based purely on photon counting statistics and are calculated using the law of error propagation.

A selection criterion has been applied to determine the acceptance or rejection of aliquots (both multi-grain and single grain). Dose estimates are accepted (both if the relative uncertainty on the natural test dose response is less than 20% and if the recycling value is within 20% of unity. Aliquots showing a dose response curve with anomalous behaviour (e.g. decreasing response as a function of dose) are discarded. These criteria lead to the rejection of approximately 98% of the measured single grains and ~ 5% of the multi-grain aliquots. Doses and their uncertainties are estimated using Analyst 3.24 (Duller, 2007). Equivalent doses were estimated by interpolation of the natural test dose corrected signal onto the dose response curve which had been fitted using either a linear or a saturating exponential function. Approximately 2% of the measured natural sensitivity corrected signals are higher than the signal measured for the highest regeneration dose point in the dose response curve. In these cases the D_e was determined by extrapolation. The uncertainties derived from Analyst 3.24 are based on counting statistics and curve fitting errors. Additional uncertainty derived from gamma dose recovery experiments (fur further details see section 3.4.4.2) are added onto individual dose estimates to account for measurable intrinsic sources of variability (Reimann *et al*., 2012; Sim *et al*., 2012; Thomsen *et al*., 2005, 2007, 2012).

2.8. **Field sampling**

Samples are collected by hammering opaque PVC cylinders (internal diameter of ~5 mm and length of ~30 cm) into a cleaned vertical exposure until completely filled with

sediment. Upon extrusion from the cliff face, these cylinders are sealed using thick duct tape. Extra sand subsamples for each sample are packed into airtight plastic containers holding approximately 200 g. These subsamples are to be used for determining the water content and the dose rate at the sample location. The cylinders of OSL samples are extruded under subdued red laboratory light from which quartz grains with sizes of 180-250 μm are extracted using routine laboratory procedures (Porat, 2006).

2.9. Sample preparation

2.9.1. Dose rate determination

For this work, the dose rate is measured in the laboratory using high-resolution gamma spectrometry on approximately 200 g of bulk material collected immediately adjacent to the OSL sample. This material is ground in a ball mill to make it homogeneous and casted in a wax mould with reproducible geometry and suitable for reliable radon retention (Murray *et al*., 1987). Water content at the moment of sampling is measured on the same fraction of sample prior to casting. Although average annual precipitation in this area might have varied during the Holocene, this is not expected to cause large changes in the humidity annual cycle of the soil; i.e. wet winters and dry summers. In this well-drained semi-arid environment, the water content values measured right after sampling were assumed to be representative of the average conditions during the burial time. Dose rates are based on the average radionuclide activities of the material collected from the area surrounding the sample location. Cosmic radiation contribution at the site is estimated following Prescott and Hutton (1994), based on depth of each sample.

2.9.2. Equivalent dose measurements

All handling of the sample is carried out under controlled light conditions to avoid bleaching the OSL signals prior to measurement.

Samples were wet sieved to fractions 90-180 μm and 180-250 μm and chemically treated to isolate quartz fraction. Samples were treated with 10% HCl until carbonates were dissolved, and H_2O_2 was used to eliminate organic matter. A solution of 40% HF was used to eliminate feldspar and to etch the quartz outer layer which would have been affected by alpha radiation.

2.9.3. Possible sources of error in sample preparation

For the first preparation of samples, a standard protocol (see Aitken, 1998 and references therein) involving two hours of 35% HCl was used. The solution reacted violently at contact indicating that these samples are carbonate rich. After two hours, the reaction had stopped and the subsequent steps in the protocol were taken. At contact with HF solution the sample reacted violently again.

At completion of the sample preparation, quartz grains had apparently been isolated and inspection confirmed that the processed subsample was composed of only white grains.

Twenty-four large multi-grain aliquots (8 mm) were measured. Approximately 20% of them had poorly defined dose response curves. ~90% of the total aliquots measured had no detectable natural signal but part of them had well defined dose response curve.

This behaviour was not expected from a pure quartz sample. Later examination of the subsample under a microscope revealed only very few crystalline grains. Subsequent X-ray diffraction experiment was carried out on one of the samples to confirm the purity fraction. It revealed that more than 95% of the sample was fluorite (CaF_2), which was not expected to be present, and less than 5% of quartz (Figure 2.11).

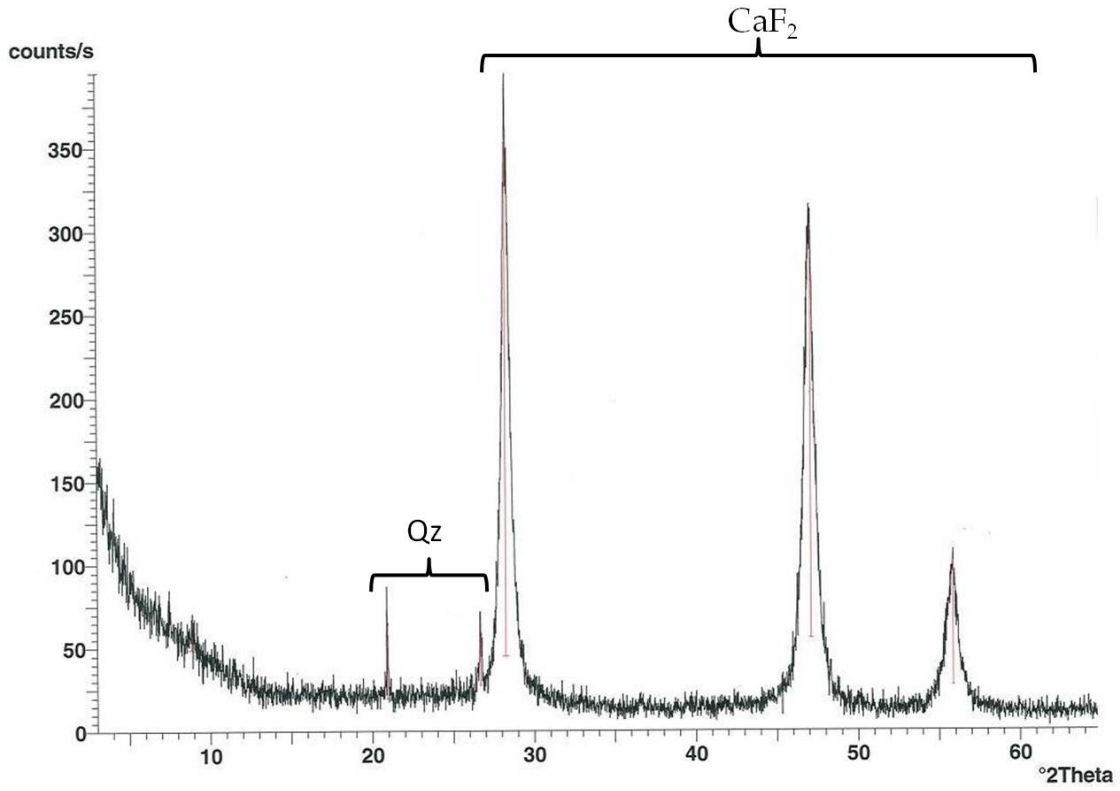

Figure 2.11. X-ray diffraction spectrum of quartz sample from T-23 after application of standard sample preparation protocol. The characteristic peaks from CaF_2 are four times more intense than those from quartz. The large concentration of fluorites was produced when HF reacted with remaining carbonates.

The formation of fluorites is likely to be a consequence of an inadequate removal of carbonates, i.e. the 2 hours treatment with 35% HCl used was insufficient. Elimination of carbonates with HCl solution is based on the reaction:

$$2HCl + CaCO_3 \rightarrow CaCl_2 + H_2O + CO_2$$

When the reaction stops producing CO_2 (bubbling stops) it may indicate the reaction has ended due to either total elimination of $CaCO_3$ or to total reaction of the existing HCl. In this case the amount of HCl used was calculated to be enough to dissolve 100% of the sample if it was pure carbonate so it was assumed that the reaction had stopped because the carbonate had been totally eliminated. The release of ions and other product compounds causes the deceleration of the reaction rate and avoids the solution

to contact and react with the remaining carbonates. Therefore, the reaction may stop even if not all carbonates have been dissolved.

Assuming the reaction had stopped because the total amount of carbonate had been dissolved, following steps in the protocol were taken and the formation of fluorites took place when adding HF solution

$$2HF + CaCO_3 \rightarrow CaF_2 + CO_2 + H_2O$$

This could only be a consequence of carbonates not being totally eliminated although the reaction with HCl had stopped.

Fluorite was just formed during sample preparation, thus it has not received enough ionizing radiation to show a detectable natural luminescence signal. Despite, it has been reported that fluorite shows luminescence response heat (TL) and blue (OSL) stimulation (Calderon *et al*., 1992; Chougaonkar and Bhatt, 2004). Therefore, even though fluorite is not expected to contribute to the natural signal, its response to ionizing radiation and stimulation may affect the dose response curve and thus will cause variations in the D_e estimation. To test the possible effect on the D_e determination a dose recovery test was carried out on a sample composed of fluorites (~80%) and quartz of known dose (~20%). The quartz grains were determined to have received a dose of 200 mGy (Bailiff *et al*., 2000). These had been extracted from bricks in the downwind area of the Chernobyl nuclear power plant to be used for dosimetry purposes. Using a standard SAR protocol, the dose was recovered accurately (recovered to given ratio was 0.99 ± 0.03 for a set of 12 aliquots measured). This result suggests that the presence of fluorites would not prevent from determining the D_e values accurately. Despite, using our natural prepared sample containing such a big proportion of fluorites caused that the majority of the multi-grain aliquots prepared contained one or none quartz grains thus resulting in a negligible natural luminescence response. In an attempt to dissolve the new formed fluorites, a treatment with 35% HCl heated at 80°C was used finding insignificant effect.

A second batch of samples was prepared paying special attention to the total elimination of carbonates. In this case the treatment with a 35% HCl solution for 30 minutes and water rinsing was repeated a total of six times until no reaction was found at contact with fresh solution. This would be the appropriate procedure to avoid incomplete reaction when treating a carbonate rich sample. Adding fresh acid solution on top of the previously used one would only result in the dilution of the acid when mixing with the remaining ions and product compounds. Rinsing the sample helps removing ions and other product compounds that might dilute the acid and slow down the reaction rate. Samples were then treated with H_2O_2 and HF following a standard procedure (Aitken, 1998).

Another fairly common problem in the chemical isolation of quartz is the contamination with feldspar. If this is caused by the prevalence of feldspar in the sample, it could be overcome with a second treatment of 40% HF solution but if feldspar is embedded as inclusions in the quartz grains (Lamothe *et al*., 1994, Baril, 2004) then, physical separation is not possible. Both feldspar and quartz emit OSL signals in response to blue/green stimulation but only feldspar responds to IR stimulation. Thus it is possible to reduce the feldspar contribution to the observed blue/green stimulation (Lamothe *et al*., 1994; Banerjee *et al*., 2001). To check the effectiveness of the IR stimulation in order to obtain a clean quartz signal it is recommended to calculate an IR depleting ratio (Duller, 2003) by including an extra cycle in the measurement. However it has been shown (Thomsen *et al*. 2008) that in some cases, IR stimulation alone is not able to reduce the feldspar OSL signal sufficiently. In such cases, instrumental separation of quartz and feldspar signal can be obtained using pulsed (POSL) stimulation as the luminescence lifetimes for latest are much shorter than those for quartz (Denby *et al*., 2006) thus showing a much faster decay curve. Figure 2.12 shows the response to a pulse of led stimulation. During the off time, it can be clearly observed the difference in the decay time of quartz and feldspar, making it possible to identify if the OSL signal comes from pure quartz or if there is feldspar contribution. (This technique, POSL, has not been further used in this study).

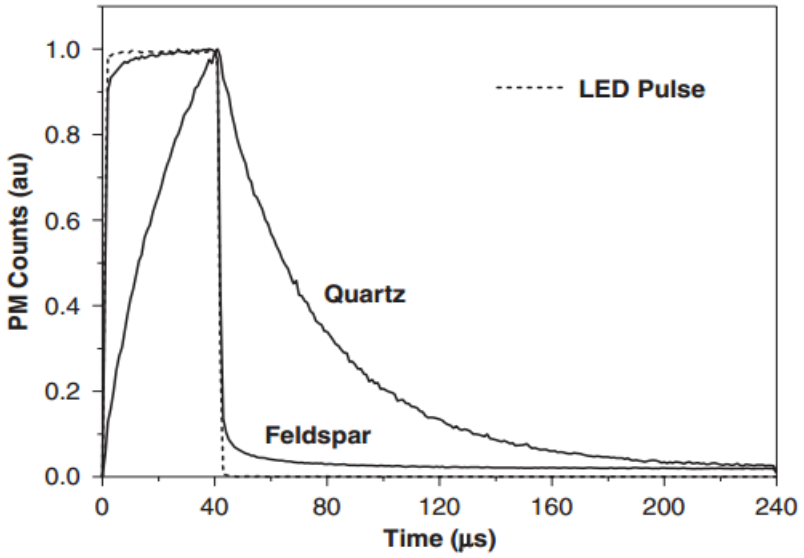

Figure 2.12. Time resolved responses of both, quartz and feldspar under pulsed stimulation (Denby *et al.*, 2006). In the off interval it can be clearly observe the slower decay of the feldspar signal.

3.

OSL dating of historical and modern paleoflood sediments

3.1. **Site description and age framework**

Sediment samples were taken from flood-related fluvial facies from the upper Guadalentin River (upstream catchment area 372 km2) in south-eastern Spain (Figure 3.1). The sediments consist of sand and silt flood sediments that accumulated from suspension during high stage floods in slack-water environments. These slackwater flood sediments accumulated during multiple palaeofloods and now form an up to 7 m thick flood bench on the right margin of the Guadalentín River, 150 m upstream of a bedrock gorge entrance. At the Estrecho site the stratigraphic section contains very well-developed sequences of multiple fine-grained flood deposits, providing evidence of at least 24 individual flood layers deposited over the last 1000 years (Benito *et al*., 2010). A schematic diagram of the section is shown in Figure 3.1.

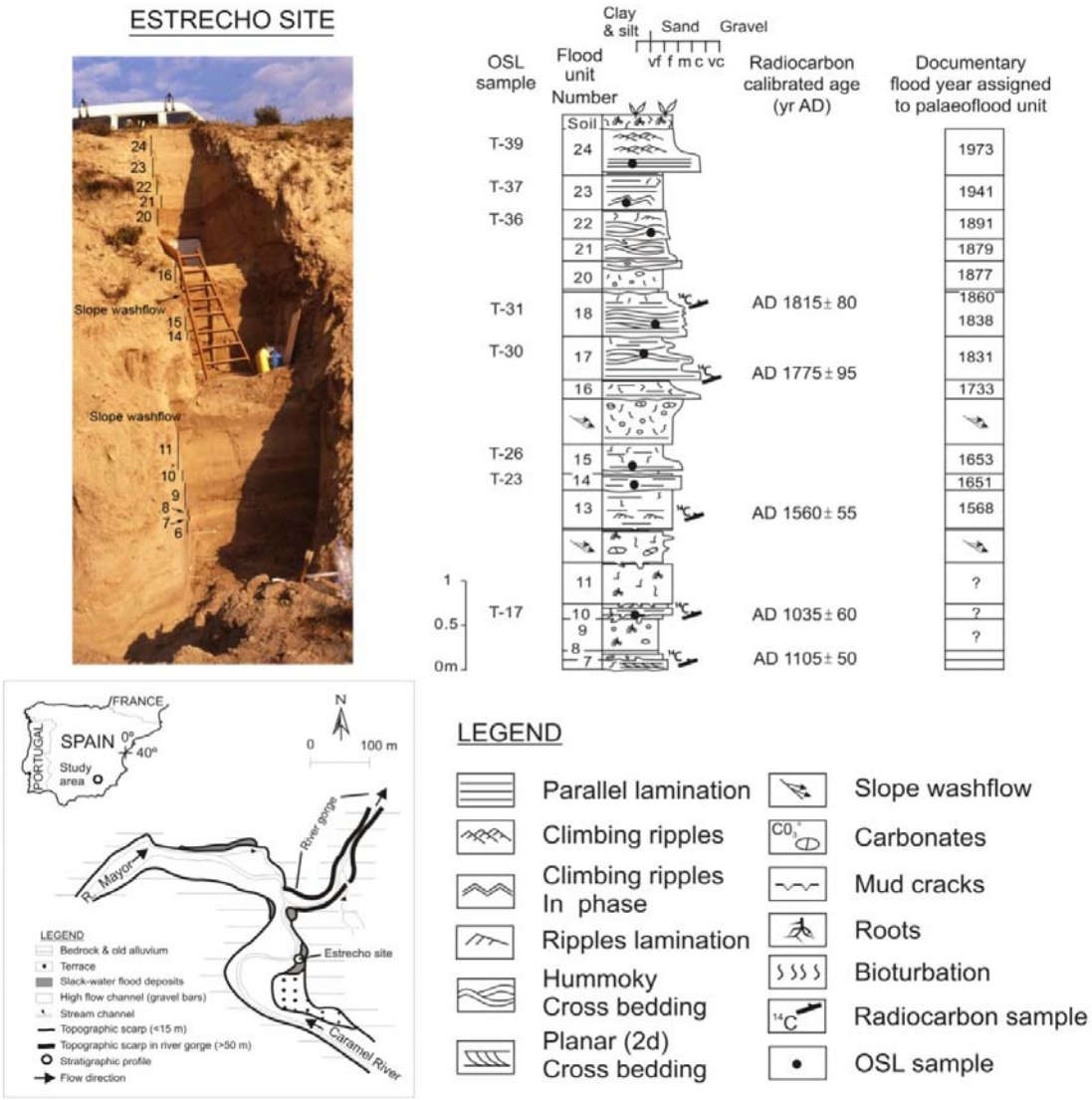

Figure 3.1. Site location, stratigraphic profile and age range association.

The lower ten flood units (only 7 to 10 are shown in Figure 3.1) were radiocarbon dated to between AD 890-1160 and 1000-1210; taken together with the evidence of very fine and fine sand grain size and the thin stratigraphic layers, this suggests a period of frequent relatively small floods. The top of this lower flood sequence is overlain by slope deposits which indicate a break in flood sedimentation of at least 250 years. Overlying this are three flood layers (13 to 15; Figure 3.1) of fine to very fine sand grain-size with the lower one radiocarbon dated to AD 1450-1650. These flood layers are capped by a 42 cm-thick colluvial layer indicating a second break in flood

sedimentation. The upper part of the sequence is represented by nine modern flood deposits, with a basal radiocarbon date of AD 1630-1890 (81.5%), a middle date of AD 1815 ± 80, and the upper flood layer most probably left by the 1973 flood. The radiocarbon age resolution for the last 250 years unfortunately prevents an accurate flood age determination. Flood deposits should contain a complete record of extreme floods (each flood exceeding a certain elevation above the channel leaving a sedimentary unit) and so it is to be expected that this sedimentary sequence should match the historically documented flood record contained in the local municipal archives. Accordingly a flood year was assigned to each palaeoflood unit recorded in the stratigraphy (Figure 3.1) on the basis of the 500-year continuous record of extreme flooding (Municipal Historical Archive of Lorca); this record contains data on the income and expenditure of the community on flood damages (Benito *et al*., 2010; Machado *et al*., 2011). Based on socio-economic damage and inundation area, floods were classified into three categories (Barriendos and Coeur, 2004): (i) ordinary (in-bank flow, no damage); (ii) extraordinary (overflowing of riverbed, damage but no destruction); and (iii) catastrophic (overflowing of riverbed, destruction of permanent infrastructures). Only floods classified as (ii) or (iii) were expected to be recorded in the flood stratigraphy.

During the period AD 1500-1900, 31 flood events were reported in the Municipal Archive, of which 15 were classified as ordinary, 7 extraordinary and 9 catastrophic (Benito *et al*., 2010). According to the archive descriptions, the most severe floods occurred in AD 1651, 1653, 1879 and 1973; these accounted for more than 2600 fatalities in the Guadalentin-Segura catchment, including the AD 1802 dam failure (Machado *et al*., 2011). The stratigraphic record at the Estrecho site is located at a protected low energy site and should include evidence of all these major floods. The three palaeoflood events (units 13, 14, 15) post-dating AD 1450-1650 are likely to correspond to three catastrophic documentary floods occurring in AD 1568, 1651 and 1653. During the first half of the 18th Century, only three large floods were documented (AD 1704, 1728 and 1733). Only one flood unit was deposited at the higher elevation in the stratigraphic section (unit 16), radiocarbon dated with a calibrated age of AD 1775 ± 95. Benito *et al*. (2010) suggest that unit 16 may correspond to the catastrophic 1733 flood at

Lorca, and that high elevation required for leaving depositional evidence (threshold censoring level) prevented deposition at this site of the extraordinary floods in AD 1704 and 1728, and the later 18th Century ordinary floods. During the second half of the 19th Century, an increase in frequency of extraordinary and catastrophic floods is reflected in both the documentary record, with high economic losses and casualties, and the palaeoflood record with high energy sedimentary structures. Benito *et al*. (2010) assigned an age to the upper palaeoflood units containing high-energy sedimentary structures (units 17, 18, 21 and 22) post-dating a calibrated radiocarbon age of 205 ± 45 years BP, to match the most extreme recent floods documented in the Lorca records. The most severe floods in the Guadalentín occurred in 1838 and 1879 and were assigned to units 18 and 21 respectively. In between these floods, the stratigraphy shows at least two flood units (units 19 and 20; the former < 7 cm in thickness), whereas the documentary records contains only one catastrophic flood (1860). An additional documented flood in AD 1877 classified in Lorca as ordinary was assigned to unit 20. The largest flood at the end of the 19th Century occurred in 1891, which was assigned to unit 22. The second largest flood in the 20th Century occurred in 1941 (palaeoflood unit 23) and the largest in 1973 (unit 24). These ages assigned to each sedimentary flood unit on the bases of documentary records are considered a good independent age control from which the robustness of OSL statistical age models can be tested.

3.2. Sample collection, dose rate and predicted doses

A total of eight stratigraphic units from the Estrecho 2 site were sampled for OSL dating (Figure 3.1). They were prepared as detailed in section 2.9.2.

Radionuclide activity concentrations, derived total beta and gamma dose rates to an infinite dry matrix, together with sampling depths, observed water contents and derived total dose rates are summarised in Table 3.1.

Sample	Depth (cm)	Water content (%)	β dose rate (Gy/ka)	γ dose rate (Gy/ka)	Total dose rate (Gy/ka)	Expected ages (ka)	Expected doses (Gy)
T-39	59	8.7	0.37 ± 0.02	0.25 ± 0.01	0.82 ± 0.04	0.04	0.033 ± 0.002
T-37	95	11.8	0.45 ± 0.02	0.31 ± 0.01	0.90 ± 0.05	0.069	0.062 ± 0.003
T-36	122	2.6	0.46 ± 0.03	0.25 ± 0.01	0.91 ± 0.05	0.119	0.109 ± 0.006
T-31	216	9.7	0.43 ± 0.03	0.29 ± 0.01	0.85 ± 0.05	0.172	0.146 ± 0.009
T-30	259	3.4	0.53 ± 0.03	0.31 ± 0.01	1.00 ± 0.06	0.179	0.179 ± 0.010
T-26	351	2.0	0.45 ± 0.03	0.30 ± 0.01	0.91 ± 0.05	0.357	0.32 ± 0.02
T-23	367	8.4	0.43 ± 0.02	0.31 ± 0.01	0.84 ± 0.05	0.442	0.37 ± 0.02
T-17	478	13.4	0.72 ± 0.02	0.42 ± 0.01	1.13 ± 0.05	0.98 ± 0.06	1.10 ± 0.12

Table 3.1. Dose rates for Estrecho 2 site.. Depth and water content at the moment of sampling, considered representative for the burial time, are summarized. Also the total beta and gamma dose rates. An internal quartz dose rate of 0.06 ± 0.03 mGy.a^{-1} has been assumed. The expected ages for all samples (excluding T-17) are based on historical records and is hence expected to be known to a precision of days (no uncertainty quoted). The expected age for the oldest sample (T-17) is based on radiocarbon dating. The expected ages have been converted to expected doses in quartz using the total dose rates.

The site is well-drained and all deposits are well above the current river level. It is assumed that the water content at the time of sampling is representative of the average site water content.

Combining the dose rate data with the information from section 3.1 (age framework) the expected quartz burial doses have been derived using

$$D_e = Age \times Dose\ rate$$

Known ages and the corresponding expected doses are summarized in Table 3.1.

3.3. **Burial dose estimation**

Dose distributions obtained from samples that were well-bleached prior to burial (e.g. aeolian samples) are generally observed to be normally distributed and the burial dose is simply estimated by using the mean of the observed doses. However, in fluvially transported samples no all grains are likely to be well-bleached at deposition and the measured dose distributions may be asymmetric and positively skewed. In such cases, estimating the burial dose using a simple mean is likely to over-estimate the true burial dose. In order to determine an accurate burial dose, the grains that were well-bleached at burial must be identified.

In the past fifteen years a number of analytical approaches and age models have been developed to estimate objectively an equivalent dose from the dose distributions obtained in the measurements. In the context of optical dating it should be understood that age models actually focus on the estimation of the equivalent doses rather than the ages themselves. Five different approaches have been used to estimate the burial dose of these eight samples:

i) As a first approach to burial dose estimation a simple arithmetic mean is calculated. In this case all dose estimates are included irrespective of the precision with which they are known. The most straightforward method to calculate the burial dose would be to use descriptive statistics calculating the mean value and the corresponding standard error with the following equations:

$$\overline{D} = \frac{\sum_{i=1}^{n} D_i}{n} \quad ; \qquad se = \frac{s}{\sqrt{n}}$$

where s is the standard deviation given by

$$s^2 = \frac{\sum_{i=1}^{n} (D_i - \overline{D})^2}{n}$$

and Di and n are the independent equivalent doses measured and n is the sample size (number of data points included). This approach is commonly

used for well-bleached samples but is likely to overestimate the burial dose for incompletely bleached samples.

ii) As a second approach, the equivalent doses were processed based on robust statistics (Turkey, 1977) which is a refinement of the arithmetic mean. Here extreme outliers are removed prior to calculation of the unweighted mean. Extreme outliers are identified to be those outside 1.5*IQR (InterQuartile Range), where IQR = Q3 – Q1 (Turkey, 1977). The first quartile Q1 separates the lowest 25% of the data whereas the third quartile Q3 separates the highest 25% of the data, (Figure 3.2). Unweighted averages and the corresponding standard deviations were then calculated from the resulting dose distributions.

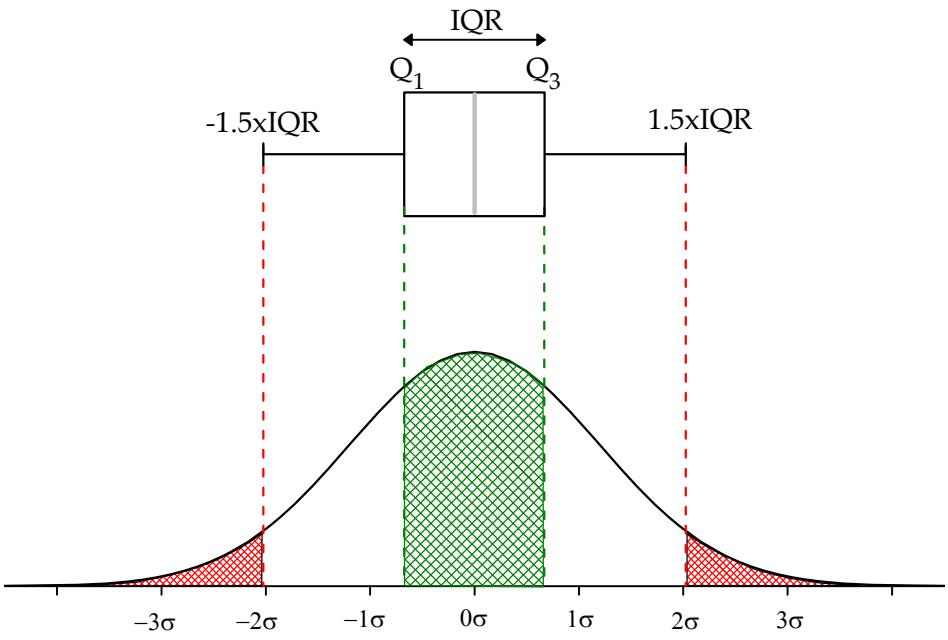

Figure 3.2. Interquartile range (IQR) and the corresponding area of the distribution which includes 50% of the data points (green area). Also shown are the areas containing the outliers defined to be those out of 1.5xIQR (red areas).

In these two approaches each data point contributes equally to the final average but since uncertainties from photon counting statistics vary between individual dose estimates it could easily be argued that a weighted average is more appropriate that an unweighted one.

iii) As a third approach, the Central Age Model (CAM) is applied. CAM is a weighted average of all doses estimates. CAM assumes that the dose distribution is log-normal, i.e. the log dose is normally distributed given by

$$\hat{\delta}_i = \delta_i + \varepsilon_i \quad \text{for i= 1, 2…, n}$$

where δ_i is the true log dose of grain i and ε_i is the error of the estimation which is assumed to be normally distributed centred around zero and standard deviation s_i. The normal distributed true log dose has a weighted average $\hat{\delta}$ and a relative standard deviation σ given by

$$\hat{\delta} = \frac{\sum_{i=1}^{n} w_i \hat{\delta}_i}{\sum_{i=1}^{n} w_i}$$

where the weight, w_i, is inversely proportional to $s_i^2 + \sigma^2$, deriving in a stronger contribution of the values with smaller uncertainty.

Most of the dose distributions presented here contains some non-positive dose estimates which prevent the direct use of CAM because of its log-normal assumption. Arnold *et al*. (2009) described a version of the CAM (CAM_{UL}) in which the log-normal assumption has been replaced by a normal assumption and thus is able to deal with dose distributions containing non-positive dose estimates. However, by using a simple exponential transformation of the data prior to the CAM (using the original scripts written by Galbraith *et al*.) identical results to those derived from the CAM_{UL} are obtained. If the individual dose values and their associated uncertainties are termed D_i and S_i, respectively, then the transformed dose value is $D_{tr_i} = \exp\ (D_i)$

Since the transformed value of the D_e, D_{tr}, is a function of a variable with its corresponding uncertainty, the propagation of this uncertainty has to be taken into account following the relation

$$A = f(x) = a.e^{\pm bx} \xrightarrow{\text{then}} \frac{\sigma_A}{A} = \pm bx$$

Then the uncertainty of the transformed data is given by $S_{tr_i} = D_{tr_i} * S_i$

iv) As a fourth approach, the Minimum Age Model (MAM) (Galbraith *et al*., 1999) is applied. MAM assumes that only a proportion of the measured doses belong to the burial dose distribution and that the remaining dose estimates are part of a log-normal distribution truncated at the burial dose. As with the CAM, the MAM has an underlying log-normal assumption preventing its application to dose distributions containing non-positive dose estimates. Arnold *et al*. (2009) developed a version of MAM, MAM_{UL}, which is based on the assumption that the dose distributions are normal. However, applying the simple exponential transformation described above also allows the use of the original (and in our experience, more stable) Galbraith *et al*. MAM scripts.

Results derived from the MAM applied on exponentially transformed data are termed MAM_{tr}. The MAM_{tr} results are identical to the results obtained with MAM_{UL}.

v) As a fifth approach, the Internal-External Consistency Criteria (IEU) (Thomsen *et al*., 2003; 2007) is applied. The IEU approach is based on the assumption that the well-bleached part of the measured dose distribution is normally distributed. grains are part of a normal distribution with an over-dispersion given by the "ideal" sample only affected by intrinsic factors. The IEU calculates the weighted mean, Z, defined as

$$Z = \frac{\sum_{i=1}^{n} D_i/\sigma_i^2}{\sum_{i=1}^{n} 1/\sigma_i^2}$$

with a standard error, α, which can be calculated as an external measurement of uncertainty combining information on the individual estimates of uncertainty, σ_i , and the deviation from the weighted mean, $D_i - Z$, given by

$$\alpha_{ext}^2 = \frac{\sum_{i=1}^{n}(D_i - Z)^2/\sigma_i^2}{(n-1)\sum_{i=1}^{n} 1/\sigma_i^2}$$

where D_i are the individual dose estimates and n is the total number of measurements.

α can also be calculated as an internal estimate of the uncertainty given by

$$\alpha_{int}^2 = \frac{1}{\sum_{i=1}^{n} 1/\sigma_i^2}$$

If σ_i is the only source of variance affecting the data and the number of measurements, n, is large, then

$$\alpha_{int}^2 = \alpha_{ext}^2$$

and $\mathcal{R} = \alpha_{int} / \alpha_{ext}$ tends to unity (Thomsen *et al.*, 2003, 2007) with the uncertainty of the ratio given by $\frac{1}{\sqrt{2(n-1)}}$ (Topping, 1955).

If the uncertainties which describe the observed variability of a well bleached sample are assigned to the individual dose estimates then *R* will tend to unity when all grains belonging to the well bleached part of the distribution are included. If incompletely bleached grains are included in the dose estimation, then α_{ext} becomes larger than α_{int} and *R* becomes less than unity. Thus, in order for the IEU to be identifying successfully the

aliquots belonging to the well-bleached part of the dose distributions it is very important that the assigned uncertainties are appropriate (see section 3.4.4.2).

3.4. Luminescence characteristics

3.4.1. Decay curves and dose response curves

Figure 3.3a shows a representative OSL decay curve from samples measured using multi-grain (~30 grains) aliquots, together with the decay curve from an aliquot of calibration quartz (known to be dominated by the fast component). The summation limits employed in the dose estimation are also shown.

The natural OSL signal decays to half its initial value in ~0.14 s and reaches background level in ~ 0.8 s; it is clearly dominated by the fast component. The average multi-grain test dose intensity is 700 ± 120 counts/Gy. The inset in Figure 3.3a shows a typical dose response curve from multi-grain aliquots, fitted with a linear function. The corresponding data using single grain measurements are shown in Figure 3.3b. In this case the dose response curve has been fitted using a saturating exponential function but the natural signal generally falls in the linear part of the dose response curves. The shapes of the single grain OSL decay curves vary significantly from grain to grain. The average test dose intensity is 400 ± 100 counts/Gy from accepted grains. No significant differences in terms of luminescence characteristics have been observed among the samples investigated here.

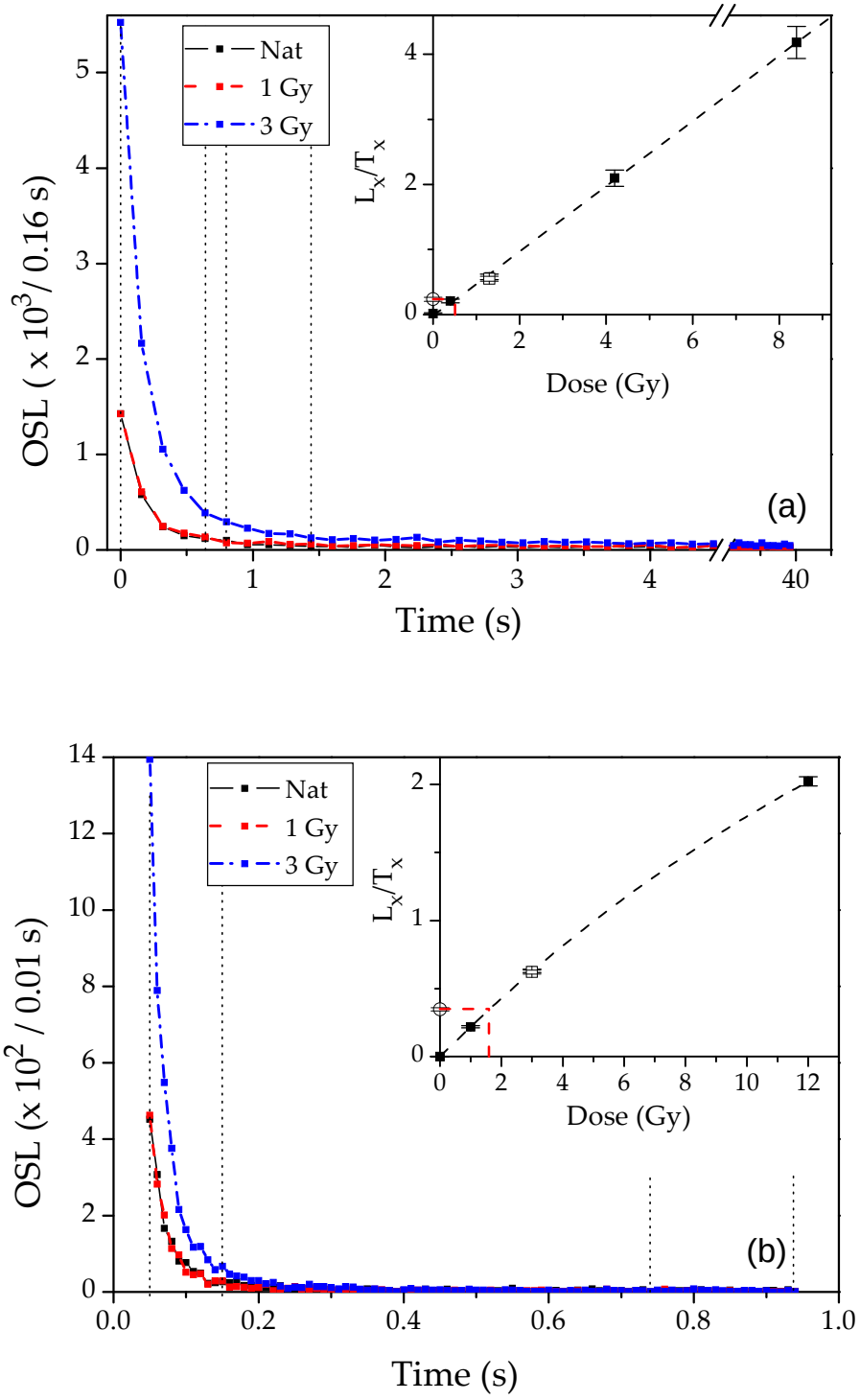

Figure 3.3. (a) OSL decay curve of natural and first and second regenerative dose points of a multigrain aliquot and the summation limits used. Inset shows the growth curve linear fitted obtained from multigrain aliquots of sample T-31; (b) OSL decay curve of natural and first and second regenerative dose points and the corresponding summation limits used. Inset shows the dose response curve fitted with a saturating exponential function for single grains of sample T-26.

3.4.2. Cumulative light summation

There is a very large variability in the intensity of the luminescence signal coming from different grains, even when they belong to the same sample and have been given identical doses. An easy way to analyse determine the contribution of grains to the luminescence signal in terms of its intensity it is to rank the grains (from a single grain measurement) in order of descending brightness and plot the cumulative light sum as a function of the proportion of grains involved. If all grains were contributing with the same intensity, then the proportion of grains contributing and the brightness would be directly proportional to each other (Duller and Murray, 2000). But this behaviour is generally not observed in natural samples where only a small percentage of the measured grains give most of the light and many of the grains have negligible contributions.

The analysis of the cumulative light sum is highly advantageous as it gives estimation on the fraction of the sample to be expected to contribute to the luminescence signal and giving an idea of what kind of behaviour could be expected from a multi-grain aliquot. A significant proportion of grains with detectable signals is not taken into account in single grain analysis due to the selection criteria (see section 2.7) but will contribute to the light measured from multi-grain aliquots. In the cumulative light sum all measured grains, including those that would be rejected by the selection criteria, contribute.

The cumulative light sum as a function of the proportion of grains for sample T-26 for both the natural and the second regeneration dose (3 Gy) is shown in Figure 3.4. 80% of the light sum is derived from less than 12% of the grains and ~60% of the grains do not contribute significantly to the total detected signal, providing less than 10% of the light sum. This results are consistent with previous cumulative light sum studies (Duller *et al*., 2000; Jacobs *et al*., 2003) concluding that 5-10% of the grains or less from a sample provide 90-95% of the luminescence signal emitted.

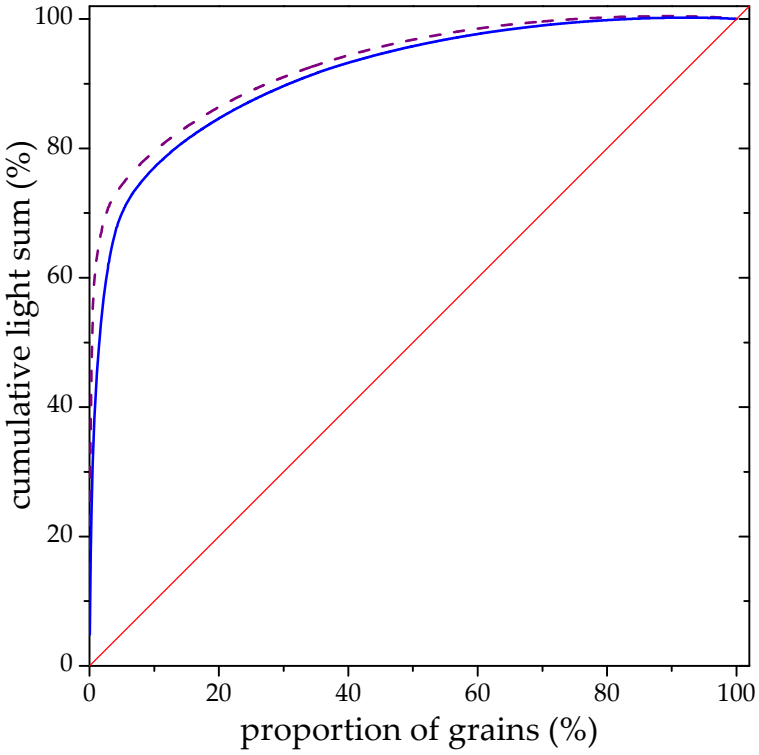

Figure 3.4. The cumulative light sum for the natural (dashed purple line) and second regeneration dose (solid blue line) of sample T-26.

A high percentage of the rejected grains (see selection criteria in section 2.7), therefore excluded from the burial dose estimation, have detectable signals. These grains will not contribute in the single grains analysis but their detectable signal will contribute if they are measured in a multi-grain aliquot. Taking into account that all grains with detectable signal contribute in a multi-grain aliquot, the percentage is low enough to assume that among the small (~30 grains) multi-grain aliquots used for this study, the light from a number of them will be derived from only one or two grains and then behaving like single grains.

Then part of them will have some will have the contribution of incompletely bleached grains but it can be expected that a number of the multi-grain aliquots will show a signal derived only from well bleached grains.

3.4.3. Thermal behaviour

3.4.3.1. Preheat plateau

In a preheat plateau test a natural sample is measured using different preheats to evaluate how sensitive the dose estimate is to choice in preheat temperature. For relatively old (e.g. older than 5000 years) samples consisting of quartz with good luminescence characteristics, the dose estimate is normally relatively insensitive to the choice of preheat temperature.

To select an appropriate thermal treatment, preheat plateau tests on multi-grain aliquots were measured on samples T-23 and T-39. For young samples one might *a priori* expect to observe an increase in dose as a function of preheat temperature because of thermal transfer of charge from light insensitive traps to light sensitive traps (e.g. Rhodes 2000, Murray and Olley, 2002). However, for these samples the average dose appears to be independent of preheat temperature up to a preheat of 300°C (Figure 3.5a). Each point displays the average and standard error of six individual dose estimates. The cutheat temperature was always 20°C less than the chosen preheat temperature. Based on these measurements, any preheat temperature below 300°C would be appropriate.

3.4.3.2. Thermal transfer

Thermal transfer was assessed by bleaching 48 fresh multi-grain aliquots of samples T-17, T-26 and T-39 in a daylight simulator (Hönle SOL 2) at a distance of 80 cm from the lamp for two hours prior to measurement. The results are shown in Figure 3.5b; each point is the average and standard error of six individual dose estimates. For preheat temperatures less than 220°C the CAM_{tr} average is consistent with zero; even at a preheat temperature of 300°C the measured dose is only ~0.25 Gy. Figure 3.5c shows the CAM_{tr} doses from similar thermal transfer experiments measured on single grains. A total of 1500 single grains of sample T-30 were measured using preheat temperatures varying between 160 and 260°C. For this sample the initial bleach was done in the reader using two blue light exposures at room temperature for 40 s with an intervening

pause of 10,000 s. The CAM_{tr} doses for this sample vary between -2 ± 8 mGy to 76 ± 25 mGy for the preheat temperature range considered here. Based on these measurements and the results of the preheat plateau test a preheat temperature of 200°C and a cutheat temperature of 180°C are chosen; this combination is commonly used for dating young samples (e.g. Madsen *et al*., 2007; Hu *et al*., 2010).

Finally, 2400 grains of sample T-39 were bleached under the daylight simulator for 2 hours and measured at a preheat temperature of 200°C. From those, 57 grains were accepted into the dose distribution (see inset to Figure 3.5c), which appear to be symmetric around the weighted mean dose of 16 ± 7 mGy. This weighted dose is consistent with that of sample T-30 measured at a preheat temperature of 200°C (12 ± 10 mGy, n=27). Combining the results from all the bleached single grains measured at a preheat temperature of 200°C, a weighted average of 15 ± 6 mGy (n = 84) is obtained; it corresponds to a residual age of 16 ± 6 years (using average dose rates for these two samples). This value is small and may not be significantly different from zero. It can be concluded that thermal transfer is negligible in these samples when using a preheat and cutheat temperature of 200°C and 180°C, respectively, thus this thermal treatment appears to be appropriate for these samples.

3.4.4. Dose recovery

3.4.4.1. Dose recovery test

Dose recovery tests have been carried out to investigate if a known dose given prior to any thermal treatment can be recovered accurately. Dose recovery tests on both multi-grain aliquots (samples T-17, T-30 and T-39) and single grains (sample T-39) using a preheat temperature of 200°C and a cutheat of 180°C have been measured. In these experiments all samples were bleached for two hours in the daylight simulator prior to dosing.

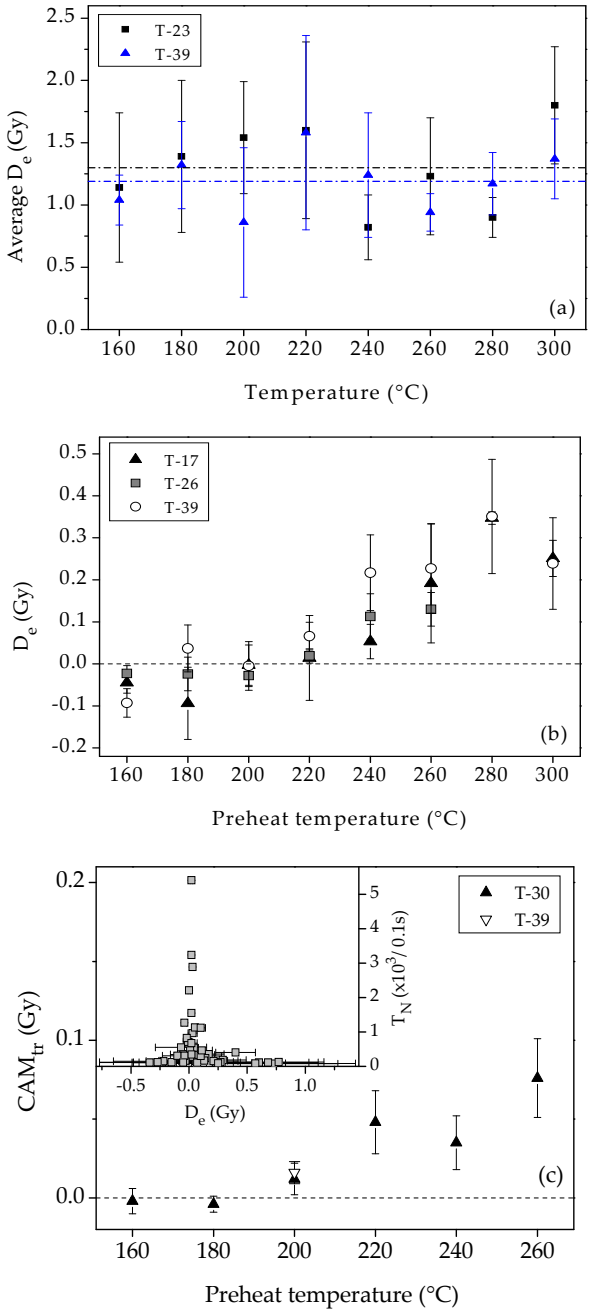

Figure 3.5. (a) Preheat plateau test carried out using multi-grain aliquots of samples T-23 and T-39. Points correspond to the average of 6 measured aliquots for each temperature. The cutheat temperature was 20°C less than the applied preheat temperature. All values are consistent with the mean within 2 standard errors showing no significant differences at increasing temperatures; (b) Thermal transfer test measured on 48 laboratory bleached aliquots of samples T-17, T-26 and T-39. Individual points correspond to the average of 6 results for each temperature. Thermal transfer only appears to become significant for temperatures above 240°C; (c) CAM_{tr} results from thermal transfer laboratory blue light bleached single grains from sample T-30 (upright triangles). The dose derived from solar simulator bleached single grains of sample T-39 using a preheat temperature of 200°C (downright open triangle) is also shown. 28-32 single grains are contributing to the CAM_{tr} values of sample T-30 and 57 single grains from sample T-39. Inset shows the dose distribution of sample T-39.

In one set of experiments, seven bleached multi-grain aliquots from each of the three samples were given an *in situ* beta dose (given in the reader) of 2 Gy. The dose recovery ratios (i.e. measured to given dose) were 0.91 ± 0.07, 0.99 ± 0.04 and 0.90 ± 0.02 for samples T-17, T-30 and T-39, respectively. Combining the results from the three samples, an average weighted dose recovery ratio of 0.93 ± 0.03 (n=21) and an over-dispersion value of 4 ± 4 % was obtained. The uncertainties assigned to individual aliquots are based on counting statistics and curve errors). If instrument reproducibility (~2.5% per dose estimate; e.g. Thomsen *et al*., 2005) is taken into account, the calculated over-dispersion would reduce to ~3 ± 4 %.

In a second experiment, 1,000 single grains of the bleached portion of sample T-39 were measured after being dosed *in situ* with 2 Gy. The dose recovery ratio was 0.98 ± 0.09 (n=18) with an over-dispersion of 16 ± 8 %. The uncertainties assigned to individual dose estimates are based on counting statistics and curve fitting errors. If instrument reproducibility (~5% per dose estimate; e.g. Thomsen *et al*., 2005) is taken into account, this calculated over-dispersion would reduce to ~15 ± 8 %. Whether this data set is indeed over-dispersed it is difficult to determine based on the few data points accepted into the dose distribution.

3.4.4.2. Assigning uncertainties to individual dose points

The uncertainty on a dose estimate is usually based on counting statistics, curve fitting errors and an additional source of uncertainty to account for instrument reproducibility (e.g. Duller *et al*., 2000). The over-dispersion observed in natural samples is often attributed to the combination of these intrinsic factors together with extrinsic factors such as incomplete bleaching and beta dose heterogeneity. Following this, the uncertainties based on intrinsic sources should be sufficient to explain the observed variability in a bleached sample, in which extrinsic sources of variability have been eliminated, but it has been reported (Reimann *et al*., 2012; Sim *et al*., 2012; Thomsen *et al*., 2005, 2007, 2012) that more intrinsic factors are contributing to the over-dispersion of the dose distributions. To evaluate the contribution from intrinsic factors to the observed variability, dose recovery tests have been carried out on "ideal"

samples, which initially were bleached in the laboratory to eliminate their natural signal and then gamma irradiated with 2 Gy prior to luminescence measurement. Sample T-39 was used for this test. The dose recovery ratio for this sample was 1.07 ± 0.03 (n=48) with an over-dispersion of 7 ± 4 % (no instrument reproducibility taken into account). The over-dispersion derived from this experiment is consistent with that derived from the beta dose recovery experiment.

The bleached and gamma irradiated portion of sample T-39 was also measured using single grains. 3,200 single grains were measured, 66 of which passed the rejection criteria outlined in section 2.7. These gave a weighted dose recovery ratio of 0.98 ± 0.04 (n=66) with an over-dispersion value of 22 ± 5 %. If instrument reproducibility is taken into account, this over-dispersion value reduces to ~21.4 ± 4 %.

From the gamma dose recovery experiments it would appear that assigning uncertainties based on counting statistics, curve fitting errors and instrument reproducibility alone is insufficient to describe the observed variability. A similar conclusion has previously been reached by Reimann *et al*. (2012), Sim *et al*. (2012) and Thomsen *et al*. (2005; 2007; 2012).

Gamma dose recovery test results were used to determine the absolute over-dispersion (OD_{abs}) as a function of the equivalent doses estimated deriving in $OD_{abs} = 0.072.D_e + 0.005$ and $OD_{abs} = 0.20.D_e + 0.02$ for multi-grain and single grains distributions, respectively. For all measurements we add in quadrature an additional uncertainty (additional to that calculated from counting statistics and curve fitting errors) of 7% and 22%, respectively. Thus, it would appear that in order to describe the variability observed from intrinsic factors we must add (in quadrature) an additional uncertainty (additional to that calculated from counting statistics and curve fitting errors) of ~ 7% to the uncertainties assigned to multi-grain dose estimates and ~22% to single grain uncertainties. This additional uncertainty is added to account for the variability in measured dose distributions arising from additional intrinsic factors; we regard this as a minimum uncertainty. If extrinsic sources of variability (e.g. small scale beta dose heterogeneity) contribute significantly to the spread in the well-bleached part of the

dose distributions then, this additional intrinsic uncertainty (7% for small aliquots and 22% for single grains) is likely to underestimate the actual variability in a well-bleached dose distribution.

3.4.5. Effect of beta source inhomogeneity

As described in section 2.5.1 any spatial variation in the dose rate provided by the in-built beta source may affect the measured single grain dose distributions. Here it is investigated if the dose rate from the beta sources used in this work is significantly inhomogeneous. To assess the effect of beta dose rate inhomogeneity on dose distributions, a bleached and gamma dosed sample has been used in order to assure that all the grains were bleached and dosed to the same degree.

Although the correction matrix has been used in all cases prior to any calculation with the measured data, the effect the source inhomogeneity could have in a natural sample has been tested. The uncorrected over-dispersion and individual CAM_{tr} dose estimates as a function of the corresponding corrected ones are shown in Figure 3.6. As expected, the values are indistinguishable since other sources of variability are contributing in the dose distribution in a natural sample and thus the effect of the inhomogeneity is within the observed variability.

This source inhomogeneity must contribute to the intrinsic over-dispersion identified in the previous section; the size of this contribution can be determined by analysing a bleached and gamma dosed sample with and without correction for inhomogeneity. The observed OD is 29 ± 6 % without correction for inhomogeneity and this decreases to 22 ± 5 % when the correction is employed, suggesting that beta source homogeneity contributes ~20 ± 5 % to the observed over-dispersion.

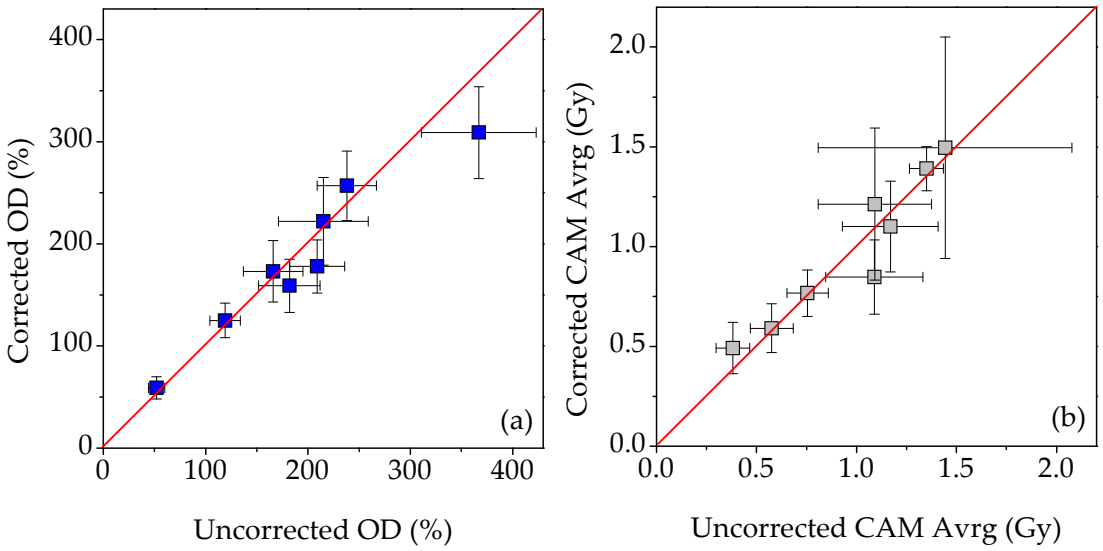

Figure 3.6. Comparison of (a) over-dispersion and (b) equivalent doses from data corrected and without correction for source anisotropy.

3.5. Dose estimations

3.5.1. Single grain results

Between 3000 and 5000 grains of each sample were measured resulting in 80-100 dose estimates per sample passing the rejection criteria described in section 2.7. Natural dose distributions showing the OSL response from the natural test dose as a function of the measured dose are shown in Figure 3.7. All dose distributions appear to be positively skewed with a minimum dose edge possibly indicating the presence of incomplete bleaching. Simple visual inspection of the dose distributions suggests that more than 60% of all grains may belong to single dose distributions located towards the low end of the observed values.

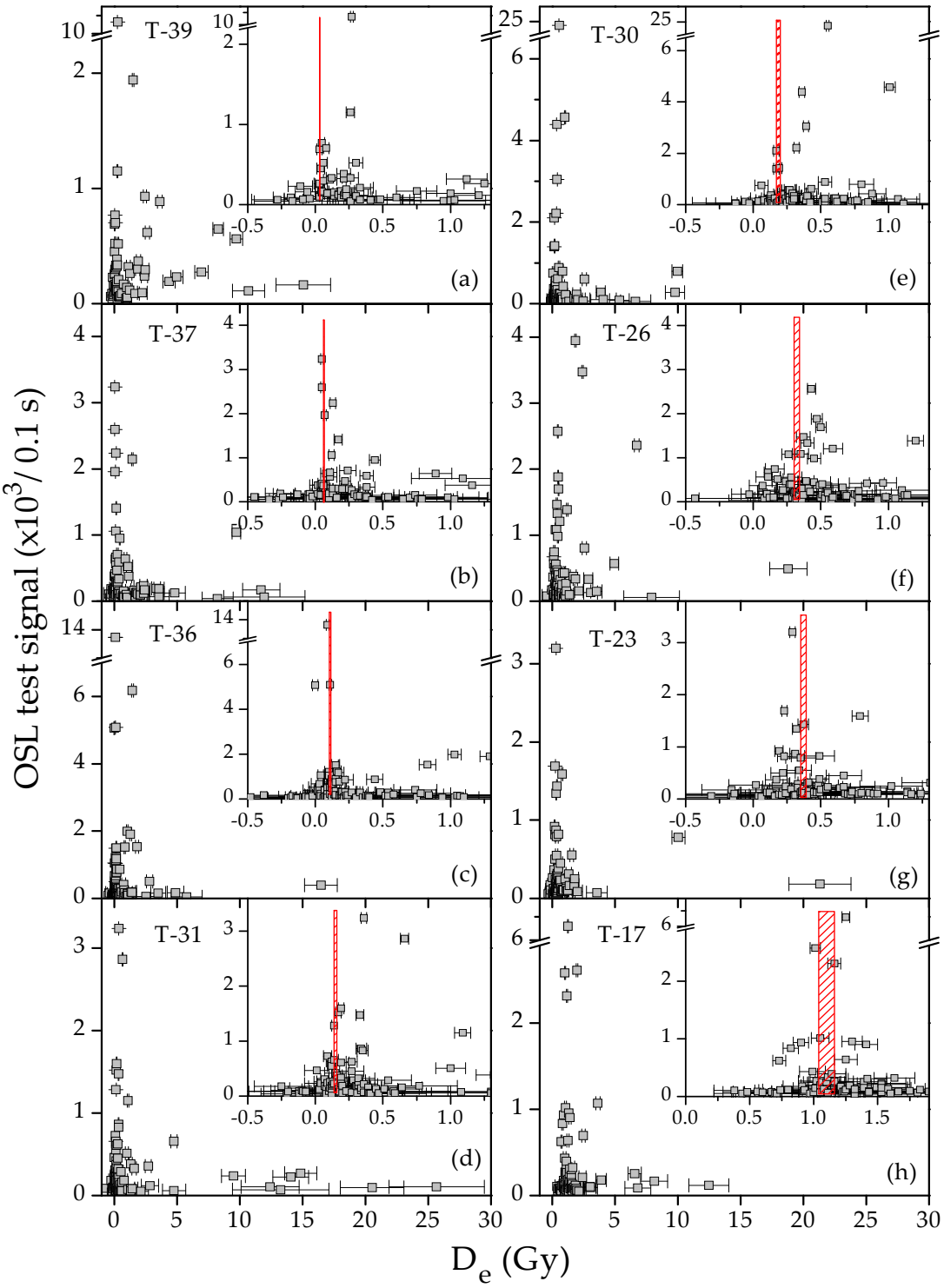

Figure 3.7. Single grain dose distributions from the eight samples measured using the SAR protocol. The signal of the natural test dose is shown as a function of measured dose. The insets show the same data from doses less than 1.3 Gy except for T-17 where doses less than 1.9 Gy are displayed. The expected doses are shown with a vertical red line/bar. These are the doses derived from the known ages. Associated error comes from the uncertainty of annual dose rate used for the conversion.

3.5.1.1. Effect of the chosen background summation limits

As discussed in section 2.7, a late background (LBG) subtraction has been used to obtain the net OSL signal from single grains; this is in contrast to the use of an early background, EBG, usually expected to minimise any effects of slower components on the net signal (Cunningham and Wallinga, 2010). A comparison of the results using EBG and LBG has been done on single grains from sample T-31. Using EBG, 2.2% of the measured grains were accepted, giving a CAM_{tr} burial dose and over-dispersion of 1.5 ± 0.6 Gy and 300 ± 50%, respectively. Estimating minimum burial doses using IEU gives 0.15 ± 0.01 Gy (n = 49). The use of LBG results in the acceptance of 3.1% of the grains, giving a CAM_{tr} burial dose of 1.6 ± 0.5 Gy and over-dispersion of 280 ± 30 %. Using IEU on this dose distribution gives a minimum burial dose of 0.13 ± 0.01 Gy (n = 54). Thus, there appears to be no significant difference between the estimated burial doses using either EBG or LBG for single grains, consistent with the results reported by Reimann *et al*., 2012 (Figure 3.8a). The over-dispersion of the dose distributions using both EBG and LBG has been calculated for all eight samples (Figure 3.8b). Again no significant differences in the ODs are observed although there is a slight systematic tendency for lower OD values when using LBG. More importantly, EBG results in a significant reduction in the number of accepted grains. Thus for these samples, it would appear that using LBG gives rise to a larger data set with no detectable cost in data quality.

3.5.1.2. Single-grains burial dose estimates

Burial doses have been estimated as detailed in section 3.3. As a first approach to burial dose estimation we calculate a simple unweighted average dose including all dose points. Such a simple approach leads to an average over-estimation of the expected dose of ~1 Gy, n = 8 (see Table 3.2), consistent with the range of values given in many reports of residual doses in modern water-lain deposits (see recent summary in Murray *et al*., 2012).

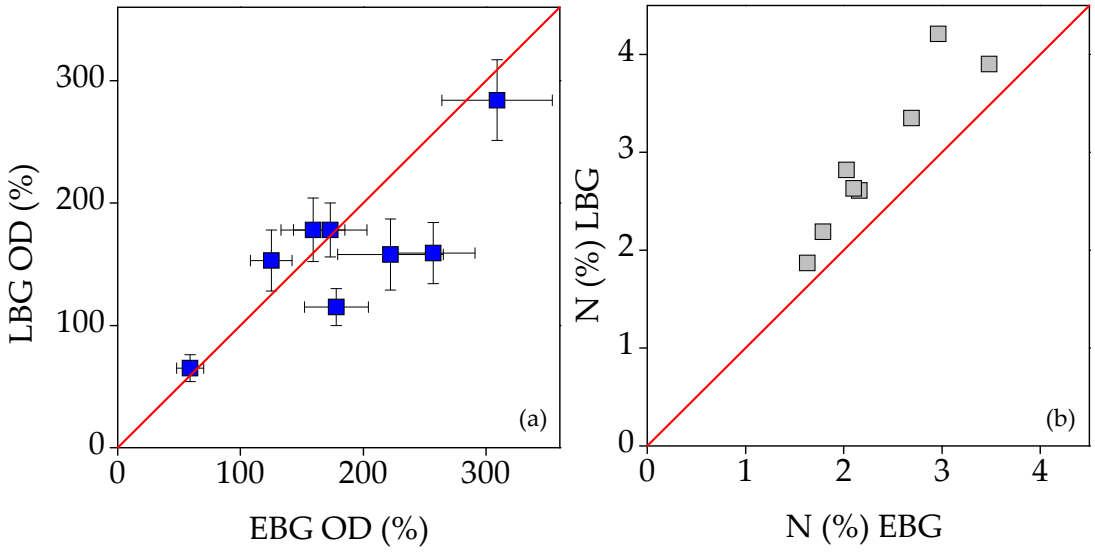

Figure 3.8. Comparison of (a) over-dispersion and (b) number of grains accepted from data using Early Background (EBG) and Late Background (LBG) subtraction.

In an attempt to improve this simple average, extreme outliers were eliminated following the 1.5*IQR criterion described in section 3.3; because of the shape of the dose distributions of these samples, all outliers identified following this criterion belong to higher dose region of the distributions and no low dose values were excluded from the calculation. The average overestimate compared to expected doses is reduced from ~1 Gy to ~0.15 Gy. Samples T-36, T-23 and T-17 now give results consistent with the expected doses within two standard deviations. The remaining samples overestimate the expected doses, with the largest overestimates for the two youngest samples (T-39 and T-37) of ~0.3 Gy. Thus, although the interquartile range criterion is not based on any physical process model, it provides a significantly better-constrained estimate of the upper dose limit to the burial dose estimate than the simple average.

The next step was to derive weighted mean equivalent doses using the CAM model on the exponentially transformed data, CAM_{tr}. Again the doses overestimate the expected values, by ~0.9 Gy on average. Clearly, the dose overestimates do not arise simply because of large, poorly known dose values.

		T-39	T-37	T-36	T-31	T-30	T-26	T-23	T-17
	Expected (Gy)	0.033 ± 0.002	0.062 ± 0.003	0.109 ± 0.006	0.15 ± 0.01	0.18 ± 0.01	0.32 ± 0.02	0.37 ± 0.02	1.10 ± 0.12
Multi-grain aliquots (SA)	Average	3.8 ± 0.8	3.7 ± 0.6	1.4 ± 0.3	1.3 ± 0.4	5.0 ± 1.3	3.6 ± 0.5	3.9 ± 1.2	4.9 ± 0.6
	Total # aliquots	90	87	80	94	79	86	95	83
	Robust avrg	1.7 ± 0.2	1.9 ± 0.2	0.63 ± 0.07	0.52 ± 0.05	1.2 ± 0.2	1.8 ± 0.2	0.73 ± 0.06	3.5 ± 0.3
	aliq incl. (%)	74	87	86	82	81	83	80	88
	CAMtr	3.5 ± 0.7	3.5 ± 0.5	1.2 ± 0.2	1.3 ± 0.3	5.1 ± 1.2	3.4 ± 0.5	3.0 ± 0.7	3.7 ± 0.3
	OD (%)	176 ± 19	139 ± 17	145 ± 20	245 ± 29	207 ± 25	126 ± 15	234 ± 29	67 ± 11
	MAMtr	0.26 ± 0.03	0.35 ± 0.06	0.19 ± 0.02	0.27 ± 0.02	0.37 ± 0.03	0.47 ± 0.03	0.46 ± 0.02	1.02 ± 0.26
	aliq incl. (%)	43	16	47	58	52	24	58	17
	IEU	0.06 ± 0.04	0.24 ± 0.03	0.11 ± 0.01	0.16 ± 0.01	0.27 ± 0.02	0.36 ± 0.02	0.37 ± 0.02	1.10 ± 0.09
	aliq incl. (%)	12	6	21	27	23	10	35	25
Single-grains (SG)	Average	1.4 ± 0.3	1.1 ± 0.3	0.6 ± 0.2	1.9 ± 0.6	0.9 ± 0.2	1.1 ± 0.3	0.9 ± 0.3	1.7 ± 0.2
	Total # grains	71	87	111	101	92	82	81	79
	Robust avrg	0.38 ± 0.07	0.36 ± 0.06	0.14 ± 0.02	0.21 ± 0.02	0.34 ± 0.03	0.48 ± 0.03	0.39 ± 0.03	1.20 ± 0.05
	grains incl. (%)	89	83	77	78	83	84	91	92
	CAMtr	1.2 ± 0.3	1.5 ± 0.2	0.36 ± 0.06	1.6 ± 0.5	0.8 ± 0.2	1.0 ± 0.2	0.68 ± 0.12	1.53 ± 0.12
	OD (%)	179 ± 25	115 ± 15	158 ± 29	284 ± 33	178 ± 22	153 ± 25	159 ± 25	65 11
	MAMtr	0.15 ± 0.04	0.23 ± 0.05	0.17 ± 0.03	0.22 ± 0.03	0.32 ± 0.03	0.41 ± 0.04	0.40 ± 0.03	1.11 ± 0.04
	grains incl. (%)	68	46	88	83	83	79	91	82
	IEU	0.057 ± 0.012	0.07 ± 0.02	0.098 ± 0.010	0.134 ± 0.012	0.201 ± 0.010	0.28 ± 0.02	0.34 ± 0.02	1.08 ± 0.04
	grains incl. (%)	38	21	70	53	53	46	77	75

Table 3.2. Equivalent doses estimated using descriptive statistics (simple unweighted average), robust statistics, CAM_{tr} and the corresponding over-dispersion, MAM_{tr} and IEU and the proportion of grains included in each approach. The expected dose (Gy) is also given for each sample. Values from both single grains (SG) and multi-grain small aliquots (SA) are summarized

These three estimates include all dose points in the distributions; one would expect these results to significantly overestimate the true burial dose in the presence of significant incomplete bleaching. It is not surprising that these methods over-estimate given the depositional environment; the shapes of the dose distributions support the expectation of at least some incomplete bleaching. For these very young samples an overestimation of ~1 Gy is unacceptable but it is important to note that such an overestimation would be trivial for older samples (e.g. > 10 ka).

We next apply the IEU and the MAM models (the latter using exponentially transformed data, see section 3.3, since distributions from all samples, except T-17, contain non-positive dose estimates). All dose estimates have an additional uncertainty of 22% added onto the uncertainty calculated from counting statistics and curve fitting errors (see section 3.4.4.2) to account for intrinsic sources of uncertainty including instrument reproducibility. Furthermore, all data sets have been corrected for beta source inhomogeneity.

MAM_{tr} results in estimates within three standard errors (sample T-26) and one standard error (samples T-23 and T-17) of the known values for the three oldest samples (> 350 years) but shows poor agreement for the other five.

The IEU approach has also been tested. For the IEU approach it is considered that the over-dispersion is not constant but dependent on the dose. The variation of over-dispersion as a function of dose is assigned by the slope and intercept of the fit linear between known values of over-dispersion and dose. The OD obtained for the gamma irradiated sample with a known dose of 2 Gy and the value for a bleached sample distribution are use to determine the dependence. For single grains of these samples it is given by the relation $OD_{abs}(Gy) = 0.207.\overline{D} + 0.021$.

The IEU doses are in good agreement with all predicted doses; the estimates are within one standard error for four of the eight samples (T-37, T-36, T-31 and T-17) and within two standard errors for the other four. This confirms that the identification of the well bleached fraction based on the gamma dose recovery over-dispersion is appropriate.

Burial doses estimated using the different approaches are summarized in Table 3.2, together with the proportion of grains making up the well bleached part of each dose

distribution. The estimated doses plotted against the expected values are shown in Figure 3.9 (a).

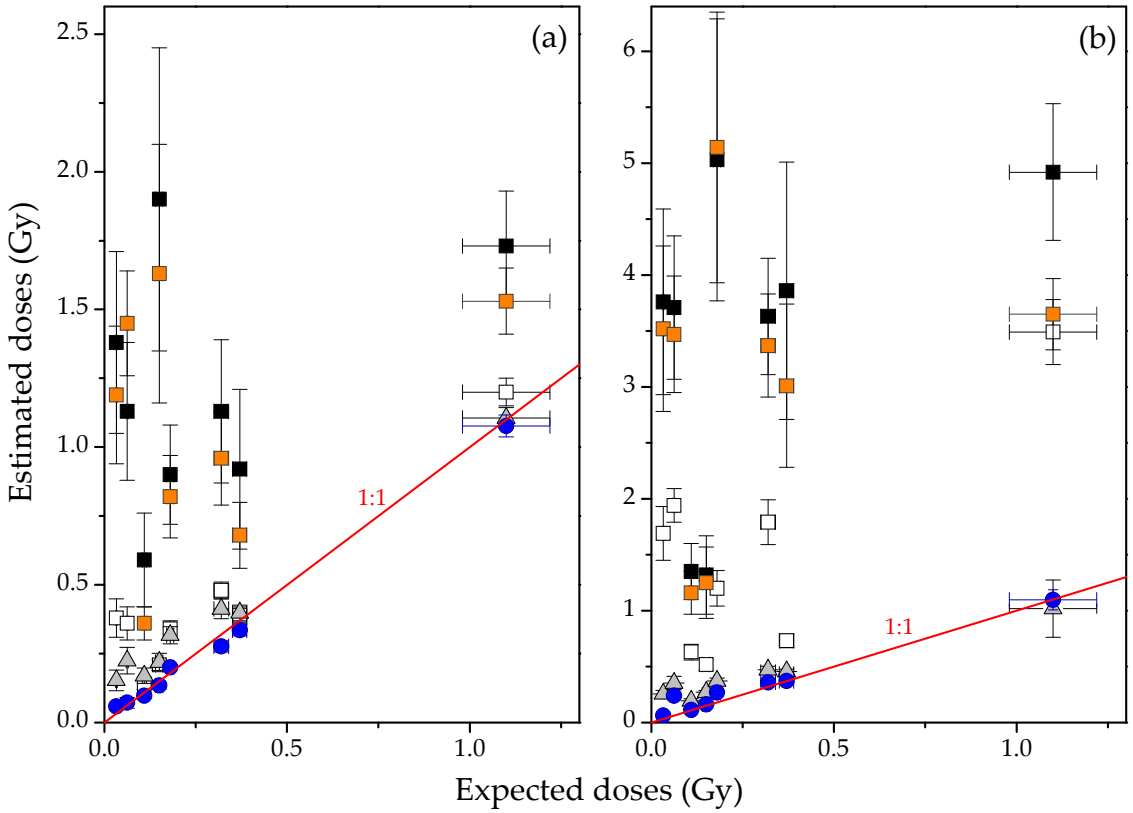

Figure 3.9. Estimated doses using (a) single grains and (b) multi-grain aliquots versus expected doses. Doses have been estimated with simple average (black squares), robust average (open squares), CAM_{tr} (orange square), MAM_{tr} (gray triangles) and IEU (blue circles). The 1:1 line is also shown. Legend is common for the two plots.

3.5.2. Multi-grain results

3.5.2.1. Natural multi-grain dose distributions

Between 80 and 100 multi-grain aliquots (each ~30 grains) were measured for each sample. Laboratory dose recovery tests gave an OD of 7 ± 4 % (n = 48; see section 3.4.4.2) and so we add an additional uncertainty of 7% to individual dose estimates to

account for intrinsic sources of variability. Observed natural dose distributions and the corresponding expected doses are shown in Figure 3.10. All distributions appear to be positively skewed and include a number of dose values significantly higher than those expected. Sample T-37 is unusual, in that even the leading dose edge seems to be off-set to higher doses compared to the expected dose. This observation is consistent with the single grain IEU analysis (see Table 3.2) which concluded that T-37 was the most poorly bleached sample with less than 20% of the grains being well-bleached (see section 3.5.1.2).

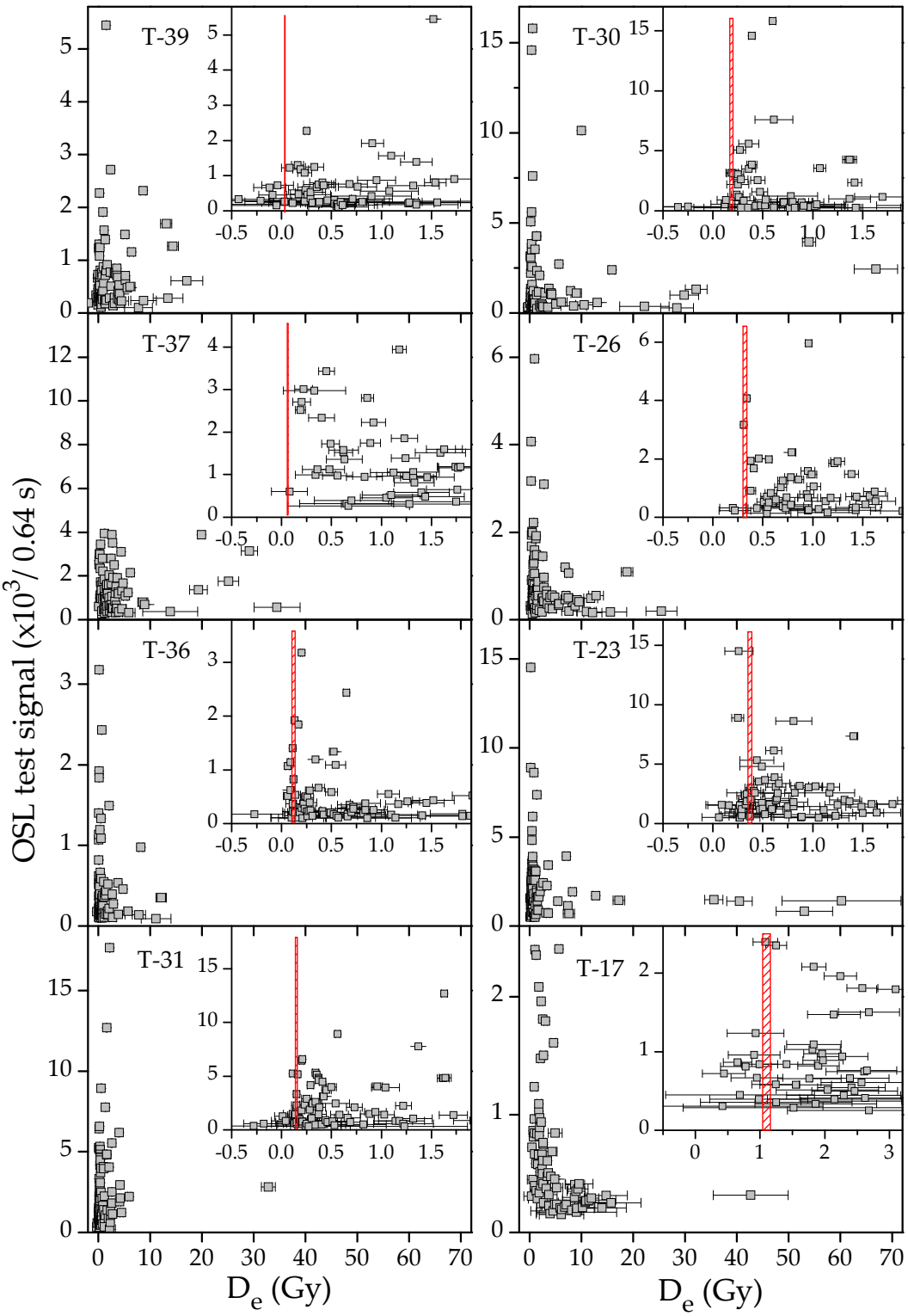

Figure 3.10. Multi-grain aliquot dose distributions from the eight samples measured using the SAR protocol. The signal of the natural test dose is plotted as a function of the measured dose. The insets show the same data from doses less than 1.8 Gy except for T-17 where doses less than 3.2 Gy are displayed. The expected doses are shown with a vertical red line/bar.

3.5.2.2. Multi-grain burial dose estimates

The over-dispersion values for the natural samples are very similar to those determined for the single grain dose distributions (see Table 3.2). The simple averages, as well as the CAM_{tr}, overestimate the expected dose by ~3 Gy on average. This confirms that if all data points are included in the burial dose estimates, then there will be a large contribution from incompletely bleached grains. The cumulative natural light sum from single grain data (section 3.4.2) shows that 80% of the total light is derived from less than 12% of the grains. Then the total light of a multi-grain aliquot of ~30 grains must be dominated by the light from ~3.5 grains. In addition IEU results from single grains indicate that 40-70% of the grains from the samples (except T-37) are well bleached. Thus, it is to be anticipated that the signal from a number of multi-grain aliquots will only be derived from well-bleached grains. Although it can usually be argued that it is inappropriate to apply statistical age models to multi-grain data sets, in this case, given the conclusion from the cumulative light sum, we analyse the multi-grain aliquot data set in the same manner as the single grain data.

The ratio of the MAM_{tr} dose and the expected dose is consistent within two standard errors of unity for the two oldest samples (T-23 and T-17) but there is poor agreement for the other six. These ratios vary from 7.8 ± 0.7 to 0.9 ± 0.1.

Results from small multi-grain aliquots in combination with the IEU approach are within one standard deviation of the expected values for six of the eight samples, but the agreement for samples T-37 and T-30 is poor. The ratios of estimated to expected doses vary from 3.9 ± 0.5 to 1.0 ± 0.1.

For the extreme case of T-37 (i.e. > 80% of the accepted grains are incompletely bleached), the presence of a large number of grains with a significant residual dose prevents accurate analysis by any of the statistical analyses used here. Estimated doses with each approach are compared with the expected ones (Figure 3.9 (b)).

3.6. **Discussion**

The aim of this study is to explore the most suitable methods for burial dose estimation for flash-flood deposits. We consider our age control (radiocarbon and historical records) sufficiently reliable to allow us to assign calendar ages to individual flood events (Benito *et al*., 2010), and so derive expected equivalent doses. A number of studies have addressed the OSL dating of individual flood layer, most of them from large fluvial catchments (e.g. Grodek *et al*., submitted). In small basins (< 500 km^2) incomplete bleaching of sediments transported by flash-floods over short distances is to be expected. Our sediments were deposited by short-lived flash floods; nevertheless the residual doses are small, and comparable with other reports of residuals in modern river sediments, including non-flood deposits. Presumably our materials were mainly bleached before final transport by the flash flood which deposited the sediment.

The approaches which include all dose points in the estimation (simple average and CAM_{tr}) overestimate the expected age significantly confirming the suggestion that some grains with significant residual dose are contributing, as expected for this type of sediments. Nevertheless, the observation that the estimates from robust statistics are close to the expected ages for three of the samples (T-36, T-23 and T-17) may indicate that incomplete bleaching is not a significant problem in these cases. This is also consistent with the results from the IEU minimum dose approach which identifies these three samples to be the ones with largest well-bleached populations, including 70%, 77% and 75% of the grains, respectively. Thus, it can be concluded that for a small percentage of incompletely bleached grains (< 30%), elimination of outliers from the single grain dose distribution is an appropriate approach to estimate accurate ages avoiding the use of more complex statistical analysis.

Since the rest of the samples contain a higher proportion of incompletely bleached grains in their dose distributions, minimum age models, MAM and IEU, were used. The dose distributions from these young samples contain non-positive dose estimates which prevent the direct use of MAM due to its log-normal assumption. This problem

has easily being overcome by using an exponential transformation of the data (and then using the original scripts written by Galbraith *et al*.). When the program has been used on exponentially transformed data they were termed MAM_{tr}. Nevertheless, MAM_{tr} estimates are consistent with the expected ages only for the three oldest samples (> 350 years), in contrast with previously published results (Arnold et al., 2009), concluding that the MAM_{UL} was providing the most accurate estimates for samples younger than 350 years old.

To confirm that ages estimated with MAM_{tr} can be directly compared with any other published results in which estimates were obtained using MAM_{UL}, burial dose for all samples has been calculated with both variations of the original MAM (MAM_{UL} and MAM_{tr}) with identical results.

Burial doses have also been estimated using small multi-grain (~30 grains) aliquots despite the expectation that samples were incompletely bleached. According to the cumulative-light sum data, a large number of the grains contained in our small aliquots will contribute very little to the luminescence signal, thus at least some of the aliquots can be expected to behave like single grains. As in the case of "real" single grains, aliquots with a significant residual dose contribution should be identified and excluded from the estimation in order to obtain accurate ages. Both minimum age models used previously (MAM_{tr} and IEU) have also been used to estimate the burial dose from multi-grain dose distributions. MAM_{tr} results in consistent ages with the known ages only for the two oldest samples.

IEU successfully identifies the aliquots with contributions from incompletely bleached grains and derives consistent estimates for six of the eight samples. Only the ages of the two youngest samples (T-39 and T-37, 40 and 70 years old, respectively) are overestimated.

However, as stated in section 3.4.4.2 it is possible that the uncertainties assigned based on the OD values determined in the gamma dose recovery experiment (22%) are too small to describe the variability in the well bleached part of the natural dose distribution. In the following it is investigate how sensitive the estimated MAM_{tr} burial

doses are to the size of the assigned uncertainty ranging from 5% to 50% using samples T-39 and T-31.

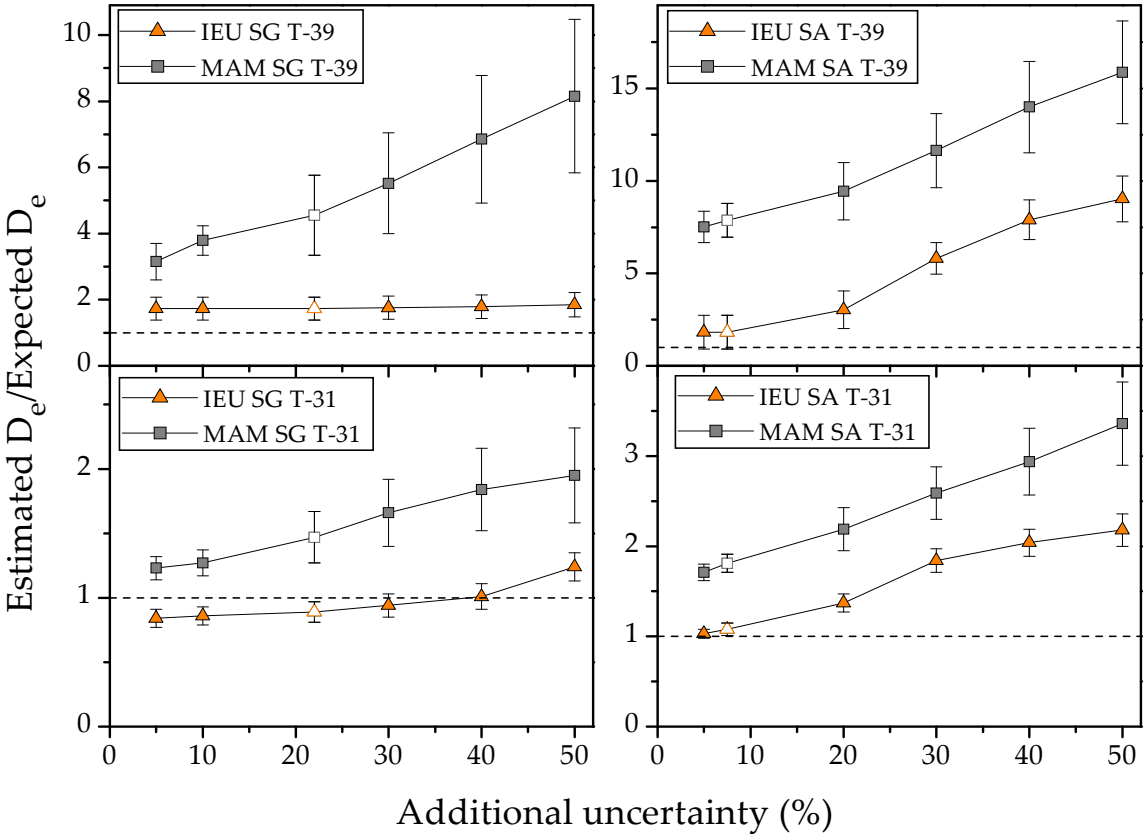

Figure 3.11. Effect of extra uncertainty added to data points on the dose estimates. Values varying from 5% to 50% were used for analysis of single grain and multi-grain dose distribution from samples T-39 and T-31. The corresponding doses were estimated with MAM_{tr} and IEU. The ratio between dose estimates and the expected doses was plotted as a function of the extra uncertainty added. Unity is shown in dashes line. The extra uncertainty values used for the final estimates are shown in open icon.

Figure 3.11 shows that for these two samples, the MAM_{tr} model overestimates the expected doses even for the lowest additional intrinsic OD tested (5%), even though the intrinsic OD must certainly be considerably greater than this.

As it has been done for the estimated MAM_{tr} burial doses, the effect of the over-dispersion assigned to the distribution on those burial dose estimates obtained with

IEU approach, has been studied adding an additional uncertainty varying from 5 to 50%. The OD as a function of the dose have been firstly plotted (Figure 3.12) for each additional uncertainty obtaining the corresponding slope (a) and intercept (b) (Table 3.3).

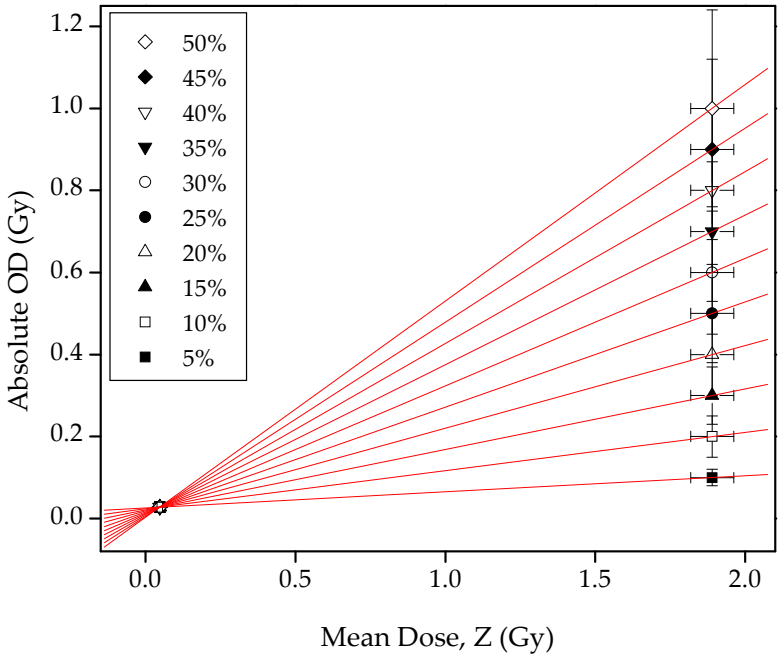

Figure 3.12. Absolute over-dispersion as a function of the mean dose providing the intercept and slope of a series of OD percentages to be used in IEU calculations.

	y(x) = ax + b	
OD (%)	a	b
5	0.039	0.026
7.5	0.072	0.005
10	0.093	0.024
20	0.193	0.014
22	0.202	0.019
30	0.310	0.013
40	0.419	0.008
50	0.527	0.003

Table 3.3. Slope (a) and intercept (b) expressed in Gy corresponding to the specified values of the over-dispersion.

In general it is found that minimum dose estimates consistent with those expected are obtained for any additional uncertainty ranging between 20 and 40% (see Figure 3.11). In Figure 3.11 the effect on the multi-grain burial dose estimate as a function of the additional uncertainty is also investigated.

Following the same procedure used on single grains, we have tested the dependence of the estimated dose on the additional uncertainty added using samples T-39 and T-31. Figure 3.11 shows that an additional uncertainty greater than ~7% results in a significant overestimate of the expected dose.

In the thermal transfer experiment a dose of 15 ± 6 mGy (n = 84) was measured. It could be argued that this dose ought to be subtracted from the final dose estimates before calculating the OSL burial age. If that is done, the estimated to expected doses ratio for all eight samples vary from 11.3 ± 4.7 to 11.2 ± 4.8 using simple average, from 3.2 ± 1.3 to 3.0 ± 1.3 for robust statistics, from 10.7 ± 4.5 to 10.4 ± 4.4, for CAMtr, from 2.1 ± 0.5 to 1.9 ± 0.1 for MAMtr, and from 1.1 ± 0.1 to 0.9 ± 0.1 for IEU. Thus, although samples T-39 and T-37 using the IEU approach and T-36 and T-31 using the MAM_{tr}, independently seem to better approach the known dose when subtracting the effect of thermal transfer it cannot be concluded that better estimates would be reached in that case as it has not significant effect on the global ratios (Figure 3.13). Thus, it can be confirmed that the effect of thermal transfer at the temperatures used can be considered undetectable.

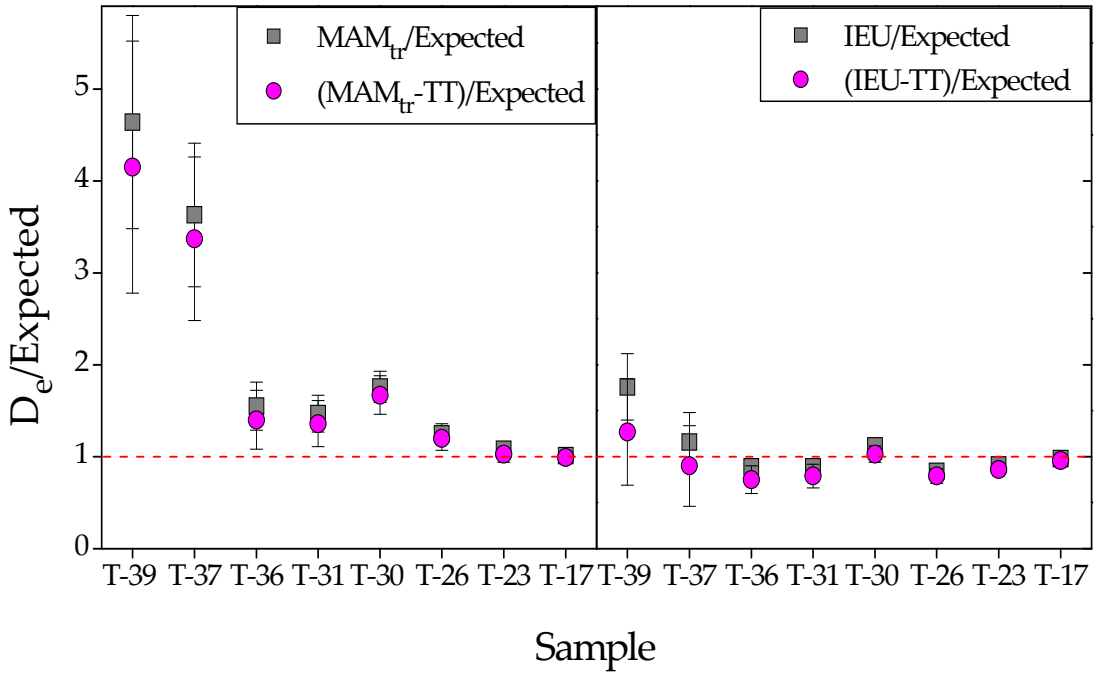

Figure 3.13. Ratio between age estimates with the MAMtr and IEU models and the expected ones (black squares). The ratios when subtracting the effect of thermal transfer from the estimated age are also shown (pink circles).

3.7. **Conclusions**

Over the last few years, single grains have been increasingly used almost routinely for fluvial deposits, despite the measurement and analysis time involved (e.g. Thomas *et al*., 2005; Arnold *et al*., 2007; Thomsen *et al*., 2007). A first general conclusion of the Guadalentín studied samples is that apparently most accurate estimates are those given by the IEU using single grain dose estimates. These estimates have been converted to ages (Aitken, 1998) and are summarized in Table 3.4 together with the estimated to expected age ratio. A second main conclusion is that considering the time and effort involved in single grain measurements compared to the use of multi-grain aliquots, these small aliquots (from ~ 30 grains) in combination with the IEU approach provided quite accurate age estimates, even though considering that in this type of flash-flood deposits were transported within high sediment load water and over a

short timing. This is in agreement with previously published results concluding that small multi-grain aliquot measurements can identify sediments containing grains with different D_e values (Olley et al., 1999; Tooth et al., 2007). In this case using small aliquots and the IEU model would result in offsets in dose of ~ 40 mGy (~40 years); even using a simple mean would only result in systematic overestimates in dose of ~ 3 Gy (~3 ka). In this study it has been found that this combination of multi-grains aliquots and IEU approach is highly reliable in dating palaeoflood deposits in Mediterranean ephemeral rivers.

Age (ka)	Depth (cm)	Simple average SG (ka)	Robust average SG (ka)	CAM_{tr} SG (ka)	MAM_{tr} SG (ka)	MAM_{tr} SA (ka)	IEU SG (ka)	IEU SA (ka)	Expected (ka)
T-39	59	1.64 ± 0.40	0.45 ± 0.09	1.46 ± 0.32	0.188 ± 0.048	0.314 ± 0.042	0.071 ± 0.015	0.076 ± 0.041	0.040
T-37	95	1.26 ± 0.29	0.40 ± 0.07	1.62 ± 0.23	0.251 ± 0.055	0.393 ± 0.069	0.080 ± 0.023	0.268 ± 0.036	0.069
T-36	170	0.65 ± 0.19	0.15 ± 0.02	0.39 ± 0.07	0.186 ± 0.033	0.213 ± 0.025	0.107 ± 0.013	0.123 ± 0.013	0.119
T-31	216	2.24 ± 0.66	0.25 ± 0.03	1.92 ± 0.57	0.259 ± 0.040	0.319 ± 0.027	0.158 ± 0.017	0.191 ± 0.017	0.172
T-30	259	0.90 ± 0.06	0.34 ± 0.04	0.82 ± 0.16	0.317 ± 0.036	0.371 ± 0.034	0.201 ± 0.016	0.269 ± 0.026	0.179
T-26	351	1.25 ± 0.30	0.53 ± 0.05	1.06 ± 0.20	0.455 ± 0.049	0.520 ± 0.047	0.305 ± 0.029	0.397 ± 0.033	0.357
T-23	367	1.09 ± 0.35	0.46 ± 0.04	0.81 ± 0.15	0.471 ± 0.043	0.539 ± 0.042	0.397 ± 0.033	0.442 ± 0.034	0.442
T-17	478	1.54 ± 0.08	1.07 ± 0.07	1.36 ± 0.13	0.983 ± 0.061	0.906 ± 0.231	0.957 ± 0.061	0.974 ± 0.095	0.975 ± 0.057

Table 3.4. Age derived from simple average, robust statistics, CAM_{tr} on single grains (SG), MAM_{tr} on single grains and small multi-grain aliquots (SA), IEU on single grains (SG) and small multi-grain aliquots (SA) and values from independent age control.

4.

Hydro-sedimentological processes, light bleaching and luminescence dating of palaeoflood deposits.

4.1. **Introduction**

Palaeoflood studies are based on geologic evidence of flood stages and channel geometry, which lead to the estimation of flood discharges. Common indirect evidence of flood palaeostages includes sediments deposited on the valley sides during high water stages. These are commonly used as palaeostage indicators (PSI's). These indicators can be correlated to define the palaeoflood water surface profiles along the river channel that subsequently are used in the estimation of the discharges associated with palaeostage indicators (O'Connor and Webb, 1988). This discharge estimation associated to flood depositional units, together with numerical dating, allows the reconstruction of flood magnitude and frequency over an extended period of time (centuries to millennia).

Robust optical dating methods should provide a precise age of flood deposits over millennia scales, including those that occurred during historical time. However, this is not simple due to methodological/instrumental problems, as well as to problems inherent to sediments in natural systems like limited light exposure of quartz grains during flood events (bleaching), poor luminescence behaviour of some quartz grains

and heterogeneous dose rates in the depositional sites due to heterogeneous radionuclide distributions.

Bleaching of quartz grains depends on exposure of sediment particles to sun light both in terms of quality and quantity. Theoretically, the washload of sediment load transported by floods is the fraction most likely to be exposed to sunlight and therefore, the best to be used for OSL dating of flood events. Moreover, depositional environments covered by shallow water during flood stage are likely to be exposed to daylight, and it may be considered to provide more reliable OSL ages. However, high sediment concentration of suspended particles transported during floods may produce high turbidity that hampers total or partially the exposure of quartz grains to daylight. In terms of exposure time, the size of a catchment or, in other words, the distance during transport of sediment, can play an important role, since the longer the distance the more chances for the particles to be exposed to light. Another factor to consider is the flood duration that can be related to the shape of the flood hydrograph. In the Iberian Peninsula, the contrasting hydroclimatic, orographic and lithological characteristics of basins draining towards the Atlantic and those to the Mediterranean result in different types of rainfall and flooding in terms of spatial distribution, seasonality and duration. In Mediterranean rivers, flood hydrographs have a short duration (a few hours) and therefore the time the sediment is exposed to light may be limited. Furthermore considering that convective storms producing flooding often occur at the end of the day. In Atlantic basins, floods are generated by the passage of frontal systems during winter months and the duration of the flood hydrographs may last for several days. Under these conditions, the potential for sediments to be exposed to light is higher even under cloud covering conditions.

This chapter aims to understand how (i) hydro-sedimentological processes and catchment characteristics may affect bleaching of quartz grains and how (ii) catchment characteristics (size, bedrock lithology, flood hydrograph duration, sediment sources) may introduce inherent errors in optical dating of the flood deposits of Iberian rivers. The initial hypothesis of this study considers that different fractions of suspended load

are bleached to varying degrees and therefore the selection of appropriate sedimentological environments may provide better dating results. Moreover, catchment characteristics may influence the light exposure time (e.g. small versus large basins, flash floods versus river floods), quartz quality (Paleozoic versus Mesozoic-Tertiary source, granite versus limestone dominate bedrocks), and annual dose rate (high content of radioactive minerals versus low contents). Testing of this hypothesis requires a detail understanding of hydraulic and sedimentological processes under which palaeoflood deposits (broad sense) are deposited within different river basin characteristics and lithologies. In the following sections, hydraulic processes and sedimentological environment intervening in the deposition of palaeoflood deposits are described. These sedimentological environments were identified at four rivers within the Iberian Peninsula where OSL dating of palaeofloods deposits were performed (Figure 4.1). OSL results are discussed to conclude with basic guidance to be considered in future OSL dating of palaeoflood deposits in Iberian rivers.

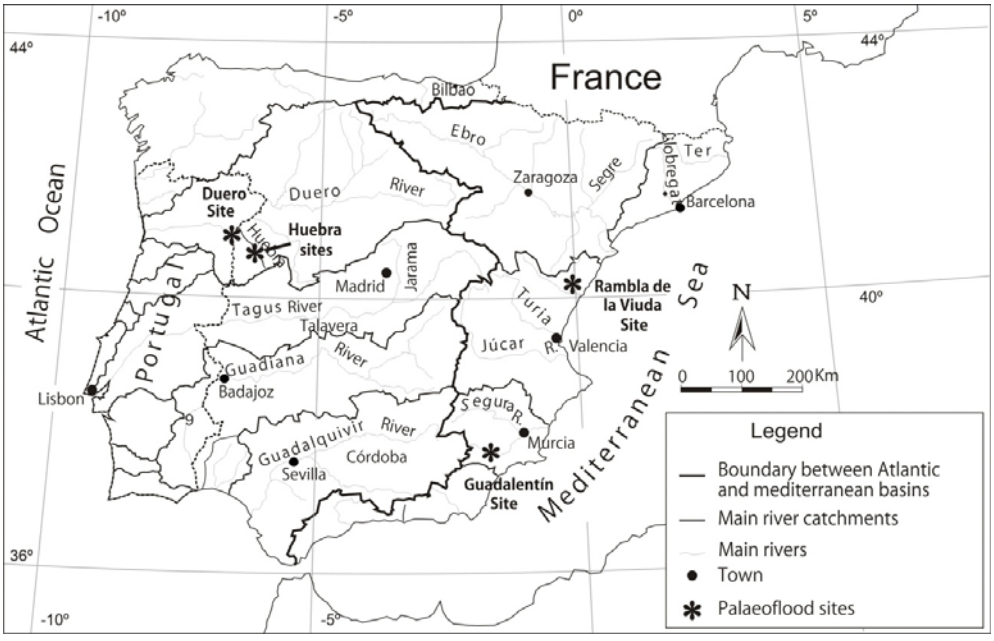

Figure 4.1. Location of the studied rivers, sites described in the text, and boundary of the Atlantic and Mediterranean river catchments. Location of the four sites where samples for this study were collected.

4.2. Palaeoflood deposits: hydraulic processes and depositional environments

Most suitable geomorphologic settings for reconstructing palaeoflood discharges are found within bedrock canyons because of their stable geometry and the sharp changes of flow energy conditions between the main channel flow and the margins of the canyon. On the flooded canyon margins, flow eddies, back-flooding and water stagnation (slack water) occur, producing a low motion which favours deposition from suspension of clay, silt and sand. These fine-grained deposits are the ones preserved in stratigraphic sequences, providing detailed and complete records of flood events that extend back several thousand of years (Patton *et al*., 1979; Baker *et al*., 1983). O'Connor (1993) distinguished two categories of suspended load deposits; the suspended load per se, and the washload. Slackwater flood deposits (SWD) are deposited in areas of flow stagnation or quiescence representing the washload component of the suspended load, whereas accumulation of other fractions of the suspended load can be found in areas of marked velocity reduction associated to recirculation zones or eddies (Eddy deposits; O'Connor 1993). Eddy deposits are commonly found in tributary mouths, downstream of obstacles or bedrock projections into the flow, and in canyon re-entrants, whereas SWD are found in wide backflooded basins and in tributary valleys where the flow is essentially stagnant (Baker, 1973; O'Connor, 1993). A question regarding OSL dating of these deposits is how the hydraulic history and particular depositional environments may affect luminescence flood ages due to total or partial bleaching of the dated grains.

4.2.1. Eddy deposits

Eddy deposits are accumulated at sites of marked reduced velocity due to flow separation from main threat of flow, and become involved in recirculation zones. These recirculation zones involve flow eddy development, having a constant supply of suspended sediment provided by the mainstream. Most geomorphologic settings of

eddy deposits are tributary mouths, canyon wall reentrants and valley expansions. Schmidt (1990) and Rubin *et al*. (1990) studied the hydraulic characteristics and sedimentation at recirculation zones in the Colorado River (Arizona, USA) focusing on valley expansion sites. According to Schmidt (1990) these recirculation zones comprise a primary eddy situated in the downstream part of the channel expansion and closer to the main threat of the flow. In the inner and upstream expansion zone, secondary eddies of changing flow direction may be developed.

The secondary flow diverges at the separation point from which water and sediment is pumped to the recirculation zone as long as the main flow maintains its stage and competency to maintain a suspended load. At the eddy's downstream sector, the convergence point varies its location along the valley margin, where eddies are developed or destroyed according to changes on flood stage. Flood sediments are deposited at these points of reduced flow velocity. Eddy deposits next to the convergence point are characterised by an elongated shape and flat surface with its highest point on the downstream end. In this convergence eddy deposits, common sedimentary structures include climbing ripples and planar cross-stratification developed by migration of the bar front towards the upstream direction (reverse flow) within the recirculation zone.

The separation eddy bars involve a larger extension that the convergence ones, in the downstream direction from the separation point. Typical sedimentary structures include climbing ripples characteristic of environments with a high content of suspension sediment, and low angle planar cross-stratification reflecting re-working by waves, characteristic of separation flow zones. Sediments in the convergence eddy bars show a coarser texture than the ones next to the separation point. In fact, convergence bars contain a grain size distribution similar to the suspended load, whereas the separation bars reflect the washload (finer fraction) of the suspended load.

4.2.2. Slackwater flood deposits

Slackwater flood deposits represent the finest fraction of the suspended load (washload), i.e. silts, sands and occasionally clays. They are located in areas of standing water (slack water) as floodwater inundates tributary streams, rock shelters or wide valley expansion zones where flow velocity is zero or close to zero. Typically, these deposits contain massive structure and/or parallel lamination, and occasionally some tractive structures such as current ripples. In this standing water of slackwater environments it is common that fine laminae of clay or silt culminate each flood unit that may be colonised by organism producing intense bioturbation. Dessication cracks are also common at these clay laminae.

4.2.3. Depositional environments

The most detailed description of the stratigraphy and sedimentology of flood deposits were provided by McKee (1938) for the Colorado River flood deposits in the Grand Canyon, by Kochel and Baker (1988) in the Pecos River slackwater sediments, and by Benito *et al*. (2003) in the Tagus River in central Spain. In the case studied, several of these sedimentary environments were identified and samples for OSL dating were collected.

These environments are:

- Channel widen (Duero River)
- Canyon expansion (Rambla de la Viuda and Huebra River)
- Bedrock obstacles (Guadalentin River)
- Back flooded tributaries (Huebra River) and tributary mouth (Rambla de la Viuda)

The first three are related with their specific position in the channel during the flood and with the specify flow conditions induced. The fourth is related also with the presence of tributary channels and their morphology. The main sedimentary sequences

associated with these depositional environments have been described in detail by Benito *et al*. (2003).

4.3. Geography and hydrology of the studied rivers

In the last two decades, a number of palaeoflood studies have been studied by the Laboratory on Palaeohydrology and Global Change of the Spanish Research Council. For this dissertation, some of the studied palaeoflood sites in Spain were re-visited to provide guidance of the most suitable deposits for OSL dating.

The Iberian Peninsula is surrounded by the Atlantic Ocean to the west and by the Mediterranean Sea to the East. River hydrology in the Iberian Peninsula is highly influenced by the Atlantic Ocean to the west and by the Mediterranean Sea to the east (Figure 4.1). This results in a distinct division between basins draining towards the Atlantic and those towards the Mediterranean. These contrasting hydroclimatic regions are therefore affected by different air masses which are responsible for different types of rainfall in terms of spatial distribution, seasonality and duration.

In the Atlantic river basins flood generation, duration and magnitude are closely related to changes in winter rainfall (Capel, 1981; Benito *et al*., 1996; Rodrigo *et al*., 1999). The heaviest rainfall in the Atlantic basins occurs when the zonal circulation is displaced towards lower latitudes (35-45° N) and the western Iberian Peninsula is affected by the entry of successive frontal systems, thus generating heavy and persistent rainfall in the basins of the Duero, Tagus, Guadiana and Guadalquivir rivers.

In Mediterranean river basins, the most intense rainfall conditions leading to extreme floods are associated to mesoscale convective systems (MCSs) (Llasat and Puigcerver, 1990) fed by moisture born in the Mediterranean and enhanced by the orographic effect of the mountain ranges near the coast. These MCSs are commonly originated during autumn months, with rainfall episodes of over 300 mm in 24 hours, leading to floods in rivers of the eastern Pyrenees and Ebro, the Júcar and Segura basins, as well

as in the southern coast rivers. Floods may reach discharges up to 11,000 times greater than mean discharge during the largest floods (Masachs, 1950). The seasonal marked temperature contrast between inland areas and the Mediterranean Sea also favours convective rainfall over the mountain ridges along the cost, leading to damaging flash floods (Llasat and Puigcerver, 1990).

These hydrological contrasting regimes are reflected both in the generated flood hydrographs and in the preservation of the palaeoflood deposits. Intense, short-lived rainfall episodes usually affect the Pyrenees and the Mediterranean coast during autumn, and are responsible for flash floods with peak hydrographs of short time duration in arroyos and ephemeral streams. During these high energy flood events, river channel and valley sides may be affected by erosion including zones of former slackwater deposition. As a result, preservation of palaeoflood deposits may be limited to 2-3 thousand of years (Benito *et al*., 2008). In the Atlantic basins, more gentle rains over extensive areas associated to winter cyclones from the Atlantic produce slower response to the cause of the flood, longer duration and lower specific discharges (rate of peak flow to the catchment surface). Here, hydrographs are normally broad-based and peak discharges may last several days (from 2 to 7 days in most cases).

Lithologically, the catchment of Atlantic basins broadly coincides with the former Tertiary continental endorheic basins (Duero, Tagus and Guadalquivir). The Tertiary bedrock is characterised by detritic sediments (conglomerates, sands and silts) associated to alluvial fan systems developed at the front of the surrounding mountain ranges, which graded to evaporitic materials (limestones and gypsum) towards the central parts of the basin where formed playa-lake systems. However, in their western part of these catchments, the basement of these basins, as well as mountain ranges, are dominated by granites, gneises, shales and schist of Precambrian and Paleozoic ages with frequent outcrops of hydrotermal deposits associated to volcanism, as well as ubiquitous ore deposits including radioactive minerals. These old rocks are part of the Hesperic Massif folded during the Hercinic orogenesis. Therefore, environmental dose

rates in Atlantic rivers are expected to be relatively high. A larger quantity of feldspar can be expected to be contained in Quaternary alluvial deposits.

The eastern part of the Iberian Peninsula is dominated by sedimentary rocks (both evaporitic and detritic) of Mesozoic age that were folded during the Alpine orogenesis. During this orogenesis most of the current Iberian mountains were developed, including the Pyrenees, Betic Cordillera, Iberian Range and Catalan Range. As sedimentary rocks are the main source of quartz, there is a wide diversity of quartz that can be found among close locations. These quartz may present different luminescence behaviour. The percentage of secondary feldspar in Mediterranean alluvial facies is low. The annual dose rate can be expected to be significantly lower than the ones in the Atlantic rivers.

4.4. **Methodology**

OSL ages have been obtained for a total of 29 samples from four rivers, two Mediterranean rivers (Guadalentín and Rambla de la Viuda), and two Atlantic rivers (Huebra and Duero) (Figure 4.1). From these, 12 were sampled from eddy bar flood environments. The remaining 17 samples were sampled from slackwater flood environments (*stricto sensu*), especially from flooded tributary streams. 8 of those samples were taken from the Guadalentin River for which independent age control from historical records and radiocarbon was available. These have been used to test the performance of the different methods for estimating the burial dose and determine the analyses that provide the most accurate results. A detailed discussion on this topic and the corresponding conclusions were presented in Chapter 3. These conclusions are applied for the estimation of the burial dose of the remaining 21 samples and to determine whether the performance of the different methods of burial dose estimation is site dependent or same behavior is repeated despite the sediment type and origin.

Burial doses have been determined using descriptive and robust statistics, CAM (CAM_{tr}), MAM (MAM_{tr}) and IEU methods. Unless otherwise stated, the ages given are

based on single grain burial doses calculated using the IEU as it was found to give the most accurate ages when studying the samples from Guadalentin river (see Chapter 3).

The stimulation curve shape and dose recovery have been analyzed for each site. Detecting any possible anomalies is crucial to establish the reproducibility of results among the different samples. Preheat plateaus and thermal transfer tests have been studied for samples from each site to determine the most suitable temperatures for the thermal treatments and quantify the thermal transfer contribution in the luminescence signal. As it was discussed in section 2.6.2 it is expected that any thermal transfer will have a less significant effect for older samples than for younger ones. Therefore, even in the case of detecting dose derived from thermal transfer, it may not be significant if the natural doses measured are high enough to be dominant.

Using the same reasoning outlined in chapter 3, the dose distribution of a bleached and laboratory gamma dosed sample is considered to be affected by the uncertainty derived from counting statistics, curve fitting error and instrument reproducibility. But as showed previously (section 3.4.4.2) other sources of error contribute to the variability of the distribution thus indicating that an extra uncertainty has to be added to account for the observed intrinsic variability. Dose recovery tests have been measured for samples from each site. The observed over-dispersion of the distributions derived from these experiments have been used to quantify the likely contribution from intrinsic sources of variability. This over-dispersion is therefore considered the minimum to account for the observed variability. But it is likely that natural samples are also affected by extrinsic factors. Then it can be assumed that the variability of the distribution, exceeding the determined minimum uncertainty is derived from extrinsic factors as partial bleaching and beta dose heterogeneity.

The over-dispersion is considered to be a function of the dose. This dependence has been based on the results from dose recovery test. The over-dispersion of the distribution of a bleached sample and that corresponding to a sample dosed with 2 Gy have been plotted as a function of the dose. This way, the absolute over-dispersion is

given by the slope and intercept of the linear fit (see sections 4.5.3 and 4.6.3 for further details).

The proportion of grains contributing to the OSL signal emitted from multi-grain aliquots has been analyzed with the aid of cumulative light sum plots for different sites. This provides knowledge on the OSL contribution that can be expected from the different type sediments analyzed.

Unless otherwise stated, LBG has been applied to single grain data as it was showed (section 3.5.1.1) that no significant differences on the over-dispersion of the distribution were caused but a bigger number of grains passed the rejection criterion. EBG has been used in multi-grain aliquots analyses to avoid contributions from slow and medium components in the dose estimates.

The selection criteria used for both, single grains and multi-grain aliquots, of the Guadalentin samples have also been used to filter the aliquots of samples from Rambla de la Viuda, Huebra and Duero rivers.

4.5. Rambla de la Viuda

4.5.1. Study area

Rambla de la Viuda, with a catchment area of 1500 km^2, is an ephemeral stream that joins the river Mijares in Almanzora (Castellón), near its mouth to the Mediterranean Sea. Its channel bed is mainly modelled by flood flows, with predominant sediment load composed by gravel and block sizes forming traversal bars (Mateu, 1974; Camarasa and Segura, 2001). The study area is located on a stretch of 6.5 km in length, between Mas de Flors (tail of Maria Cristina reservoir) and Costur road. In this reach, the river goes through a bedrock valley cut on limestones and marls of Cretaceous age, and conglomerates of Pliocene and Pleistocene age. The area has a typical Mediterranean climate with average annual rainfall ranging between 500 and 650 mm

and average temperatures of 10°C in winter and of 25°C during summer. Large floods are produced by mesoscale convective systems fed by humidity from the Mediterranean Sea during autumn months. Between 1959 and 1984, an average of three "running" flow events per year was recorded in the Rambla. However, large floods only occurred in 1920, 1962 and 2000, with the later causing a crack in the structure of a dam located at the end of the studied reach. In Rambla de la Viuda, the 1962 flood was estimated to be 1500 m^3s^{-1}, whereas discharge of the 2000-flood was estimated to be 640 m^3s^{-1}.

4.5.1.1. Slackwater flood deposits stratigraphy

Sediments transported by the Rambla (term for arroyo in the Spanish Mediterranean area) are dominated by gravels and boulders, but a careful inspection of the valley sides revealed important accumulations of slackwater flood deposits. These slackwater flood deposits, emplaced by high stage floodwaters, show a complete stratigraphy from which we can reconstruct long-term records of floods and environmental changes.

A total of ten stratigraphic profiles were described, located in areas of prevailing deposition of suspended clay, silts and fine sands, during flood events, along the canyon margins (five of them are shown in Figure 4.2). Palaeoflood deposits were accumulated forming a bench morphology on the valley side, mainly at valley expansion reaches and at confluence of tributary streams.

A total of ten samples for OSL dating were collected from three of these stratigraphic profiles: RVD2 (3 samples), RVD5 (4 samples) and RVD8 (3 samples). Chronologies of these flood units have been constrained with a number of radiocarbon ages and by historically documented floods in book archives of the riberine villages (see Table 4.1).

HISTORICAL FLOODS	Year	Month	Day
Mijares	1580	–	–
Mijares	1581	9	18
Mijares	1597	–	–
Rambla de la Viuda	1617	–	–
Rambla de la Viuda	1783	11	24
Mijares	1787	10	8
Mijares and others	1801	11	18
Mijares and others	1883	10	9
Rambla de la Viuda	1900	9	14
Rambla de la Viuda	1962	10	15
Rambla de la Viuda	1969	10	7
Rambla de la Viuda	2000	10	25

Table 4.1. Documentary flood record reported for the Mijares and Rambla de la Viuda rivers (Segura, 2001).

Profile RVD2 is located in the most downstream part of the studied reach (Figure 4.2) and belongs to a fluvial bench composed by sand and silts, with up to 6 m in thickness, placed on the confluence of a tributary stream at the right margin of the main river. In this stratigraphic profile (Figure 4.3) at least nine palaeoflood units were deposited during the last 500 years as indicated by a radiocarbon date collected at the second most bottom flood unit (radiocarbon dated as 335 ± 40 years BP).

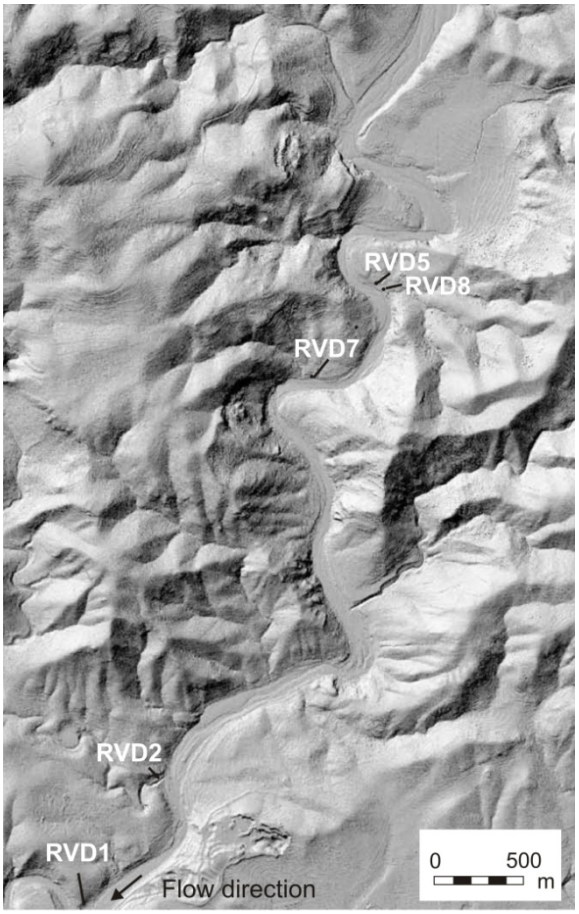

Figure 4.2. Rambla de la Viuda sites. Location and position of stratigraphic profiles described.

The stratigraphy shows three clusters of palaeoflood units separated by two colluvial units. These colluvial units indicate periods with a lack of major floods and lateral (slope) dominant processes. The bottom section shows three palaeoflood units (7 to 9); the lowest one dated as 335 ± 40 years BP (cal. AD 1464-1644). The middle section shows five palaeoflood units (2 to 6); the intermediate one dated as 220 ± 30 years BP (cal. AD 1775-1800). The upper section only shows one flood unit overlying a thick (over 1 m) twin-bed composed by colluvial deposits. The colluvial units across the palaeoflood sequences indicated times of slope instability and dominance of slope processes, that may be related with periods of drought conditions and soil degradation due to cattle, as it is reflected on the high nitrogen content of these units. Discharge

estimates from the HEC-RAS hydraulic model indicates a minimum flood discharge of 1400 m^3s^{-1}, to deposit sediments at the bottom section of this stratigraphic profile, whereas the upper most unit is associated with a minimum discharge of 2800 m^3s^{-1}.

In the upstream reach, flood deposition at an expansion reach has developed two flood benches above the channel bottom. The highest one, RVD8, shows at least eight flood units, with some contacts marked by stone lines and soil development indicating long periods with lack of flood deposition (Figure 4.4). The second one at the bottom section shows a large thickness (over 2 m) that it is unusual in slackwater flood deposition, reflecting either multiple floods with non-evident contacts or being deposited by a single large flood event with multiple pulses. There is not geochronological control on this profile due to the lack of organic material. Hydraulic calculations indicate a minimum discharge estimate of 550 m^3s^{-1} required to deposit sediment at the bottom section and of 1600 m^3s^{-1} for the upper most flood unit.

4.5.1.2. Eddy flood deposits: site RVD5

In the same valley expansion, a lower flood bench inserted in the previously described RVD8 bench shows a ~5 m thick sand and silt flood deposition from more recent flood events, as evidenced by the non consolidated sand material. A trench dug on this inserted bench (profile RVD5) shows at least nine flood units deposited in two periods (3 + 6 events) interrupted by a colluvial unit (Figure 4.5). The lower flood cluster is composed of three flood units (7 to 9) post-dated by a radiocarbon age of 160 ± 30 years BP (cal. AD 1670-1810). The upper flood cluster (units 1 to 6) corresponds to young flood deposition. OSL samples for dating were taken in units 2, 3, 5A and 5B. In RVD5, minimum discharge required for deposition varies between 350 m^3s^{-1} and 1300 m^3s^{-1}.

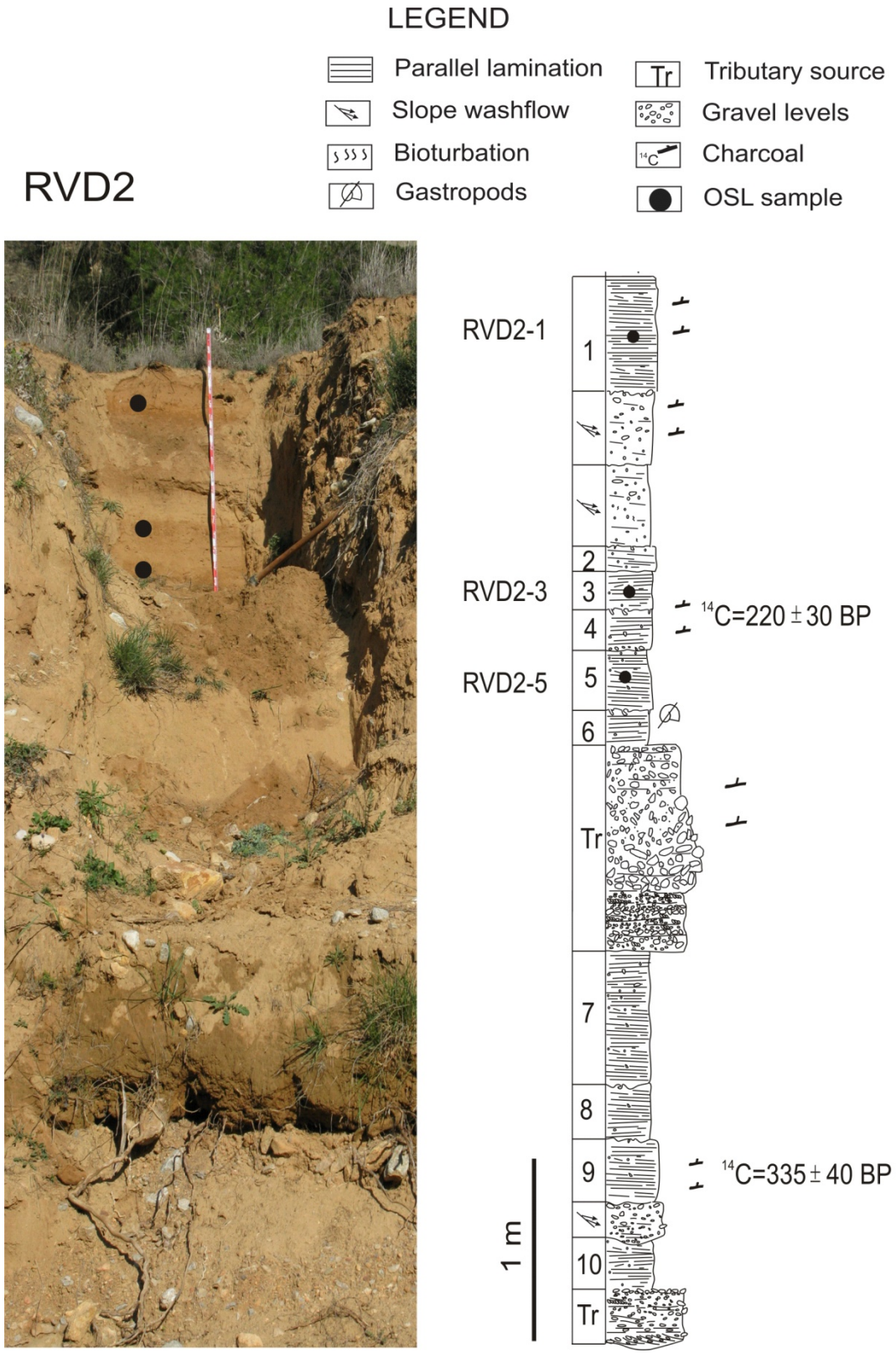

Figure 4.3. Stratigraphic profile of site RVD2.

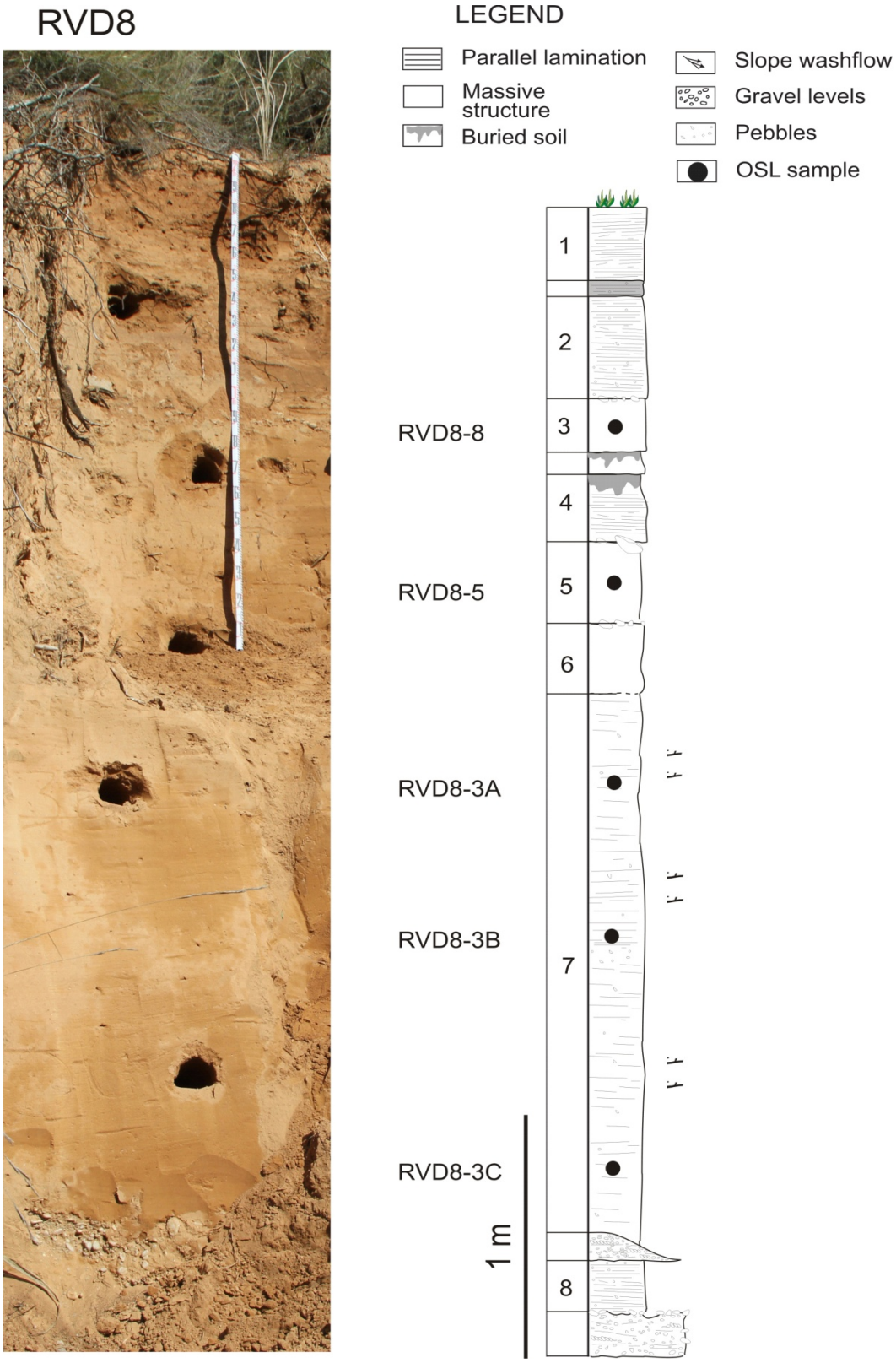

Figure 4.4. Stratigraphic profile of site RVD8.

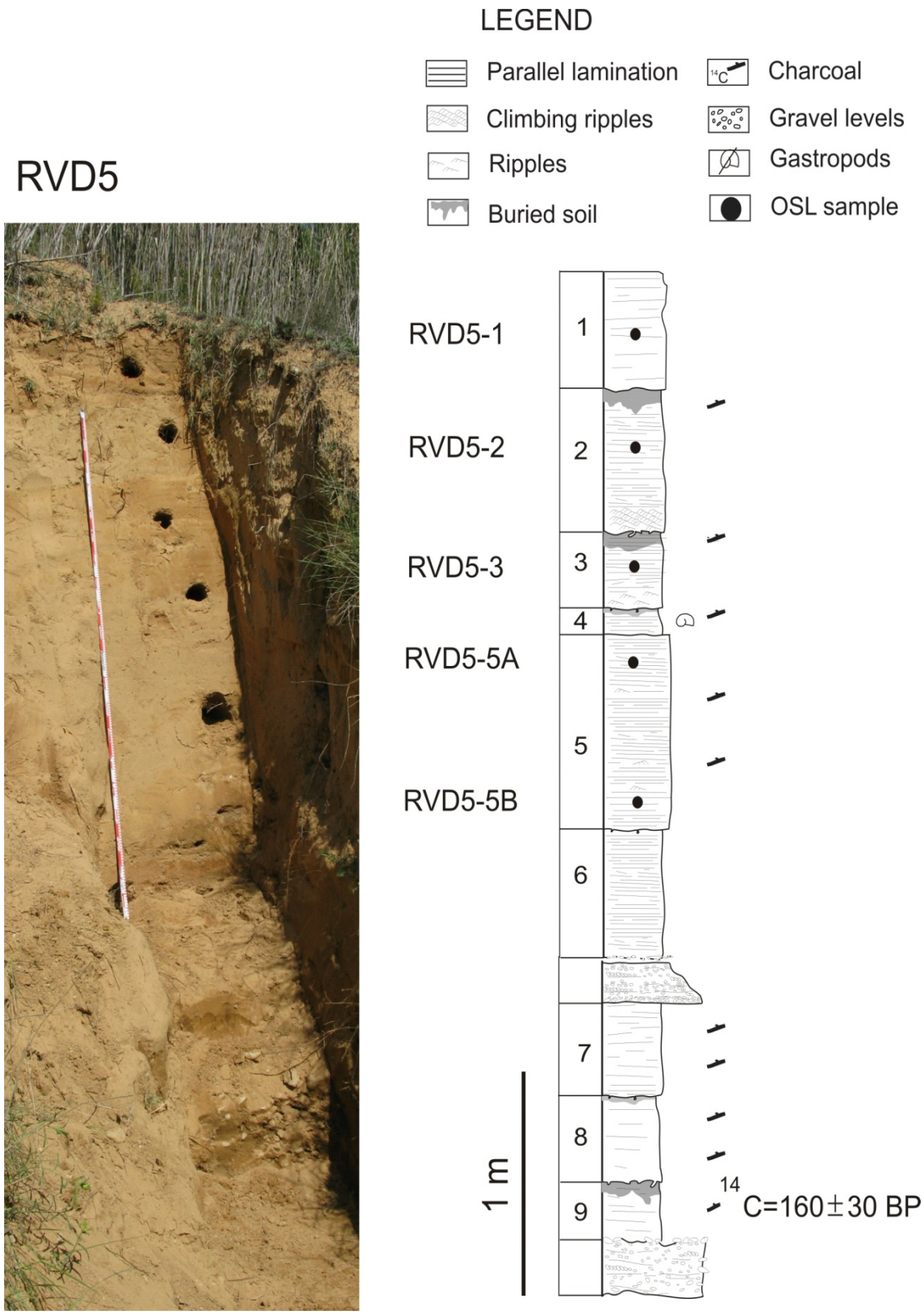

Figure 4.5. Stratigraphic profile of site RVD5.

4.5.2. Dose rate

Dose rates were measured by high resolution gamma spectrometry (section 2.4). The samples are assumed to be surrounded by a homogeneous matrix. Thus, the dose rate reaching the sample is considered homogeneous and constant during the burial time.

Annual variation in rainfall during the burial time is not expected to have caused significant changes in the water content of the soil over long periods (i.e. Mediterranean climate prevailed over mid-late Holocene) and thus the water contents measured right after the sampling are assumed to be representative for the burial time.

The cosmic radiation contribution has been estimated according to the depth of the sample location Prescott and Hutton (1994). Concentration of the measured radionuclides, total dose rates, depth and water content used for the calculation are summarized in Table 4.2.

Sample	Depth (cm)	Wat. cont. (%)	^{226}Ra (Bq/kg)	^{232}Th (Bq/kg)	^{40}K (Bq/kg)	Total dose rate (Gy/ka)
RVD2-1	20	7	21.2 ± 0.7	24.6 ± 0.7	363 ± 11	2.05 ± 0.09
RVD2-3	100	7	19.9 ± 0.5	18.9 ± 0.6	271 ± 8	1.59 ± 0.07
RVD2-5	135	7	17.7 ± 0.6	17.3 ± 0.6	279 ± 9	1.63 ± 0.08
RVD5-2	50	8	16.9 ± 0.5	18.1 ± 0.5	342 ± 9	1.79 ± 0.08
RVD5-3	90	9	21.7 ± 0.5	24.0 ± 0.5	369 ± 8	2.00 ± 0.09
RVD5-5A	123	7	18.9 ± 0.3	20.1 ± 0.3	329 ± 6	1.79 ± 0.08
RVD5-5B	167	7	19.7 ± 0.4	23.5 ± 0.4	324 ± 7	1.88 ± 0.08
RVD8-8	82	8	22.4 ± 0.5	25.3 ± 0.6	341 ± 9	1.85 ± 0.08
RVD8-5	150	8	23.1 ± 0.6	24.0 ± 0.6	370 ± 10	1.99 ± 0.09
RVD8-3C	332	12	23.1 ± 0.5	27.7 ± 0.5	329 ± 9	1.98 ± 0.09

Table 4.2. Depth of the sample, water content of each unit (this value was assumed representative of the total burial time), radionuclides concentration and total dose rates calculated.

4.5.3. Luminescence behaviour

Figure 4.6 shows the normalized natural OSL signal of a representative single grain from sample RVD5-3. Also shown is the normalized OSL signal from a grain of calibration quartz (dominated by the fast component). The shape of single grains OSL decay curves are highly variable but still it can be observed that generally the OSL from these samples is dominated by the fast component, reaching background level in ~0.15 s. A similar comparison for a multi-grain aliquot of same sample has been made confirming that the signal from both, single grains and multi-grain aliquots, are dominated by the fast component.

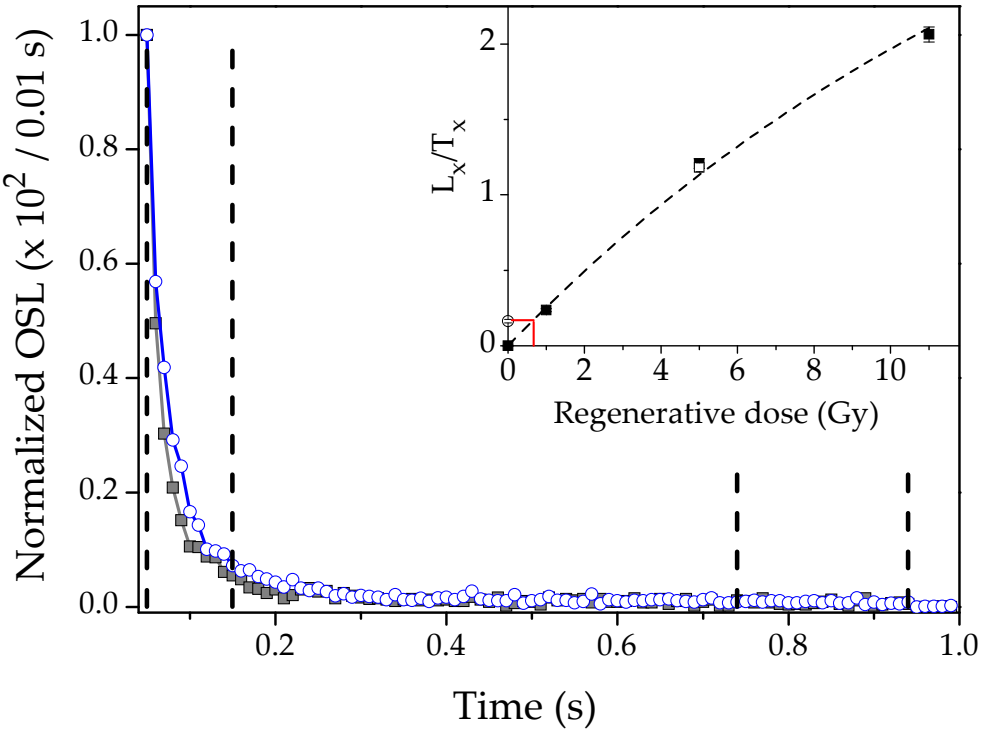

Figure 4.6. Normalized OSL decay curve of natural signal (closed gray squares) of sample RVD5-3 and decay curve of a calibration quartz single grain (open blue circles) known to be dominated by the fast component. For the multi-grain aliquot, the dose response curve exponentially fitted is shown in the inset. The corrected natural signal (L_x/T_x) is indicated by an open circle

Cumulative light sums show that most of the light is derived from a small percentage of grains. This has been quantified on samples RVD2-5 and RVD8-3C for which the intensity of the background subtracted natural OSL signal has been plot as a function of the grains contributing (Figure 4.7). Both samples show similar behavior with 80% of the total light detected being derived from less than 10% of the grains. ~70% of the grains have a very small contribution providing less than 10% of the total light detected. Therefore, in a 30 grain multi-grain aliquot, as those measured in this work, in average less than 10% of the grains will dominate the luminescence signal (Duller, 2008).

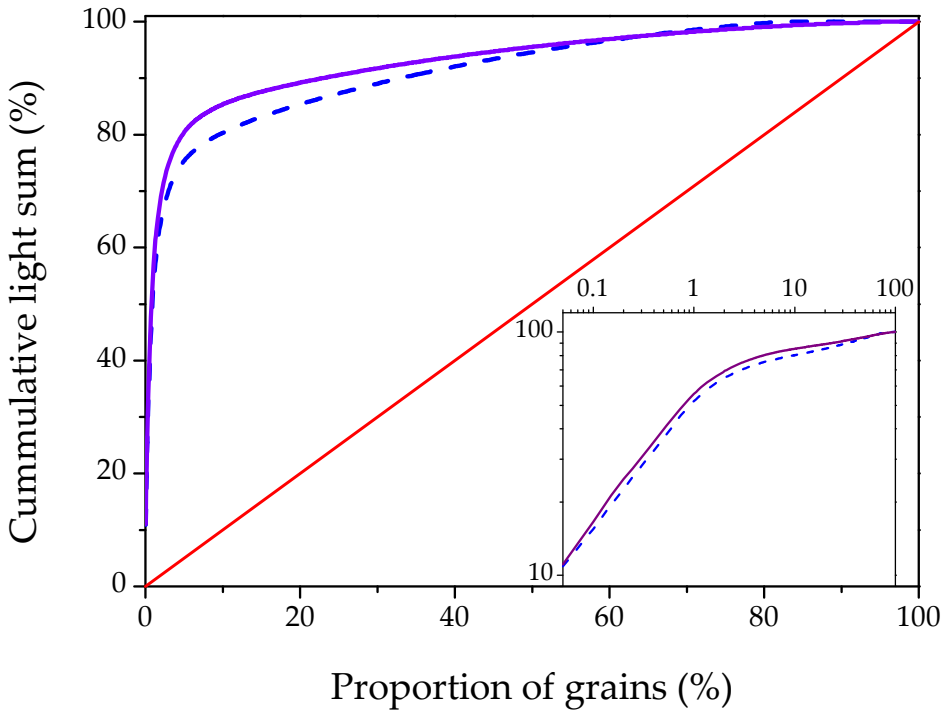

Figure 4.7. Cumulative light sum from samples RVD2-5 and RVD8-3C as a function of the proportion of grains contributing. The plot shows similar results for both samples with 80% of the total light coming from less than 10% of the measured grains. ~70% of the grains do not contributing significantly, providing less than 10% of the total light detected. The 1:1 line is showing the dependence if all grains were equally contributing to the luminescence signal. The inset shows the plot on a log scale.

Preheat plateau test based on the determination of D_e values using temperatures ranging from 160°C to 260°C (ΔT = 20°C) has been carried out. Six fresh multi-grain aliquots of sample RVD5-3 have been measured at each temperature. Measured doses at all temperatures are consistent with each other showing no detectable variation. Thus, it can be concluded that measured D_e are independent on the preheat temperature used for the range 160°C to 260°C.

Possible thermal transfer has also been measured as it can be significant for the burial dose estimation of young samples (Rhodes 2000, Murray and Olley, 2002). A fraction of sample RVD5-3 has been bleached under solar simulator for 2 hours and subsequently it has been measured using small multi-grain aliquots and preheating temperatures ranging from 160°C to 260°C (ΔT = 20°C). This way, if any signal is detected it can be assumed to be derived from the thermal treatment since effect of absorbed dose has been eliminated by the artificial bleaching of the sample. Eight aliquots have been measured for each temperature and their independent D_e values determined are also shown on Figure 4.8. Average values at each temperature are consistent with each other. Therefore thermal transfer appears to be insignificant for the temperature range investigated here.

Given the lack of dependence on the choice of preheat temperature up to 260°C a preheat temperature of 200°C and cutheat of 180°C, used in previous works on young samples (e.g. Madsen *et al*., 2007; Hu *et al*., 2010), were chosen for the thermal treatment in the SAR protocol applied, unless otherwise stated.

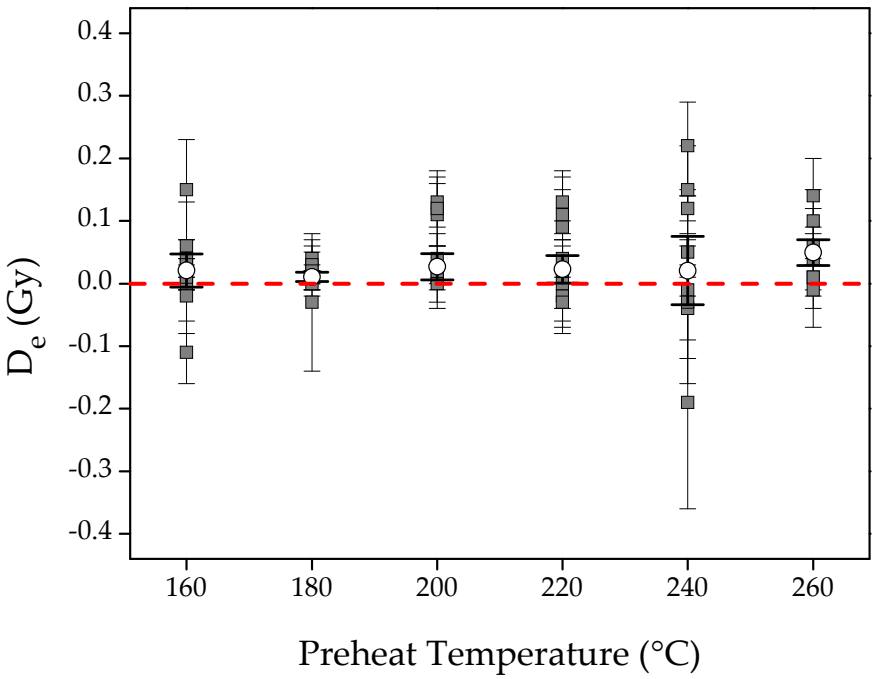

Figure 4.8. Results of thermal transfer test. Eight small multi-grain aliquots (~30 grains) of a bleached fraction of sample RVD5-3 have been measured at each temperature ranging from 160°C to 260°C (ΔT = 20°C). Individual D_e values (solid squares) and averages at each temperature (open circles) are shown.

An extra cycle at the end of the SAR sequence including IR stimulation prior to the blue stimulation and OSL measurement was added (Figure 4.9). This extra cycle was used to determine the IR depletion ratio (i.e. the difference in the blue-OSL signal when stimulating the sample with only blue light and when stimulating the sample with IR prior to blue-OSL measurement) The IR depletion ratio has been measured for all aliquots (both multi-grain and single grains) to detect possible feldspar contribution to the signal. "Extended" SAR protocol including the extra cycle at the end of the standard SAR, in which an IR bleaching step was included prior to the blue stimulation has been used for this purpose.

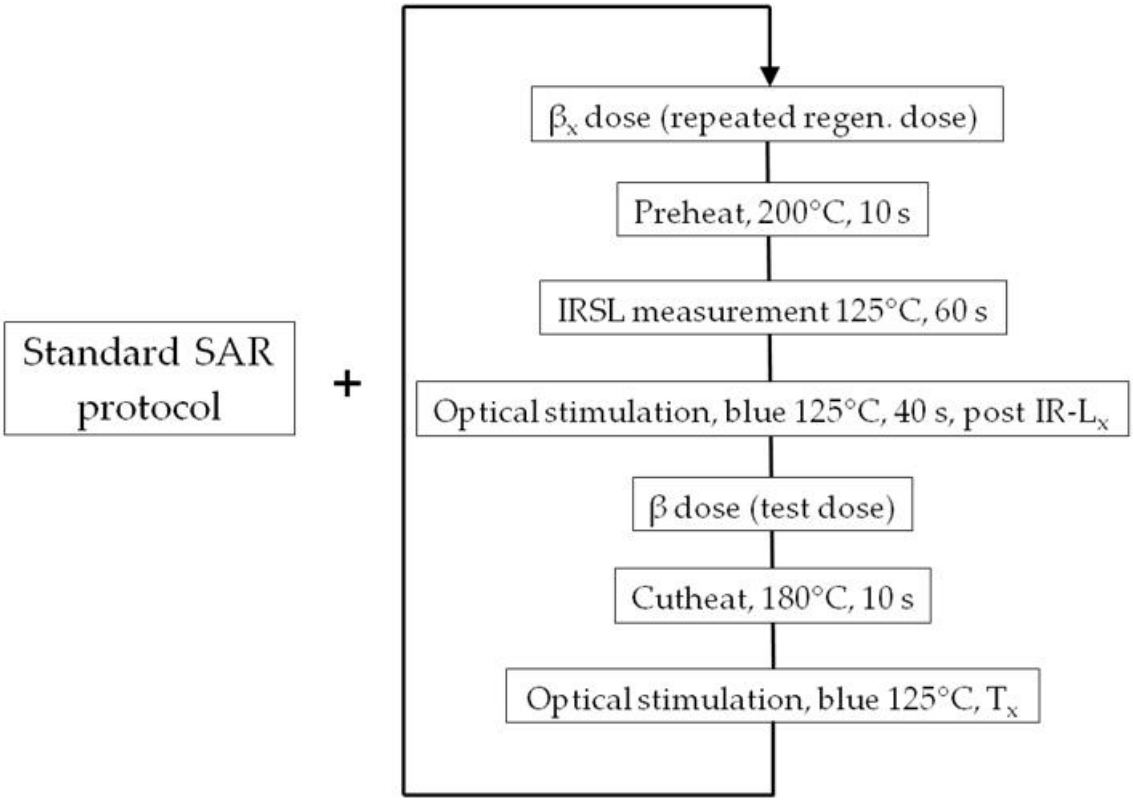

Figure 4.9. SAR protocol including an extra cycle at the end of the standard SAR protocol to determine the IR depletion ratio. This extra cycle includes IR stimulation prior the blue-OSL measurement keeping the second part of the cycle (test dose and subsequent cutheat and blue-OSL measurement) constant.

For single grain measurements, those grains showing response to IR stimulation have been dismissed based on the fact that either they are feldspar grains themselves or they are quartz grains with feldspar inclusions. In either case they would contribute to the signal when measuring the response to blue stimulation. For this work, those grains were discarded based on the IR depletion ratio. In addition, if they were to be included in the age estimation, the contribution for the internal ^{40}K to the dose rate from a grain presenting feldspar inclusions should be taken into account (Huntley *et al*., 1993). Some (~10%) multi-grain aliquots had a detectable IR signals, but their average IR depletion

ratio was not significantly different from unity thus, feldspar do not appear to contribute significantly to the quartz OSL signal.

Dose recovery tests have been measured on six multi-grain aliquots of each sample to confirm that a given dose can be recovered accurately. Aliquots have been bleached under the solar simulator for two hours followed by a beta dose of 2 Gy given in the luminescence reader. For all samples the beta dose given has been recovered obtaining results consistent within two standard deviations.

A gamma dose recovery test has been carried out to quantify the variability arising from intrinsic factors. In this test, a fraction of sample RVD5-2 was bleached and subsequently gamma dosed (section 2.5.3) with 2 Gy. The dose distribution of this bleached and gamma dosed sample has an over-dispersion of 20 ± 4% when measured on single grains and 11 ± 2% when using small multi-grain aliquots similar to those used for measuring the natural samples. From these results it is assumed that when using single grains, an extra 20% uncertainty should be added to the uncertainties based purely on counting statistics and curve fitting errors to account for the observed variability. Analogously, an extra 11% should be added when using multi-grain aliquots. It is implicitly assumed that the relative over-dispersion is constant as a function of given dose, although Thomsen et al., (2012) showed that this assumption breaks down at doses larger than 10 Gy. (see section 4.6.4.1 for further details). In addition to the CAM mean and over-dispersion values for the bleached and gamma dosed sample, CAM mean and over-dispersion have also been determined for a bleached fraction of the same sample. Dose distributions for both, the bleached fraction and that gamma dosed with 2 Gy after being bleached, show a peak centred at the mean value in each case (Figure 4.10). CAM averages are shown with dashed lines on the dose distribution. The over-dispersion associated to each mean dose value is used to determine the variation of over-dispersion as a function of dose. This can be assigned by the slope and intercept of the fit linear between these two measurements. For single grains it is given by the relation $OD_{abs}(Gy) = 0.193 \cdot \overline{D} + 0.012$, where $\overline{D}$ is

the mean dose. For multi-grain aliquots this dependence is given by $OD_{abs}(Gy) = 0.093 \cdot \overline{D} + 0.030$.

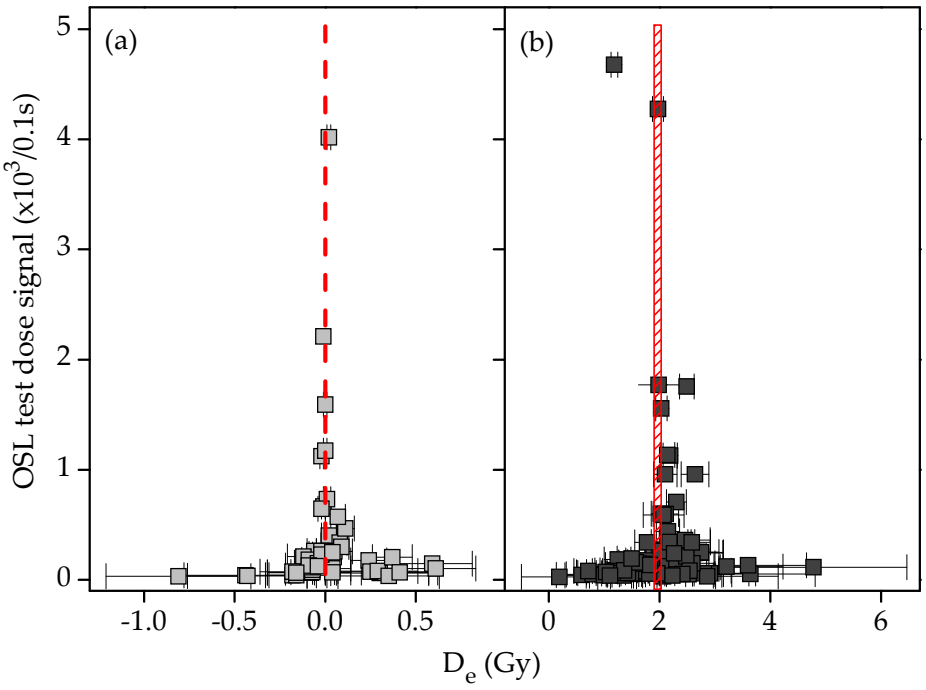

Figure 4.10. Single grains dose distributions from the fractions measured to determine the dependence of over-dispersion with dose, on (a) the bleached fraction and on (b) gamma dosed fraction, which shows an over-dispersion of 20 ± 4%. CAM averages are shown in each case (dashed line/bar).

4.5.4. Natural dose distributions

4.5.4.1. Single grain dose distributions

For each sample from Rambla de la Viuda sites, 2500 to 3500 grains have been measured resulting in 90-160 passing the rejection criteria outlined in section 2.7; ~5% of the total measured. The natural dose distributions showing the natural test dose signal as a function of the D_e measured are shown in Figure 4.11.

The CAM_{tr} average is shown on the plots (red dashed line/bars). The distributions appear positively skewed (except RVD8-5 and RVD8-3) The CAM_{tr} average is off-set from the majority of doses because of a high dose tail of high doses. These high dose points have generally a low natural test dose response, which typically means that they are known with poor precision. These high dose tails may indicate the presence of incompletely bleached grains. Simple visual inspection of these positively skewed dose distributions suggest that more than 70% of the D_e values belong to an imaginary single Gaussian centred on the low dose peak. These distributions are similar to those observed on single grains from Guadalentin river site (see section 3.5.1).

The dose distribution of the upper most sample from RVD8 site, RVD8-8 (sampled at 82 cm depth), shows a similar behaviour, clearly positively skewed, with a peak centred around the lowest doses and a number of higher D_e values. In contrast, dose distributions of samples RVD8-5 and RVD8-3, sampled at 150 and 332 cm, respectively and therefore older than the overlying units -and their corresponding samples described above-, show a different shape. In these two samples, the distributions are symmetric around the mean value, showing a Gaussian shape which contains more than 90% of the measured D_e values. This offers for consideration that a simple identification of outliers and its exclusion from the calculations could be a suitable approach for burial dose estimation as well as the CAM_{tr} model. The CAM_{tr} averages for dose distributions from samples RVD8-5 and RVD8-3 are consistent with the majority of points thus it will not bias the estimated values. These suggest that these two samples are not affected by incomplete bleached grains. This may therefore indicate a difference in the events causing the deposition of these two units from the events causing the deposition of the remaining units measured in this work.

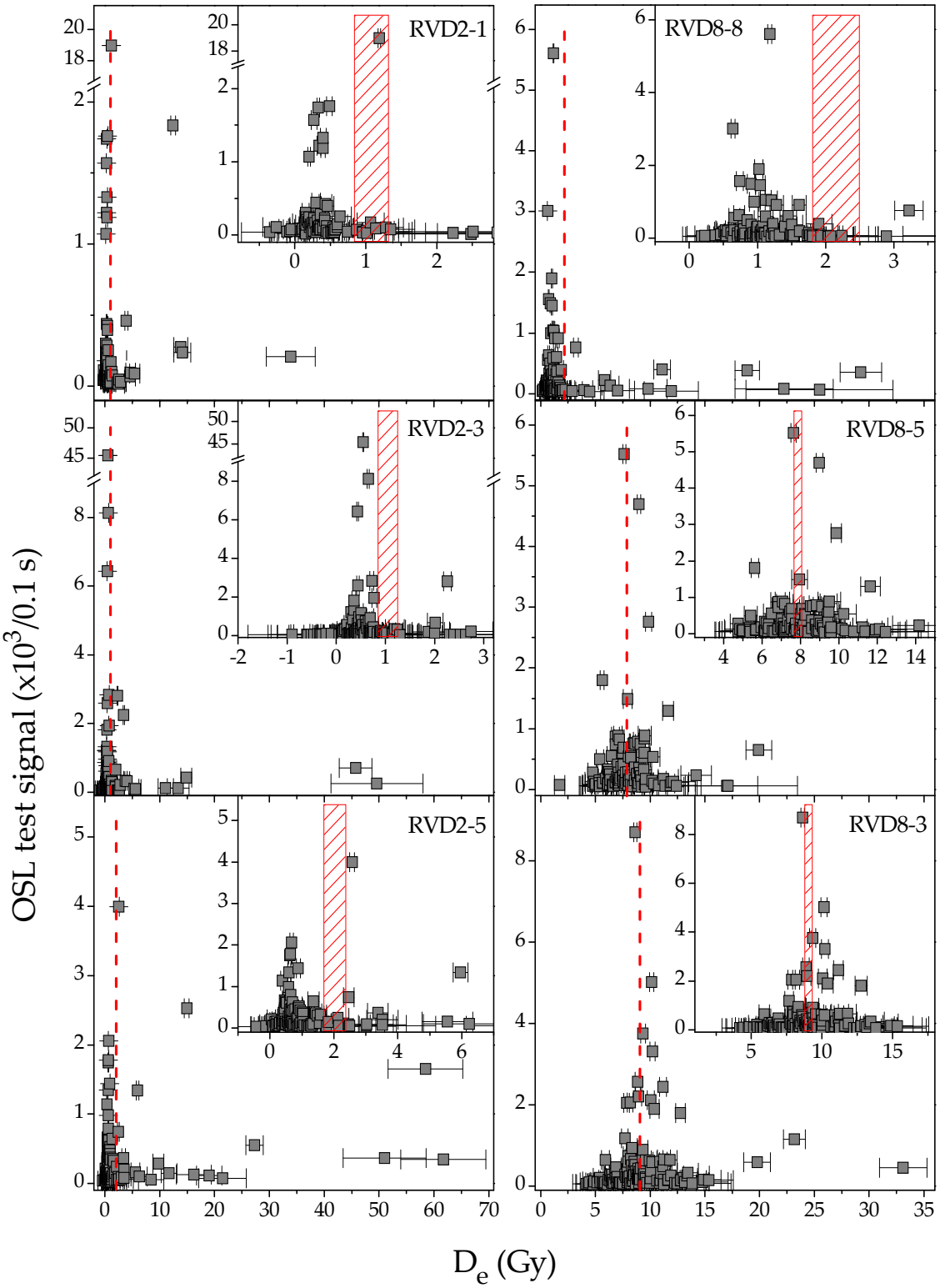
RVD2-1
RVD8-8
RVD2-3
RVD8-5
RVD2-5
RVD8-3
OSL test signal (x10^3/0.1 s)
D_e (Gy)

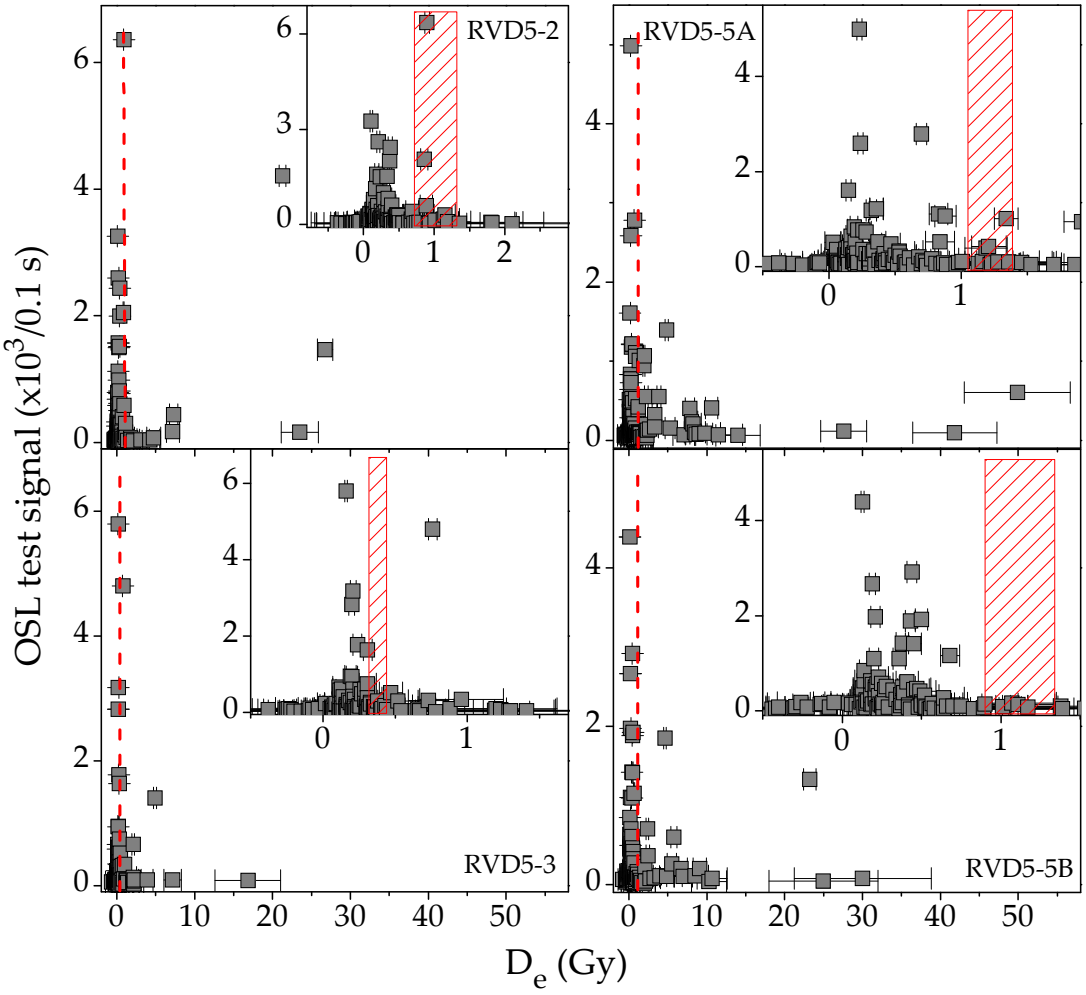

Figure 4.11. Dose distributions of samples from Rambla de la Viuda sites: RVD2, RVD8 and RVD5. CAM_{tr} averages (dashed red lines/bars) are shown on the figure. Insets show a close up of the data.

Samples from the RVD5 site were collected from different stratigraphic units located at depths varying from 50 cm to 170 cm. Thus, different ages are expected for them and therefore different burial doses (accounting for the similar dose rates measured, Table 4.2). In contrast to the expectation, the dose distributions of these four samples show a main peak centred on the approximately same dose value. It can be anticipated that

estimating the slight differences in their ages may not be possible even using minimum age models.

The estimated burial doses using each approach, over-dispersion of the natural distributions estimated with CAM_{tr} and the percentage of grains contributing in each case are summarized in Table 4.3.

Sample	Average	Robust average		CAM_{tr}			IEU		MAM_{tr}	
	D_e (Gy)	D_e (Gy)	n (%)	D_e (Gy)	n	OD(%)	D_e (Gy)	n (%)	D_e (Gy)	n (%)
RVD2-1	1.5 ± 0.5	0.36 ± 0.03	82	1.1 ± 0.2	90	203 ± 29	0.28 ± 0.02	63	0.33 ± 0.03	82
RVD2-3	1.7 ± 0.5	0.50 ± 0.03	86	1.0 ± 0.2	135	198 ± 36	0.38 ± 0.02	59	0.48 ± 0.03	86
RVD2-5	3.3 ± 0.8	0.70 ± 0.04	80	2.0 ± 0.3	129	181 ± 26	0.61 ± 0.02	75	0.65 ± 0.02	80
RVD5-2	1.1 ± 0.3	0.27 ± 0.02	83	1.0 ± 0.3	127	321 ± 32	0.19 ± 0.01	60	0.29 ± 0.03	83
RVD5-3	0.6 ± 0.2	0.20 ± 0.02	77	0.38 ± 0.06	125	153 ± 19	0.19 ± 0.01	76	0.22 ± 0.03	77
RVD5-5A	2.1 ± 0.5	0.45 ± 0.04	80	1.2 ± 0.2	158	162 ± 20	0.22 ± 0.01	54	0.32 ± 0.03	80
RVD5-5B	1.6 ± 0.4	0.31 ± 0.03	80	1.1 ± 0.2	129	220 ± 23	0.16 ± 0.01	45	0.28 ± 0.03	80
RVD8-8	3.0 ± 0.7	1.08 ± 0.04	86	2.2 ± 0.3	108	159 ± 22	0.94 ± 0.03	74	0.99 ± 0.03	86
RVD8-5	8.1 ± 0.2	7.59 ± 0.14	90	7.9 ± 0.2	113	24 ± 3	7.7 ± 0.2	97		90
RVD8-3C	9.2 ± 0.3	8.6 ± 0.2	93	9.1 ± 0.3	130	32 ± 4	8.5 ± 0.2	93	8.7 ± 0.2	93

Table 4.3. Estimated doses for Rambla de la Viuda samples measured single grains using simple average, robust average, CAM_{tr}, IEU and MAM_{tr}. No results was obtained for sample RVD8-5 using MAM_{tr} model. The over-dispersion of the distributions calculated with CAM_{tr} is summarized. The percentage of grains included in each estimation and the total number of grains (n) passing the rejection criteria are also shown. Samples from each site are summarized following increasing depth order.

4.5.4.2. Multi-grain small aliquots distribution

Three of the samples were also measured using small multi-grain aliquots containing ~30 grains each. From the single grain dose distributions is likely that multi-grain aliquots from the RVD2 and RVD5 sites and sample RVD8-8 are very likely to contain grains with significant residual doses. On the other hand, from cumulative light sum plot it is shown that the luminescence signal is dominated by the signal from less than 10% of the grains. Therefore, in a multi-grain aliquot of ~30 grains, it is expected only 1-5 grains giving OSL signal and thus, it can be assumed that a number of the multi-grain aliquots measured will behave like single grains. From the analysis of single grain dose distributions it has been estimated that ~50-70% of the grains are well-bleached. Putting these conclusions together, it is likely that the light derived from some multi-grain aliquots will come only from well-bleached grains. Some others will be affected by grains with a residual dose and thus a minimum age model has been applied to identify the aliquots with only well-bleached grains contribution from those showing a dose corresponding to incompletely bleached ones. This is same procedure used in chapter 3 as multi-grain aliquots measured were showing this same behaviour (section 3.5.2). The use of minimum age models makes it possible to obtain accurate burial dose estimates using small multi-grain aliquots even for samples suffering from incomplete bleaching.

4.5.5. Age calculation

The burial dose and the corresponding ages have been calculated for each sample (Aitken, 1998). The same methods as those used to estimate the burial doses in the Guadalentin samples have been applied to these samples from Rambla de la Viuda; although for determining final age estimates, those derived from the IEU approach using single grains have been chosen as it was previously observed, when comparing to known ages, that this approach obtained the best estimates.

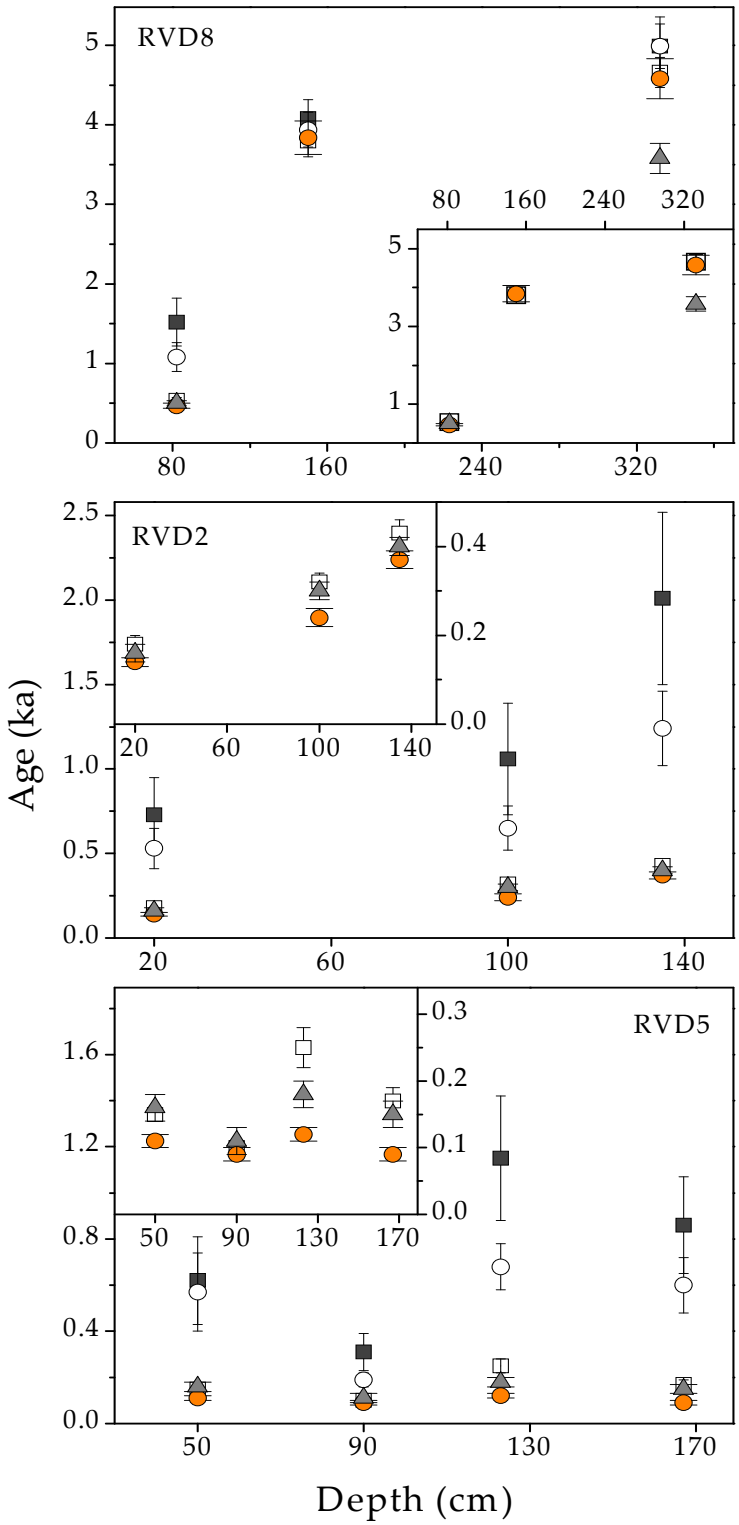

Figure 4.12. Estimated ages for all the samples from the RVD2, RVD5 and RVD8 sites using the different approaches: simple average (solid square), robust average (open square), CAM (open circle), IEU (solid circle) and MAM_{tr} (solid triangle). MAM_{tr} estimate is not shown for sample RVD8-5 as the model did not converge to a result. Inset shows a close up of the three approaches believed to get the most accurate results: robust average, IEU and MAM_{tr}.

Comparison of the corresponding calculated ages is shown in Figure 4.12. As expected for samples with contribution of incompletely bleached grains, both, simple average and the CAM_{tr} model, clearly over-estimate de burial dose deriving in an average over-estimation of 800 years (500%) and 500 years (300%) for simple average and CAM_{tr}, respectively, from those obtained using the IEU approach. That is not the case of the two oldest samples from RVD8 site, RVD8-8 and RVD8-5, for which the determined ages, despite being also over-estimated, the over-estimation is less than 40% (~1.4 ka) the values from the IEU approach. This is in agreement with the conclusions from observation of the dose distribution which showed a symmetric distribution with a peak centred at the mean value, characteristic of well-bleached samples, for these two samples.

Robust statistics derives in age estimates consistent within two standard errors with those from the IEU approach. Specifically, the estimates for samples RVD8-8 and RVD8-5 are similar to those from the IEU approach.

The MAM_{tr} and the IEU obtain very similar values; those from MAM_{tr} presenting a slight systematic tendency to older ages: ~50 years. Converging problems were found when applying MAM_{tr} to sample RVD8-5.

4.5.6. Discussion

Intense, short-live rainfall episodes associated to mesoscale convective systems, commonly originated during autumn months, lead to extreme floods in the in the Mediterranean river basins (Llasat and Puigcerver, 1990). During these high energy flood events, river channel and valley sides including areas of slackwater deposition and thus, palaeoflood deposits, may be affected by erosion. Due to this erosion, palaeoflood deposits older than 2-3 thousand years are not expected to be found (Benito *et al*., 2008).

The fast transport of sediments during the events brings for consideration the possible partial bleaching of the grains within the deposits, and due to the young age range expected for the collected samples, that effect may be significant to the age estimation

(Jain *et al*., 2004; Medialdea *et al*., 2011). As stated by several authors (e.g. Olley *et al*., 1999; Ballarini *et al*., 2007) the presence of poorly bleached grains within a sample could be identified by dose distribution analysis of single grains thus, samples from Rambla de la Viuda have been measured using single grains.

Dose distributions for RVD8-8 and RVD8-5, and the fact that the age estimates do not vary significantly among the different approaches used, indicate that all grains from these two samples were completely bleached. However, this is not the case of the remaining eight samples which show clear indications of contribution from partially bleached grains. This suggests that samples RVD8-8 and RVD8-5 were exposed to light time enough to bleach homogeneously all grains prior to deposition, most probably due to a slower deposition rate at a shallow stagnated depositional environment, as could be expected from slackwater deposits.

Samples collected from RVD5 correspond to four different flood units. These four units comprise a total thickness of 120 cm. Their estimated ages do not show a coherent stratigraphic order. The IEU and the MAM_{tr} approaches show consistent values with a mean age of 100 ± 10 years and 150 ± 20 years, respectively. This suggests that all four units were deposited in a high suspended load environment and/or with a fast deposition rate. However the gap time between deposition of RVD5-3 and RVD5-2 was long enough to allow vegetation to develop on their respective buried soils (see Figure 4.5). Observation of the stratigraphic profile together with these results might also indicate that samples RVD5-5A and RVD5-5B belong to the same flood event or the time elapsed between the two is too short to be discerned by luminescence dating (less than 10 years).

The measurement of multi-grain aliquots from three of the ten samples shows that despite the contribution of incomplete bleached grains, IEU succeeds identifying the aliquots with contribution from only well-bleached grains thus, achieving accurate burial doses. Results from cumulative light sum analysis, consistent with previous studies (Duller *et al*., 2000; Jacobs *et al*., 2003) suggest that a number of the small multi-

grain (~30 grains) aliquots measured behaved like single grains (Rhodes, 2007) and thus, minimum age models can be used estimate the true burial dose.

The cumulative light sum plot shows a similar behaviour to that found among samples from Guadalentín river; showing that 80% of the total light comes from less than 12% of the grains thus indicating that luminescence response is similar in both cases, in agreement with previously published results (Duller, 2008). Despite these similarities, 5% of the grains from Rambla de la Viuda passed the selection criteria outlined in section 2.7 while only 2% of grains from Guadalentín passed it. Since, from cumulative light sum, it is known that this is not related to the number of grains with luminescence emission, it might be indicating that grains in either site come to the deposition location from different sources.

4.6. **Huebra River**

4.6.1. Study area

The Huebra River is a tributary of the Duero River with its confluence at Saucelles, in the international reach known as Arribes de Duero. The Huebra River has a length of 122 km and a catchment surface area of 2880 km^2. Lithology at the Huebra catchment is dominated by granitoids, palingenetic granites with two micas and calcoalcalinic granite of Paleozoic age, related with the Hercinic orogenesis. Other lithologies outcroping in the catchment are metamorphic rocks linked to the granite intrusion, namely schists and gneis, and pre-hercinic materials, as well as Cambrian and Ordovicic roks including shales and quartzites. The river valley is incised in the described lithologies with frequent bedrock gorges which are more prominent towards its lower reach at the confluence with the Duero River in the Arribes region. The slackwater flood deposits described in this chapter are located in this lower reach between the villages of Cerralbo and Bermellar (Figure 4.13).

Figure 4.13. Sites location map showing the confluence of Duero and Huebra rivers.

The Huebra's flow regime shows maximum mean discharge at the end of the winter and early spring; the former associated with the Altantic frontal systems crossing the Iberian Peninsula and the later due to snowmelt contribution from its headwaters at the Sierra de Francia (Central Range). The minimum discharges are produced during summer and early autumn. Floods occur mainly in January and February, with a second maximum in May. The highest flood frequency occurred during the 1960s (peak flow reaching 865 m^3s^{-1} on January 31st, 1966), end of the 70s (peak discharge of 519 m^3s^{-1}), as well as a higher irregularity at the end of the 20th Century (maximum peak discharge reaching 563 m^3s^{-1} and minimum of de 4.9 m^3s^{-1}). In the recent pre-instrumental record, the largest floods occurred in 1909 and 1936, with a magnitude higher to the 1966 flood (865 m^3s^{-1}), the largest of the instrumental period. The Huebra river has no flood documentary record, although it is expected a similar flood hydrology behaviour as that exhibited by the Tormes river. The Tormes river in Salamanca shows an increase in flood frequency in the periods around 1500, 1750-1800

and 1850-1900. The largest documented flood in the Tormes River occurred on January 26th - 27th, 1626.

The slackwter flood deposits are located in two reaches, 3 km apart, named as Puente de Resvala and Barrera, respectively (Figure 4.14).

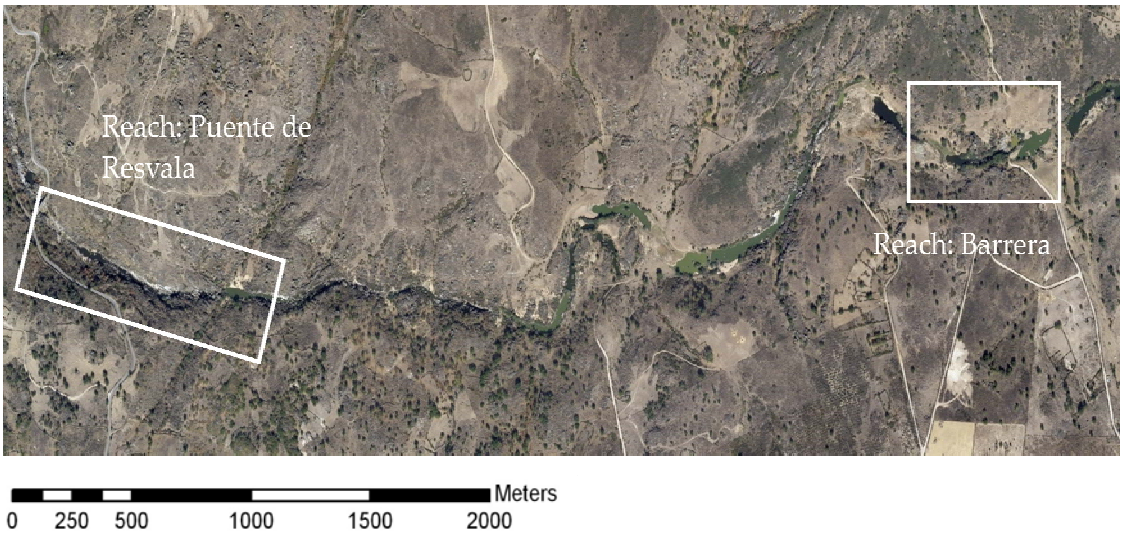

Figure 4.14 Orthophoto showing the two reaches of Huebra river where the palaeoflood study has focused: Puente de Resvala and Barrera.

4.6.1.1. Puente de Resvala

The Puente de Resvala reach is 600 m in length where the river is forming a gorge on pegmatitic rocks. The slackwater flood deposits are located at a junction with a tributary stream entering on the right margin, approximately 50 m upstream of a hydrological gauge station. The geomorphology corresponds to a complex of at least two major eddy bars overlapping the nearby hillslopes. The lower eddy bar (closed to the river course) was deposited by smaller-frequent floods and they were re-worked by the largest floods. The higher eddy deposits were accumulated by the largest floods. In these higher deposits a trench was dug to describe the flood stratigraphy named as R5.

The profile R5 is located at a 3 m cut exposed by the tributary stream. An exposed trench shows at least ten palaeoflood units composed by medium to fine grain sands, with massive structure and frequent bioturbation (Figure 4.15).

Only the four highest units showed horizontal contacts, whereas the lower units showed irregular contacts and occasionally disappear laterally (units 5, 6 and 7). A radiocarbon date at unit 9 provided an age of 4140 ^{14}C years BP (cal AD 2130-2240). The flood discharge associated with the elevation of this profile varies between 400 m^3s^{-1} and 865 m^3s^{-1} for the lowest and upper most units (10 and 1 respectively). In this profile, four samples were collected for OSL dating; two of them, R5-1 and R5-3, were used for this study.

4.6.1.2. Barrera study site

The site is located about 3.2 km upstream of Puente de Resvala site (Figure 4.13). Here the river is incised on pegmatitic rocks that contain dykes with high content of quartz minerals which are highly resistant to erosion. This lithological scheme produces on the river valley expansion reaches where slackwater flood sediments are deposited, alternating with narrow stretches with an effective hydraulic control. In the expansion reaches, flood deposits are accumulated forming "benches" that interfingers with slope deposits. The thickest bench is located at the right side of the Huebra River, near Barrera village.

A stratigraphic profile was described for OSL sampling (B6), although in a previous field work campaign, other profile in similar position was analysed.

4.6.1.3. Profile B6

The profile B6 is 2.7 m in thickness exposing at least six flood units (Figure 4.16). The lowest one (unit 6) shows high bioturbation, and oxides (iron) precipitation indicative of former anoxic conditions. The other five flood units are between 20 and 65 cm in thickness, composed by fine to very fine sands with massive structure and clear stratigraphic contacts although occasionally irregular. All the flood units have

developed an upper incipient soil containing high bioturbation (mainly due to former grass) and darker colour. The lower unit was radiocarbon dated as 5550 ^{14}C years BP (cal 4394 ± 56 BC). Flood units 3 and 6 showed a light brown colour with unit 3 dated as 2210 ^{14}C years BP (cal 272 ± 68 BC). The minimum flood discharge associated with this these levels varied from 463 $m^3 s^{-1}$ for unit 7, between 485 $m^3 s^{-1}$ and 710 $m^3 s^{-1}$ for units 6 to 3, and between 830 $m^3 s^{-1}$ and 905 $m^3 s^{-1}$ for units 2 and 1, respectively.

4.6.2. Dose rate

Dose rate is measured on a 200 g subsample taken from the volume immediately adjacent to the OSL sample. This subsample is prepared for high-resolution gamma spectroscopy as detailed in section 2.9.1. Water content has been measured shortly after sampling. This water content value has been considered representative of the average conditions during the burial time. The cosmic radiation contribution has been estimated according to the depth of the sample location Prescott and Hutton (1994). Depth, water content, contribution of ^{232}Th, ^{226}Ra and ^{40}K to the dose rate and the estimated annual dose rate for each unit have been summarized in Table 4.4.

Sample	Depth (cm)	Wat. cont. (%)	^{226}Ra (Bq/kg)	^{232}Th (Bq/kg)	^{40}K (Bq/kg)	Total dose rate (Gy/ka)
B6-1	22	2	45.0 ± 0.7	44.9 ± 0.7	764 ± 14	4.2 ± 0.2
B6-B	47	5	47.2 ± 0.8	39.7 ± 0.8	912 ± 18	4.4 ± 0.2
B6-2	63	4	41.4 ± 0.7	36.4 ± 0.7	845 ± 17	4.1 ± 0.2
B6-3	104	5	37.5 ± 0.6	36.7 ± 0.7	940 ± 17	4.2 ± 0.2
R5-1	20	6	53.4 ± 0.9	46.7 ± 0.9	849 ± 17	4.4 ± 0.2
R5-3	75	9	57.6 ± 0.9	54.1 ± 1.0	861 ± 18	4.5 ± 0.2

Table 4.4. Annual dose rate of samples from Huebra River. Radionuclides concentration, water content and depth used for the calculation are also summarized in the table.

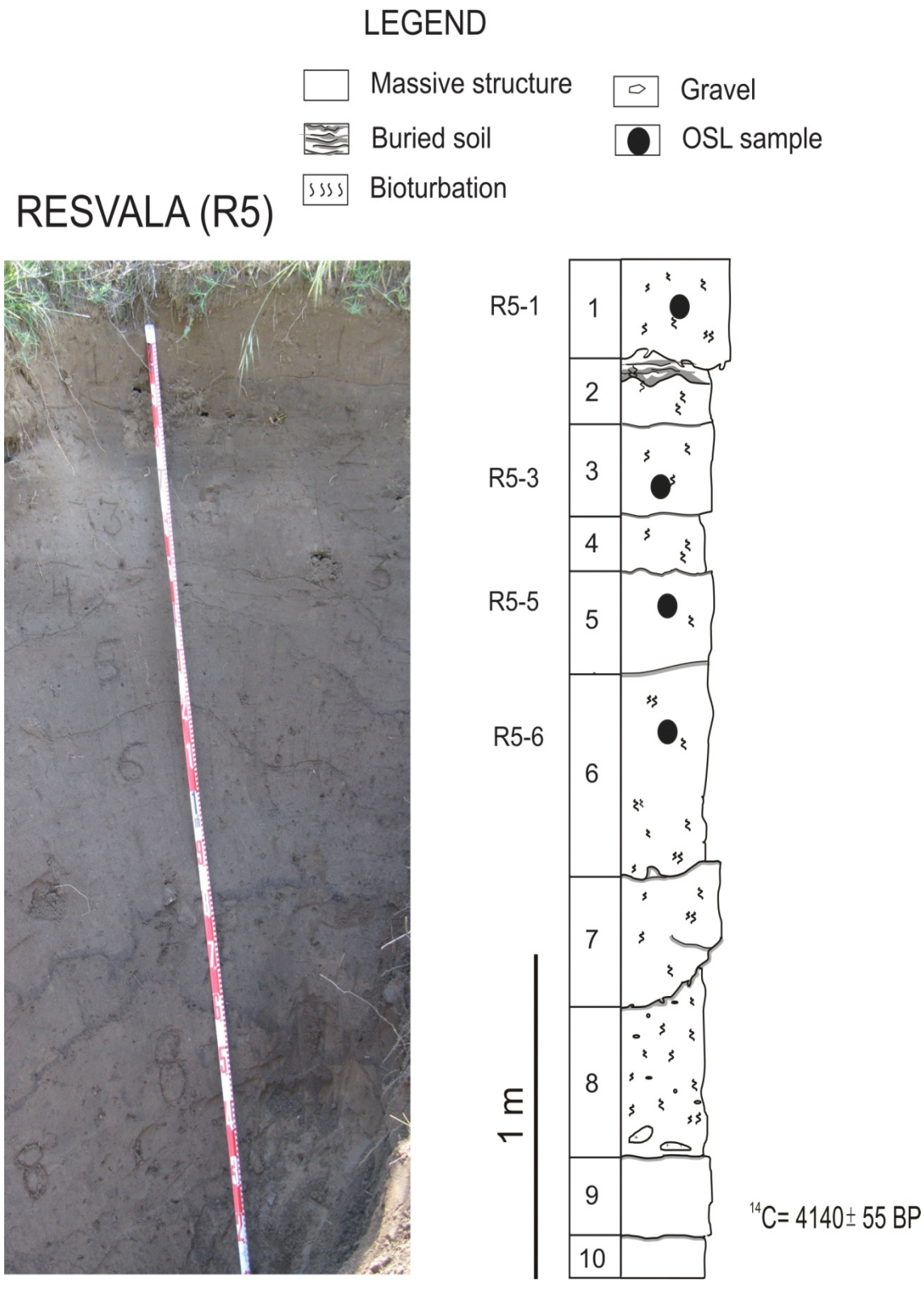

Figure 4.15. Stratigraphic profile R5 (Puente de Resvala site).

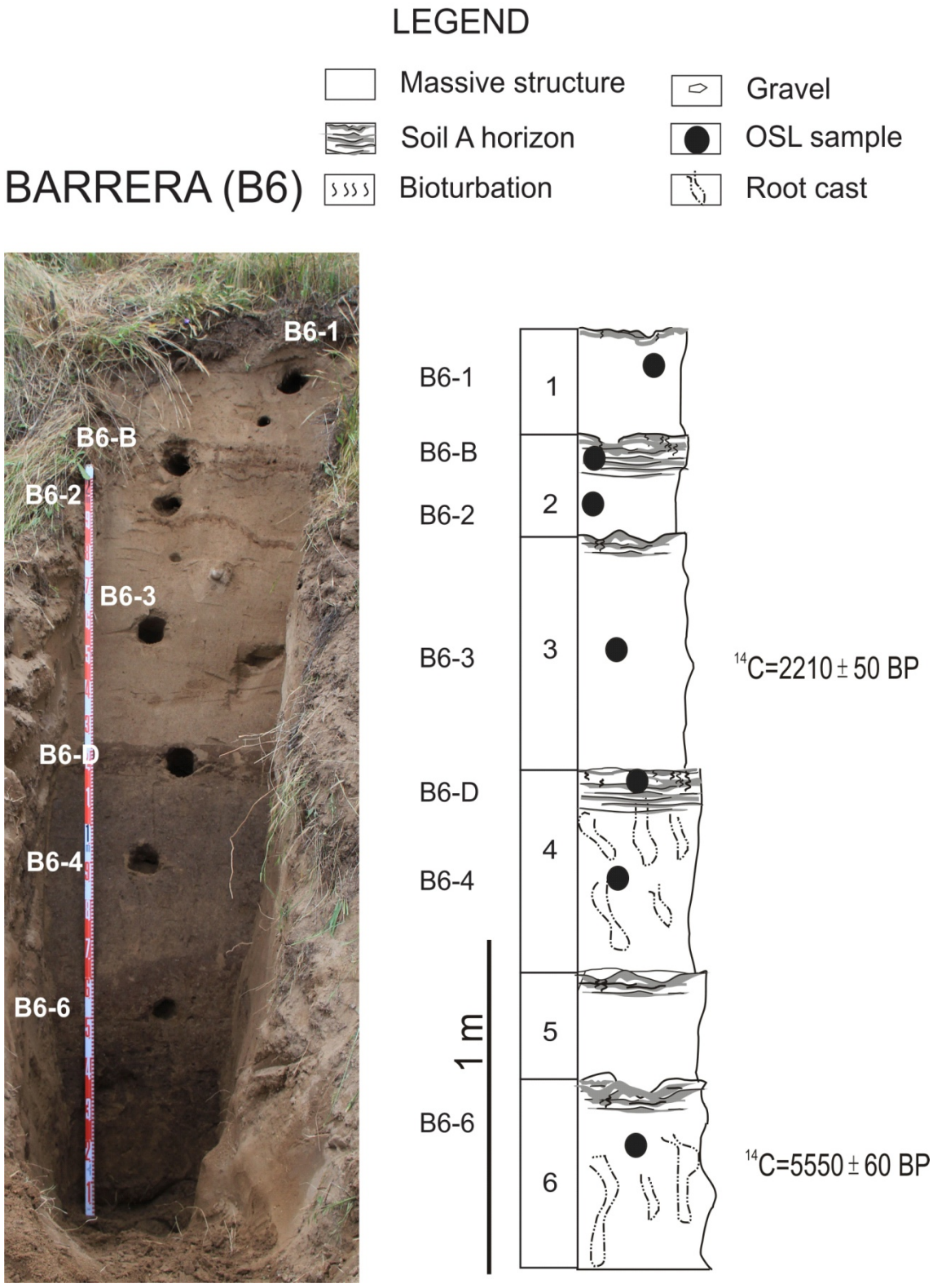

Figure 4.16. Stratigraphic profile B6 (Barrera site).

4.6.3. Luminescence behaviour

Samples from the two sites sampled at Huebra River, B6 and R5, show a large presence of mica after preparation of the quartz fraction. And additional step was included to remove mica by flotation. Mica has been considered not to be reliable as a natural dosimeter but its luminescence emission, both TL and OSL, has been reported (Bárcena *et al*., 1999; Kortekaas and Murray, 2005). In order to avoid possible contribution of the mica luminescence signal on the blue stimulation measurement, an extra step was included in sample preparation to remove mica by flotation to negligible proportion.

Preheat plateau test (data not shown) on multi-grain aliquots (~30 grains) from sample B6-2 indicates that the determined equivalent dose is independent of the choice of preheat temperature in the range 160°C to 260°C. Thermal transfer test on an artificially bleached portion of sample B6-3 has been carried out. As for the preheat plateau test, multi-grain aliquots (~30 grains) have been used to determine the effect of thermal transfer. Preheat temperatures ranging from 160°C to 260°C has been used and an average dose of 30 ± 10 mGy has been measured. These samples are expected to be old enough for this dose caused from thermal transfer to be considered insignificant. Temperatures of 200°C and 180°C have been employed for preheat and cutheat treatments, respectively.

The cumulative natural light sum from single grain measurement of for samples B6-B and B6-2 is shown in Figure 4.17. Both samples show similar behaviour, with 90% of the total light coming from ~3% of the grains measured. 90% of the grains do not contribute significantly to the total light detected contributing with less than 1%. This is in agreement with previously published studies (Duller *et al*., 2000; Jacobs *et al*., 2003) concluding that it is common that 90-95% of the luminescence signal emitted from a sample is derived from 5-10% of the grains or less. On the inset in Figure 4.17 the relation on log scale is shown. The cumulative light sum from a test dose of 10 Gy was also analyzed showing similar results as those from the natural signals.

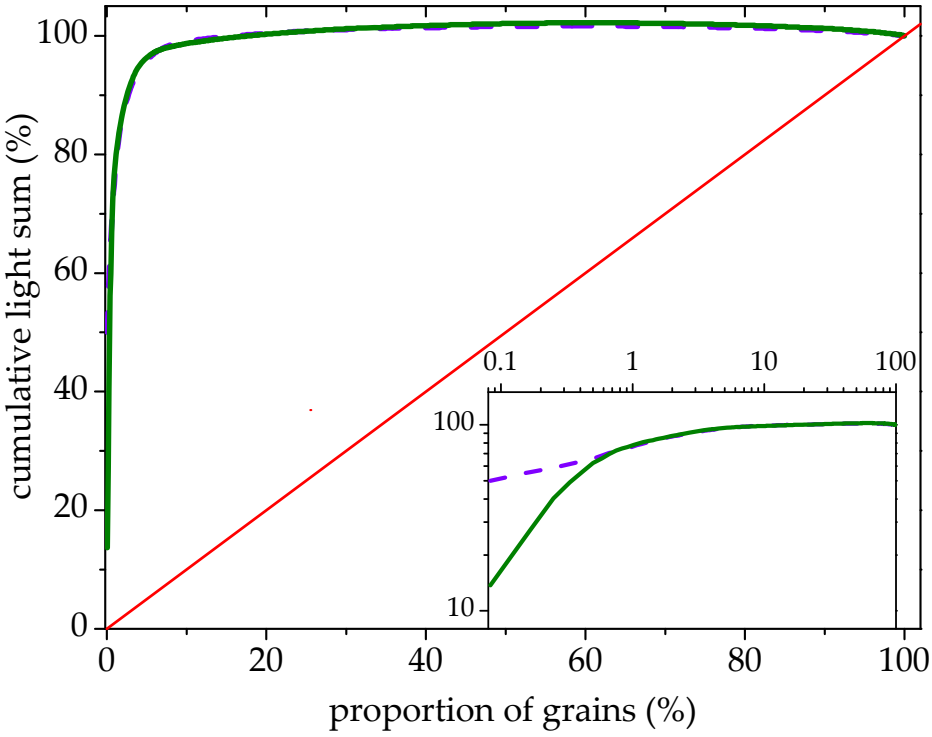

Figure 4.17. The cumulative light sum of the natural signal of single grains from samples B6-B (dashed line) and B6-2 (solid line). The 1:1 line shows the relation in the case all grains where contributing equally. On the inset, the light sum is shown on a log scale. For both samples 90% of the light is derived from ~3% of the grains. ~90% of the grains contribute to less than 1% of the total light sum.

Samples from profile B6 (B6-1, B6-B, B6-2 and B6-3) have been measured using both, single grains and small multi-grain aliquots (~30 grains).

The natural OSL decay curve from a small (~30 grains) multi-grain aliquot has been plotted together with the decay curve of calibration quartz (tested to guarantee its purity) known to be dominated by the fast component. OSL signal (blue upwards triangles on Figure 4.18) show a slower decay than the signal expected from quartz dominated by the fast component (downwards orange triangles). Under the suspicion of feldspar contribution, IR depletion ratio has been measured for samples B6-B, B6-2 and R5-1, by adding an extra cycle including IR stimulation (Figure 4.9). IR depleting ratios are poor, giving average ratios of ~0.8 ± 0.1. In addition, an IRSL signal resulting from IR stimulation is detected through the UV filter (i.e. same filter used to detect the

blue-OSL from quartz). No IRSL signal should be observed if sample were pure quartz (Stokes, 1992). The IRSL detected signal and the poor depletion ratios show that feldspar contribution to the OSL signal is significant for these samples, in contrast with the observation for samples from Rambla de la Viuda for which feldspar contribution could be considered negligible.

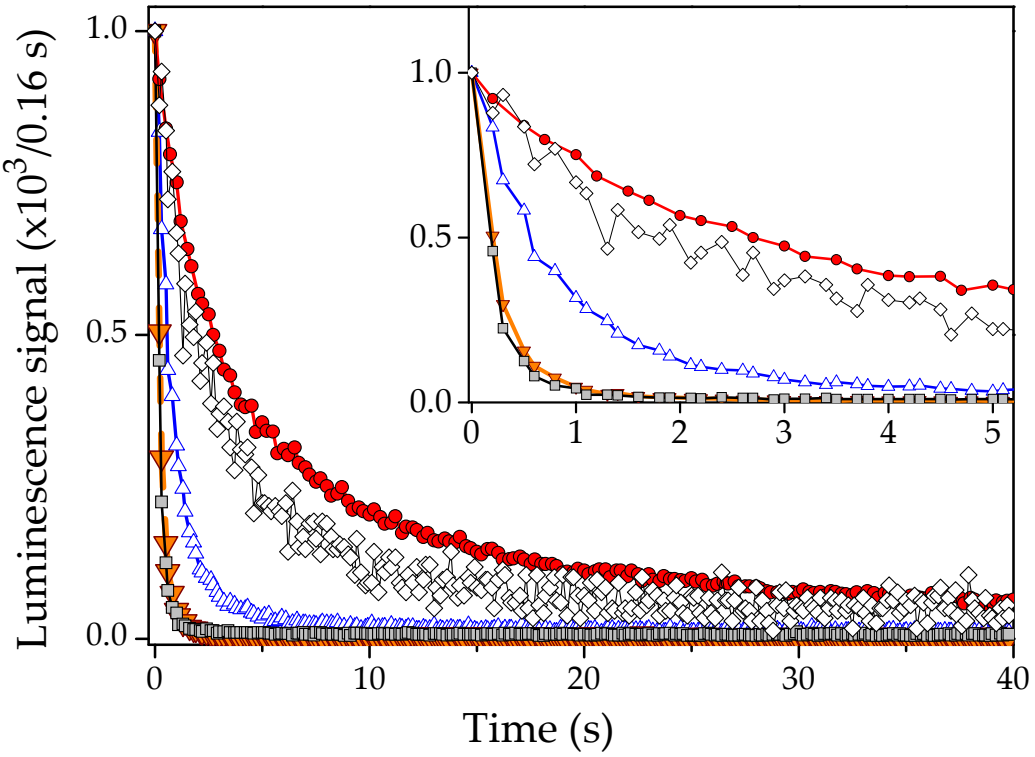

Figure 4.18. Decay curves from sample B6-3. The decay curve when measuring the blue-OSL signal (blue triangles), blue-OSL after IR stimulation (gray squares), both measured using a UV filter, and IRSL signal (red circles) measured through a blue filter. The decay curve of calibration quartz, detected through UV filter is also shown. On the inset the first 5 s of the same normalized decay curves are shown.

Banerjee *et al*., 2001 proposed a "double SAR" procedure to reduce the influence of feldspar. This procedure make use of the IR bleaching step prior to each blue stimulation to reduce the contribution from feldspar to the measured blue stimulated OSL signal. After each preheat, aliquots were stimulated with IR at 125°C and the

corresponding IRSL signal was measured. Blue stimulation at 125°C was then used and the OSL signal was measured. The cycle was repeated after dosing the sample with a test dose to trace and correct possible changes in sensitivity, as it would be done in a standard SAR protocol.

The stimulation with IR results in IRSL and depletes the blue stimulated signal from feldspar. This depletion of the feldspar signal allows enhancing the relative contribution of quartz when the subsequent blue-stimulated OSL is measured. The feldspar contribution is likely to have been reduced significantly but it has been reported that for a polymineral chemically untreated sample the determined D_e values even after IR are affected by the feldspar contribution (Duller and Bøtter-Jensen, 1993).

Therefore, in order to succeed in depleting the feldspar signal to negligible levels, this procedure using IR stimulation, should be applied on samples which have already been treated with fluorhydric or fluorosilicic acid to remove the feldspar (Roberts, 2007). Given that feldspar usually gives very much stronger OSL signal than quartz it is entirely possible that although the feldspar OSL signal has been reduced significantly it is still contributing significantly to the mixed OSL signal. Thus, elimination of a significant portion of the existing feldspar by chemical treatment helps achieving negligible levels of its signal. The blue OSL signal measured after the IR stimulation (i.e. post-IR OSL, gray squares on Figure 4.18) is compared with the decay signal from the calibration quartz (orange downwards triangles). The Post-IR OSL decay curve is clearly dominated by the fast component thus indicating that the depletion of the feldspar signal to negligible levels has been achieved.

All samples from the Huebra River have been measured using the double SAR procedure because all of them had detectable IRSL signals, even after 40% HF treatment. Nevertheless, when using double SAR procedure, estimated doses can be based not only on the blue OSL signal but also on the IRSL signal (Roberts and Wintle, 2003).

A dose recovery test has been measured using a bleached and gamma dosed portion of sample B6-2 to establish whether the applied protocol is able to recover a laboratory

dose. The gamma dose given was 2 Gy and the single grain dose recovery ratio is 1.01 ± 0.06 (n = 100). An over-dispersion of 22 ± 4% was observed in the corresponding dose distribution. Therefore, it can be concluded that the dose cannot be estimated to better than 22% when using single grains. In addition to the uncertainty calculated based on counting statistics an additional uncertainty of 22% is added in quadrature to each individual estimate of uncertainty to account for all quantifiable sources of intrinsic uncertainty.

A dose recovery test on bleached gamma dosed samples was also measured using small (~30 grains) multi-grain aliquots. The dose recovery ratio is 1.2 ± 0.1 (n = 28) and the over-dispersion of the resulting dose distribution is 11 ± 3%.

4.6.4. Burial dose estimates

4.6.4.1. Single grains

1200-1500 single grains were measured for each of the four samples from the Barrera site, 10% of which passed the selection criteria. These four distributions show a similar shape with a symmetric Gaussian centred at the mean value (Figure 4.19). CAM averages are shown on the plots. The over-dispersion values range between 24 ± 4% and 33 ± 5%.

Descriptive statistics calculating the simple average, robust statistics by excluding outliers from average calculation, the CAM model, the MAM model and the IEU have been used to estimate the burial dose. For samples from Barrera site, the exponential transformation (see section 3.3) used for the previously studied sites, Guadalentín and Rambla de la Viuda, was not necessary before applying CAM and MAM as none of the distributions contain negative or zero values.

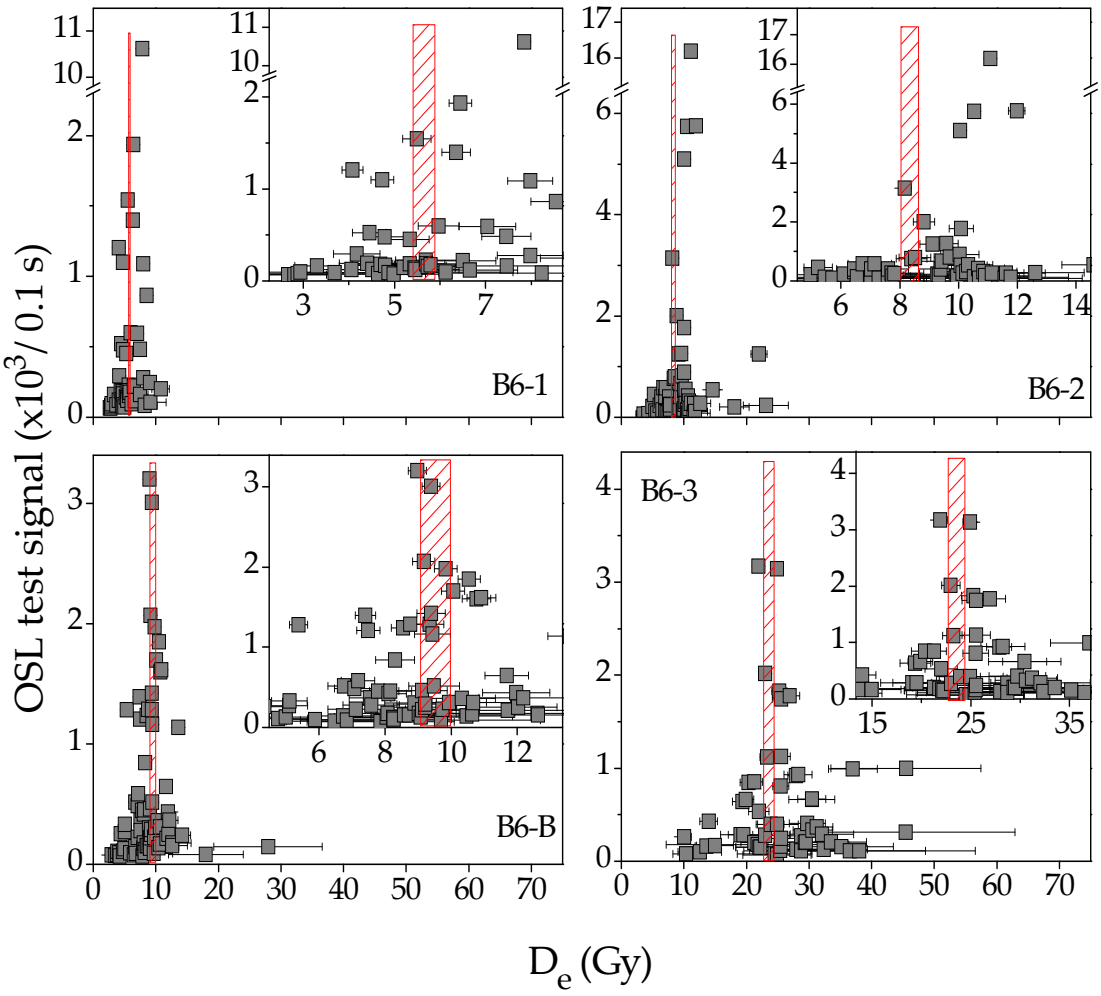

Figure 4.19. Single grain dose distributions of the four samples from the Barrera site. Insets show a close up of the same data. CAM averages are shown in dashed bars (b) Multi-grain aliquots dose distributions of samples from Huebra river: Barrera and Puente de Resvala sites. CAM averages are shown in dashed bars.

When using robust statistics, outliers are identified to be those outside 1.5*IQR (see section 3.3). In all the previous cases studied in this work (Guadalentin and Rambla de la Viuda) all identified outliers belonged to the high dose part of the distributions; none of the lowest D_e values were identified with this criterion as outliers. However, three (B6-B, B6-2 and B6-3) out of the four samples from the Barrera site have low dose outliers indicating a more symmetric distribution. The robust average has been calculated excluding all the identified outliers. The proportion of grains included in the average and the values obtained are summarized in Table 4.5. The robust average is

systematically a little smaller than the arithmetic average but the difference is mainly insignificant confirming the symmetry of the dose distributions.

The weighted average has been calculated using the original CAM (Galbraith *et al*., 1999). Estimated burial doses are very similar to those estimated using both, the arithmetic mean and the robust average.

The fact that these three approaches give very similar results indicates that any possible existing contribution from incompletely bleached grains is not significant. On the other hand, if the samples were completely bleached at deposition and if there are no additional sources of uncertainty other than those derived from intrinsic sources then, the over-dispersion of the natural distributions should be similar to that obtained from the gamma dose recovery test (22 ± 4%). The calculated over-dispersions in percentage for the natural dose distributions are 26 ± 5, 29 ± 5, 33 ± 5 and 24 ± 5 for B6-1, B6-B, B6-2 and B6-3, respectively. These over-dispersion values are systematically higher than those from the gamma dose recovery (22 ± 4%). These differences may arise from other sources of extrinsic uncertainty than incomplete bleaching such as small scale beta dose rate heterogeneity (Mayya *et al*., 2006), but at this point the contribution of incompletely bleached grains cannot be discarded. However it may also be that the variability arising from intrinsic factors has been underestimated. Thomsen *et al*., 2012 showed that the relative over-dispersion in their dose recovery experiments was not constant as a function of dose (Figure 4.20).

	Sample	Average	Robust average		CAM			IEU	
		De	De	n (%)	De	n	OD (%)	De (Gy)	n (%)
Single grains	B6-1	5.7 ± 0.3	5.5 ± 0.2	94	5.6 ± 0.2	48	26 ± 5	5.2 ± 0.2	87
	B6-B	8.9 ± 0.4	8.8 ± 0.2	86	8.3 ± 0.3	76	29 ± 4	6.0 ± 0.3	96
	B6-2	9.7 ± 0.5	9.0 ± 0.3	88	9.5 ± 0.4	58	33 ± 5	8.8 ± 0.3	67
	B6-3	25.4 ± 1.0	25.2 ± 0.7	90	23.6 ± 0.8	59	24 ± 4	23.2 ± 0.8	92
Multi-grain aliquots	B6-1	5.4 ± 0.1	5.3 ± 0.1	82	5.39 ± 0.13	74	21 ± 3	5.27 ± 0.14	69
	B6-B	8.9 ± 0.3	8.2 ± 0.2	89	8.7 ± 0.3	72	25 ± 4	8.4 ± 0.2	97
	B6-2	11.3 ± 0.5	10.3 ± 0.4	91	11.2 ± 0.5	54	33 ± 5	9.5 ± 0.4	44
	B6-3	25.2 ± 0.4	25.0 ± 0.3	92	25.2 ± 0.4	64	12 ± 2		
	R5-1	3.1 ± 0.3	2.3 ± 0.2	88	2.9 ± 0.2	94	82 ± 9	0.73 ± 0.05	12
	R5-3	21.6 ± 0.4	20.8 ± 0.3	92	21.5 ± 0.4	104	17 ± 2	21.5 ± 0.4	100

Table 4.5. Burial dose estimates of samples from Huebra River using simple average, robust average, CAM model and IEU model. MAM model presented converging problems thus, no dose estimates were obtained. Results correspond to measurements using single grains for samples from B6 site and measured using small (~30 grains) multi-grain aliquots for samples on B6 and R5 sites. IEU approach was not able to estimate a dose for sample B6-3 measured using small multi-grain aliquots, very likely due to a wrong uncertainty assigned to the calculation.

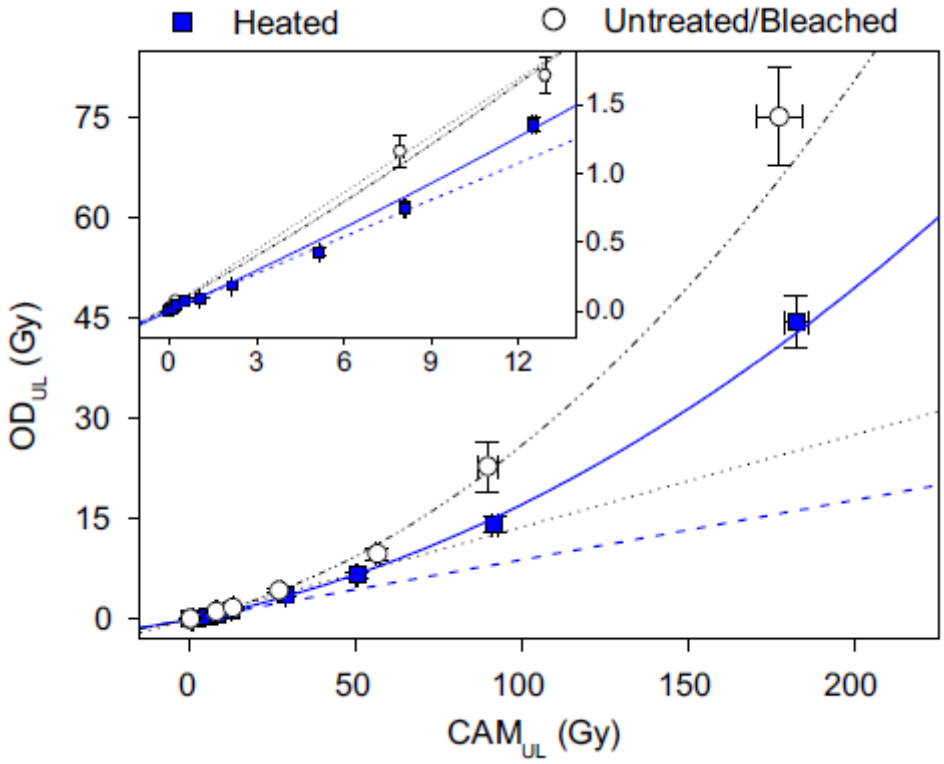

Figure 4.20. Over-dispersion as a function of CAM dose. The closed squares represent heated samples, the open circles represent untreated/bleached samples. For both data sets a second order polynomial fits is shown (solid line and dash dot line, respectively. A linear fits for doses <10 Gy is also shown. The inset shows a close up of the same data for doses less than 13 Gy. Taken from Thomsen et al., 2012.

The implication of this observation is that one should perform the dose recovery experiment at a dose similar to the natural dose. The gamma dose given here was 2 Gy but the natural doses range between ~6 and 24 Gy. Thus, it may be that the intrinsic variability is larger for a larger given dose. If this is the case, IEU estimates would be higher. Dose recovery experiment at doses higher than 2 Gy has not been carried out so the possibility of uncertainty being underestimated cannot be discarded.

Other possible cause of the additional dispersion observed could be the beta dose rate heterogeneity. If this was to be the cause then the CAM dose estimate can be considered the most appropriate.

4.6.4.2. Bleaching degree assessment

It has been reported that the difference between the relative bleaching rates of quartz and feldspar can be used to assess if quartz was well-bleached prior to deposition (Murray *et al.*, 2012). It has been shown that the IRSL signals from feldspar bleach much more slowly than the OSL signals from quartz (e.g. Godfrey-Smith *et al.*, 1988; Thomsen *et al.*, 2008; Buylaert *et al.*, 2011). The difference in bleaching rate between quartz and potassium-rich feldspar measured at 50°C is approximately one order of magnitude (Figure 4.21).

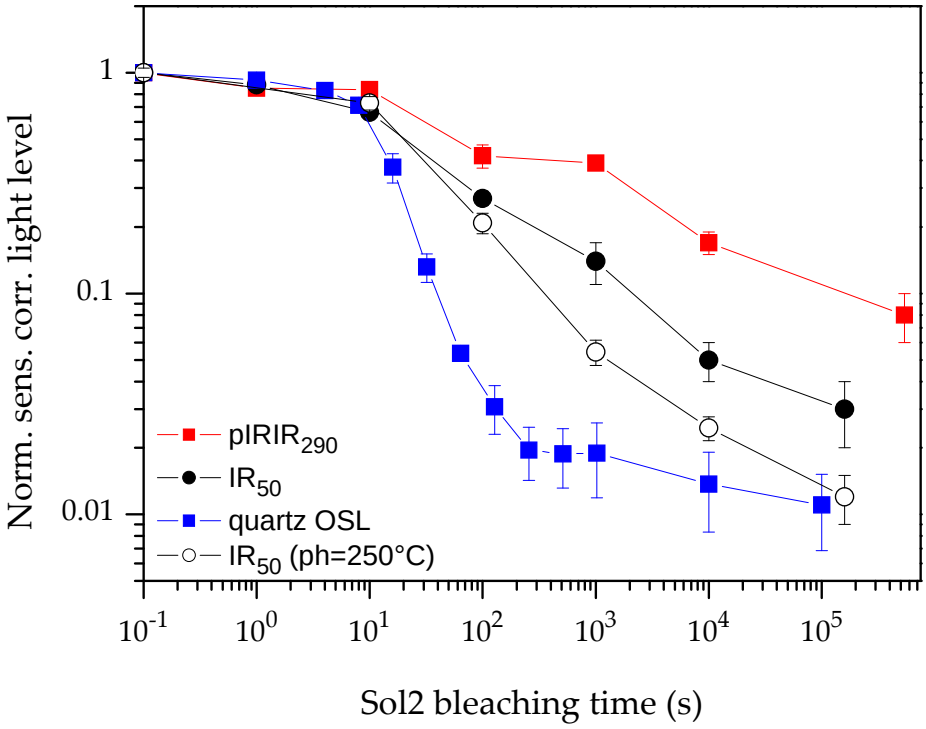

Figure 4.21. Sensitivity-corrected feldspar IR50, pIRIR290 and quartz OSL plotted against exposure time in a Hönle SOL2 solar simulator. Each data point is an average of three samples and error bars represent one standard error. For feldspar at least three aliquots of each sample were measured at every exposure time; for quartz, at least eight aliquots were measured per sample at every exposure time. Taken from Buylaert, 2012.

Thus, if quartz and feldspar give comparable dose estimates then quartz has to be well-bleached. For this purpose, six multi-grain aliquots of each sample have been stimulated with IR at 50°C and the corresponding signal has been detected through the standard blue filter combination (2 mm BG 39 and 4 mm 7-59). These measurements have been done on the feldspar contained in the quartz fraction since feldspar fraction was not kept during preparation of these samples. A normalized IRSL decay curve of sample B6-3 is shown in Figure 4.18 (red circles). The slower decay the quartz signal can be observed.

SAR protocol was applied using 250°C during 60 s for preheat and cutheat. A test dose of 10 Gy was used. IR at 180°C was employed and the consequent IRSL signal was measured through the standard blue filter combination (2 mm BG 39 and 4 mm 7-59). At the end of each cycle, a clean out with IR at 280°C was used to guarantee that no signal was left from the previous cycle. The estimated doses resulting from the IRSL signal of the feldspar within the quartz fraction prepared are similar to those estimated using the post IR OSL signal from quartz. To estimate an accurate burial dose from feldspar, the fading of the signal should be taken into account. If feldspar were incompletely bleached, the dose estimate derived from feldspar would be significantly higher than that from quartz so no more precise estimates are necessary to confirm the complete bleaching of feldspar. The ratios between the dose estimate based on the blue-OSL from quartz and the IRSL from feldspar vary between 1.09 ± 0.13 and 0.99 ± 0.08. Therefore it can be concluded that the feldspar contained in the quartz fraction of samples from B6 are well-bleached and consequently it can be concluded that quartz grains are well-bleached.

4.6.4.3. Small multi-grain aliquots

It was previously concluded that, based on results from Guadalentín River and Rambla de la Viuda, accurate burial doses can be estimated using small multi-grain aliquots.

Even though, small multi-grain aliquots (~30 grains) have also being used for these samples to confirm that the different lithology of the sediments do not affect this conclusion. 48-80 aliquots have been measured for each of the four samples from Barrear site. Dose distributions from multi-grain aliquots of B6 samples are similar to those found using single grains (Figure 4.22). The CAM model is used to estimate the burial doses finding consistent results with those obtained from single grains. Also robust average obtains consistent estimates and even unweighted simple average including all dose points results in consistent values, though showing a systematic tendency to higher estimates (~2% higher). This behaviour is to be expected from a well-bleached sample confirming that the conclusion achieved in section 4.6.4.2.

The confirmation of the complete bleaching of these sample show that a dose estimate derived from the measuring of multi-grain aliquots and the calculation of a weighted mean (i.e. CAM model) will result in accurate values. Again in this case, the use of single grain measurements was not necessary to estimate accurate burial doses.

Therefore, the remaining samples from Huebra River, the two samples (R5-1 and R5-3) from Puente de Resvala site, are directly measured using small multi-grain aliquots of quartz, applying IR stimulation prior to the detection of the blue-OSL signal to deplete contribution from feldspar. Burial doses have been estimated using robust average since it has shown to give similar results to those obtained from CAM. Dose distributions and the CAM averages are shown on Figure 4.22.

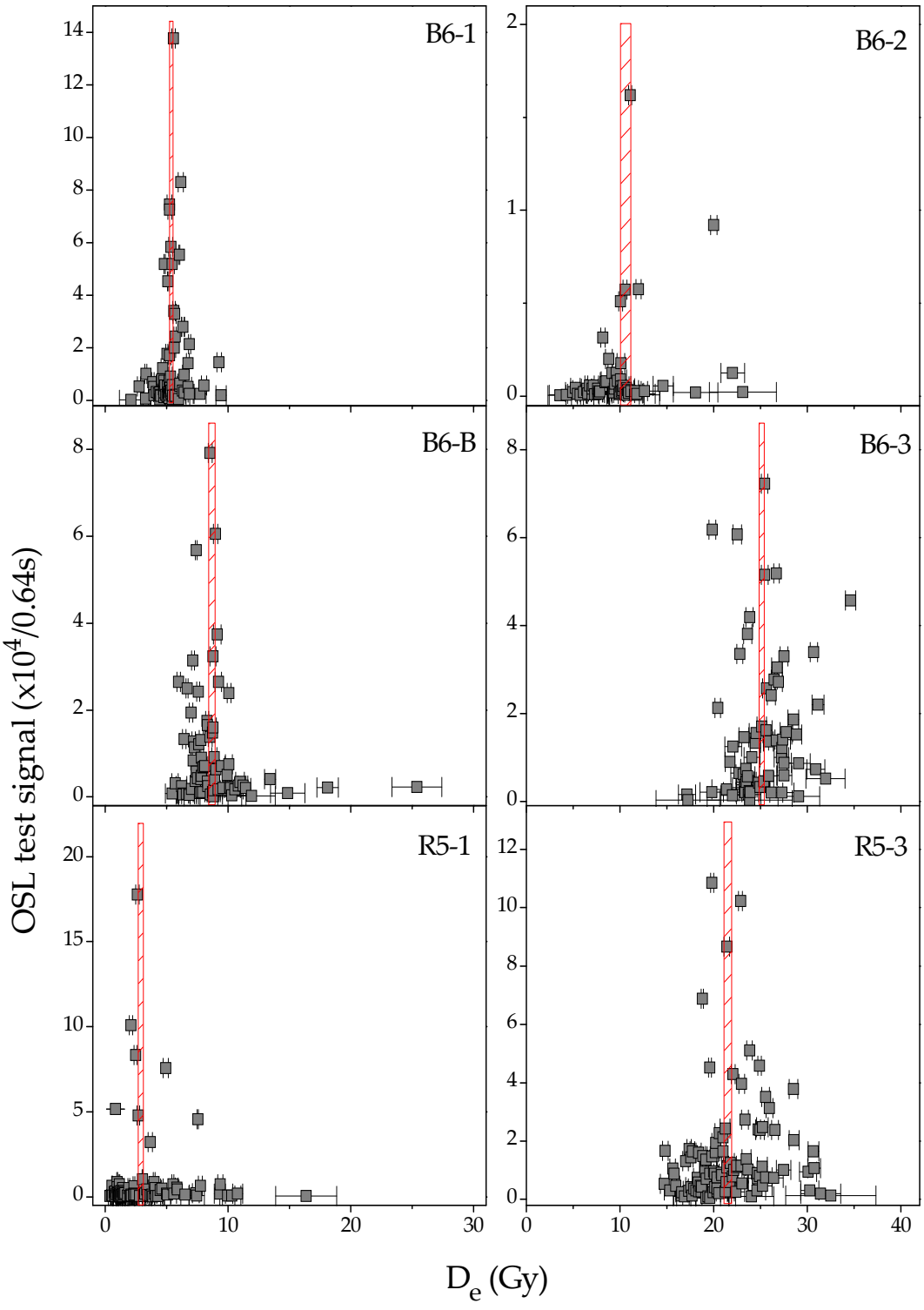

Figure 4.22. Multi-grain aliquots dose distributions of samples from Huebra river: Barrera and Puente de Resvala sites. CAM averages are shown in dashed bars.

4.6.5. Minimum age models applied to well-bleached samples

Minimum age models were originally made to analyze single grain dose distributions of young samples -although they have been applied is some cases to old samples, e.g. Olley et al., (2004) which applied MAM to samples with burial doses of ~30 ka and also Gabraith et al., (1999) use MAM on dose distributions from old samples- containing certain contribution of incomplete bleached grains. These are identified and either assigned a smaller weight in the dose calculation (MAM model) or they are excluded for the burial dose estimation (IEU model).

Given the shape of the dose distribution and the relatively small over-dispersion it seems very likely that the most appropriate way to estimate the burial dose is to calculate an average/CAM. However in the following, the minimum age models are applied to investigate if they can be used for well bleached samples as well.

In an attempt to use the MAM, model conversion problems were encountered for all four samples from Barrera site. The profile log-likelihood function of the mean (μ), sigma (σ) and proportion of well-bleached grains (ρ) do not show a bell shape and do not have well-defined confidence intervals. This lack of convergence for one or more of the parameters should be taken as evidence that the estimated burial doses are unreliable (Arnold *et al.*, 2009) and we are thus unable to provide MAM burial dose estimates.

The IEU approach is not expected to be limited by the bleaching degree of a sample but it has a strong dependence on the assigned uncertainties.

To apply IEU, results from gamma dose recovery experiments are used. IEU considers that the extra uncertainty necessary to account for the observed variability is not constant but varies with the dose. This dependence has been determined using the values of dose and over-dispersion of a bleached sample and the dose and over-dispersion of the 2 Gy gamma dosed sample from gamma dose recovery test. The fit linear between these values gives the relation $OD_{abs}(Gy) = 0.210 \cdot \overline{D} + 0.014$.

The model identifies over 85% of the measured grains to be well-bleached in samples B6-1, B6-2 and B6-3 and burial dose estimates are consistent within one sigma with estimates determined using the weighted mean (CAM). For sample B6-B, only 40% are identified to be well bleached and the burial dose estimate is significantly lower than that estimated with CAM but still keeping the coherence with the stratigraphy (further details in section 4.6.6).

Thomsen et al., 2012 showed that the relative over-dispersion in their dose recovery experiments was not constant as a function of dose (Figure 4.20) but was increasing with the dose for doses over 10 Gy. Therefore, in order to assess an appropriate over-dispersion to account for the intrinsic variability, the dose recovery test should be performed at a dose similar to the natural dose. In the Barrera site samples, the natural doses range between ~6 and 24 Gy. Therefore, the assessed uncertainty based on the results obtained from the 2 Gy gamma dose recovery experiment may lead to smaller uncertainties than those necessary to account for the observed variability at higher doses.

To confirm whether the assigned uncertainties are appropriated, IEU has been applied when adding different values of extra uncertainty. The over-dispersion of the 2 Gy gamma dosed sample was 22 ± 4 %, which is the one used to determine the extra uncertainty to be added assuming that the over-dispersion increases linearly with the dose. If a faster increase of the over-dispersion is considered for higher doses, the IEU finds problems converging for samples B6-1, B6-B and B6-3 indicating that the assigned over-dispersion is larger than that necessary to account for the observed variability. In contrast, if it is considered that over-dispersion does not increase linearly with the dose but have a slower increase for higher doses then, the IEU clearly underestimate the burial dose resulting in values which do not include the doses belonging to the main peak of the dose distributions. On Figure 4.23 the dose distribution of sample B6-B is shown. Identified outliers are indicated with open squares. For this distribution, the burial dose estimate when applying IEU using the values obtained from the dose recovery test at 2 Gy (extra 22% added to the uncertainty) is shown with a solid line. It

is approximately centred at the main peak. Also shown is the IEU value obtained with a slightly smaller uncertainty (17%) is added. In this case the approach includes only 25% of the D_e values in the estimation, none of which belong to the main peak and thus it can be assumed that this burial dose is under-estimated. 17% is clearly a too small uncertainty to account for the observed variability. But in contrast, if the extra uncertainty added is increased to 30%, then the IEU does not converge to results showing that the D_e values from the natural distribution have a smaller over-dispersion than 30% and thus, it can be assumed that 30% is too big. It can then be considered that the 22% extra uncertainty is appropriate although it was obtained from a sample dosed with lower dose (2 Gy) than those received in nature (~6 to 24 Gy).

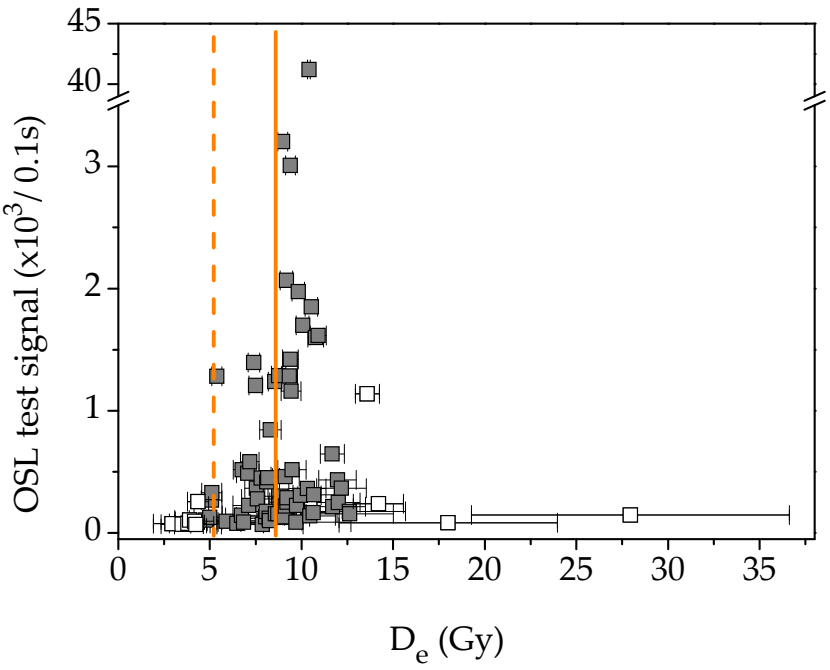

Figure 4.23. Dose distribution of sample B6-B showing the burial dose estimated with IEU when the value obtained from dose recovery test on a 2 Gy gamma dosed sample is measured and an extra 22% is added to the individual uncertainties (solid orange line). Also shown is the value when a lower uncertainty is considered and an extra 17% is added (dashed orange line). In this latest case it is clear that the estimation is not including the doses contained in the main peak and thus the burial dose obtained can be considered to be underestimated. The outliers identified to be those out of 1.5*IQR are shown in open squares.

4.6.6. Discussion

In agreement with previously published results (e.g. Duller *et al*., 2000) the cumulative light sum plot shows that a small percentage of the grains contributes with detectable signal to the total light. ~3 % of the grains measured emit ~90 % of the total light detected and 90% of the grains do not contribute significantly to the total light providing less than 1%. In addition, from the analysis of single grain it has been determined that ~10% of the single grains measured passed the selection criteria. Therefore, it can be concluded that all grains with detectable signal, not only the 3% providing most of the light but also those with dim signal, have been accepted indicating that they have a good luminescence behaviour. This results contrast with those from samples of the Guadalentin River; in that case a higher proportion of grains showed detectable signal but a smaller proportion passed the selection criteria. This may indicate that differences in the lithology derived in luminescence behaviour differences finding agreement with observations from Murray and Wintle (2003).

All grains belonging to the samples from Barrera and Puente de Resvala sites, which passed the selection criteria (section 2.7), have been found to be completely bleached. Therefore it is assumed that reliable burial dose estimates can be achieved using simple average, robust statistics or CAM model and no more complex approaches are required. Out of the three procedures it is considered that the weighted mean used by the CAM is more appropriate, assigning less weight to poorly known values. Despite, for these samples, all three methods provide consistent estimates.

Ages have been determined and results are summarized in table 4.6. Only values derived from CAM are shown as these are considered the most accurate in this specific case.

Complete bleaching indicates a good exposure to sun light during transport that it may be favoured by the river length to the studied sites (~100 km), and good hydrological behaviour of the Huebra River with flood hydrographs lasting for over one day (Masach, 1948). From this it can be concluded that the extra time consumed in

measuring and analyzing single grain results from Barrera site was not necessary in this case as it has not provided any additional information to that obtained using multi-grain aliquots (Rhodes, 2007).

Huebra	Ages (ka)
B6-1	1.30 ± 0.07
B6-B	2.00 ± 0.12
B6-2	2.76 ± 0.19
B6-3	5.97 ± 0.31
R5-1	0.65 ± 0.06
R5-3	4.79 ± 0.25

Table 4.6. Summary of age estimates derived from burial doses estimated using CAM model.

The performance of minimum age models have been tested on the Barrera site samples, although they have shown to be well-bleached. MAM model (Galbraith, 1999) presents converging problems when applied to these samples, indicating that it is not appropriate, either due to the age range or to the scarce population of incompletely bleached grains.

The IEU (Thomsen *et al*., 2003; 2007) for three palaeoflood units (B6-1, B6-2 and B6-3) identifies that these are well-bleached and includes over ~90% of the D_e in the estimation. However, when applying IEU approach to sample B6-B (soil A horizon) only 40% of grains are included, suggesting that 60% of the grains measured have a residual dose (usually arising from incomplete bleaching, Thomsen *et al*., 2003; 2007).

In the Barrera site, most palaeoflood units show incipient buried soils (A horizon) developed on the upper 10 cm, mainly due to root bioturbation and arthropod activity. Buried soils can be successfully radiocarbon dated using the humic acid components of the soil organic matter (e.g. Wang *et al*., 1996) being interpreted as minimal ages for the length of soil formation (Cherkinsky and Brovkin, 1991). Sample B6-B was collected

from an A horizon developed on the former surface of B6-2 unit in contrast with the other three samples which had been collected from units of flood deposits. Thus, different luminescence behaviour for B6-B may be expected. Since sample B6-B was collected from a soil developed on the surface of B6-2 unit same burial is to be expected.

Burial doses consistent with each other are estimated for B6-B and B6-2 units when applying simple, robust or weighted average but if a minimum age model is applied, then 60% of the grains are considered to have higher doses than those identified by the model to be the "true" burial dose. In the case of incompletely bleached sample, for which minimum age models are usually applied, the lower doses are considered to be the ones indicating the true burial dose and high doses are considered to be grains with contribution of residual doses due to incomplete bleaching. Different argument has to be understood from the results of the buried soil. In this case, the higher doses are the ones that correspond to the true burial time of unit B6-B, indicating that it has similar burial dose (and thus similar age, accounting for the small variation in the annual dose rate) to the sediment on which it has developed, B6-2. The grains showing lower doses are a contribution of the sediment deposited above filling cracks and root tubular openings thus, the burial dose estimated with the identified lower doses (identified by the model as the well-bleached fraction) give similar results to the sediment above, B6-1. The difference in the burial dose of these two grain populations provided in fact the age during which soil has been developed. This research reveals that (i) most sand and silt incorporation into the peds and conducts within the soil proceeded from the following flood event, and (ii) statistical analysis of grain distribution of a single sample can be used to date processes on which incorporation of external material is involved. Previous attempts to date soils are very scarce and mainly focussed on soils formed on loess sediments (Jia *et al*., 2008). Recently, Sweeney *et al*., (2010), applied optical dating to provide ages for grains accumulated in aeolian-derived vesicular A soil horizons developed beneath desert pavements, showed that grains from dust origin were translocated along the horizon as a result of soil forming processes.

However, this analysis was based on multiple luminescence measurements of aeolian sand contained in soil peds.

4.7. Duero River

4.7.1. Study area

The Duero River (Douro River in Portuguese) drains the northern part of the Spanish Plateau (Meseta), with an E-W elongated basin with headwaters in the Iberian Range and its mouth into the Atlantic Ocean near Porto (Figure 4.1).The Duero River is one of the largest rivers in the Iberian Peninsula, with a total surface of 98.073 km^2, 20% in Portugal and 80% in Spain. This river runs along 120 km the natural border between Portugal and Spain, known as the Arribes de Duero, carving a spectacular bedrock gorge of ~150 m in depth. In this Arribes reach the lithology is composed by granite and granodiorite rocks of the Hercinic basement. The climate is Mediterranean continental with Atlantic influence. The mean annual precipitation is about 500 mm, although with a high interannual variability between 350 and 800 mm. Rainfall regimen is mainly associated with Atlantic frontal system crossing the Iberian Peninsula during winter. Extreme floods are related to persistent rain during winter that may be combined with snowmelt from the mountain ranges surrounding the basin, producing discharges over 30 times the mean stream flow. According to Pardé (1949), the Duero River is the river with largest floods in Europe compared to similar size rivers. Therefore, reconstructing long-term flood records and its relationship with climate variability is a critical issue for flood hazard assessment.

The palaeoflood Saucelle site is located ~500 m downstream of the Duero-Huebra confluence, between the municipalities of Saucelle, Spain, and Freixo, Portugal (Figure 4.13). The palaeoflood depositional environment compresses a canyon expansion of about 1.3 km in length and 200 m wide. Slackwater deposits are preserved in a thick,

high-standing bench along its left margin of the canyon expansion (Spanish side) and at tributary mouths.

In these marginal zones, standing or slow-moving water (eddies) allow a better preservation of flood deposits through time. One high palaeoflood bench, composed of multiple flood units, eventually interfingered by slope deposits, was recognised at the left side canyon margin (Spanish part).

The bench is located 15.5 m above the present channel bottom. Two trenches were cut in this bench along the study reach (profiles DOL and MOR). Profile DOL is 2.5 m in thickness and is composed of fine-medium sand units, with well marked contacts, brown to yellow in colour, diffuse lamination to massive structure, with intercalation of slope deposits and stone lines in the palaeoflood unit contacts (Figure 4.24). The profile shows at least five flood units within two clusters (units 1, 2 and units 3, 4, 5) separated by 40 cm colluvial bed. A total of five samples were collected from this site for OSL dating and used in this study.

A second stratigraphic profile of 3.2 m in thickness was described in the same bench about 20 m upstream of the previous one (Moreras profile). This profile is composed by 12 flood units separated by diffuse to well marked contacts (stone lines). The lowest flood units (6 to 12) are thicker (average of 35-40 cm) than the upper ones (typical average thickness of 10-15 cm). Five samples were taken for OSL dating from each of the slackwater flood units (not processed in this study).

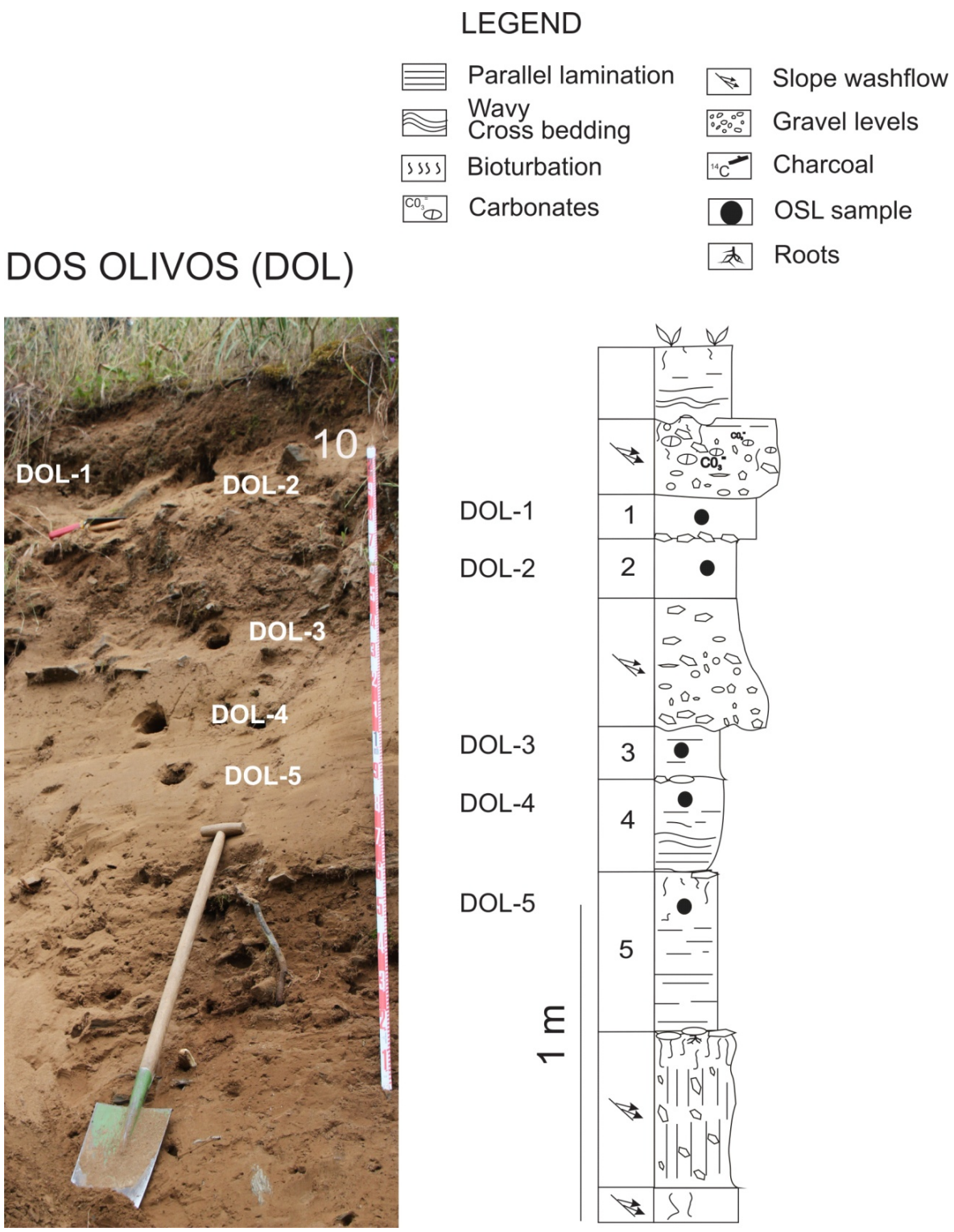

Figure 4.24 Stratigraphic profile Dos Olivos site.

4.7.2. Dose rate

Approximately 200 g of material surrounding each collected sample were taken for high-resolution gamma spectrometry. Water content at the moment of sampling has been assumed to be representative of the average water content during the burial time. The cosmic radiation contribution was calculated taking sample depth into account (Prescott and Hutton, 1994). Depth of the sample, water content, contribution of ^{232}Th, ^{226}Ra and ^{40}K to the dose rate and the estimated annual dose rate have been summarized in Table 4.7. As expected, annual dose rate values are similar to those from Huebra River.

Sample	Depth (cm)	Wat. cont. (%)	^{226}Ra (Bq/kg)	^{232}Th (Bq/kg)	^{40}K (Bq/kg)	Total dose rate (Gy/ka)
DOL-1	45	3	36.8 ± 0.8	42.1 ± 0.9	843 ± 18	4.2 ± 0.4
DOL-2	55	4	46.3 ± 0.8	57.0 ± 0.9	797 ± 16	4.3 ± 0.2
DOL-3	122	4	43.8 ± 0.5	62.9 ± 0.7	638 ± 11	3.9 ± 0.2
DOL-4	149	4	37.8 ± 0.4	52.8 ± 0.6	521 ± 9	3.2 ± 0.2
DOL-5	174	7	44.1 ± 0.8	56.0 ± 0.9	551 ± 13	3.4 ± 0.2

Table 4.7. Depth and wáter content of the samples. ^{232}Th, ^{226}Ra and ^{40}K radionuclides concentration and total dose rate of each unit from Dos Olivos site are summarized.

4.7.3. Luminesce behaviour

Similar luminescence behaviour as that observed on samples from Huebra River is present on samples from Duero River. Blue-OSL decay curves show a slower decay than that expected from a pure quartz sample dominated by the fast component. From observation on the Huebra samples collected from B6 and R5 sites, it is assumed that this slower decay is a consequence of feldspar contribution. IR depletion ratio was measured to check if feldspar contribution could be considered negligible when

measuring the blue-OSL signal, as observed on samples from Rambla de la Viuda. The depletion ratios are poor, with values around 0.7 ± 0.1, showing a significant contribution from feldspar. Thus, double SAR procedure (i.e. including IR stimulation prior to blue-OSL measurement) was used to deplete the contribution of feldspar and maximize quartz signal when measuring the blue OSL. Post-IR blue-OSL decay curve has been compared with the decay curve from calibration quartz, confirmed to be dominated by the fast component. The comparison indicates that IR stimulation succeeds in depleting the feldspar signal and the resulting blue-OSL decay curve is clearly dominated by the fast component.

Preheat plateau test were carried out. Values measured at the different temperatures are consistent with each other finding no dependence of the dose with preheating temperature for the range 160°C to 280°C.

The burial dose range varies from ~1.5 to 4 Gy thus thermal transfer, if it occurs, will be negligible for the estimated doses. Therefore no thermal transfer test has been carried out for these samples.

A fraction of sample DOL-3 was bleached under solar simulator for four hours and subsequently beta dosed with 2 Gy *in situ* (i.e. in the luminescence reader). This fraction was measured using small (~30 grains) multi-grain aliquots similar to those used for measuring the equivalent dose. It has been reported (Thomsen *et al*., 2005) that multi-grain aliquots of gamma dosed samples and beta dosed samples show similar recovered dose distribution. In addition, all measurements of natural samples from Duero River will be done using multi-grain aliquots; single grains, which could be affected by the beta source heterogeneity, will not be used in this case. Therefore it is considered appropriate to use the in-built beta source for all the irradiations involved in the analysis of samples from Dos Olivos site. The 2 Gy beta dose given is accurately recovered resulting in a given to recovered dose ratio of 1.03 ± 0.05. The over-dispersion of the beta dosed aliquots (n = 48) is 11 ± 2.

4.7.4. Natural dose distributions and burial dose estimates

Based on conclusions achieved during the analysis of samples from Barrera and Puente de Resvala sites, (i.e. single grain analysis was not necessary to estimate accurate burial doses) multi-grain aliquots have been used in this case to determine the true burial doses. To complete the understanding on the behaviour of the different approaches, burial doses have been estimated following the same procedure employed previously. MAM has not been applied as it showed converging problems when applied to well bleach samples (section 4.6.5). Simple average and CAM model obtains consistent results with each other. Robust average reaches similar results with a slight tendency to lower values. The IEU approach show a coherent behaviour.

Dose distributions of the five samples from this site are shown in Figure 4.25. CAM (red bars) and IEU approach (blue bars) dose estimates are shown on the distributions. Samples DOL-2, DOL-3, DOL-4 and DOL-5 have very symmetric distributions and CAM estimates seem centred at the main peak. The over-dispersion of these distributions varies between ~20 and 60%. Results using IEU are consistent so in this case no additional information is added when using this approach. For these four samples CAM estimates are considered appropriated. Dose distribution for sample DOL-1 shows a number of high equivalent doses and an over-dispersion of ~110%. These higher D_e values show larger uncertainties associated but in contrast with previous samples analyzed in this thesis, this high dose points show a bright signal. In previous dose distributions presenting relatively high D_e values, these were part of a tail of high doses poorly known (with low test dose signal). When applying the CAM model to dose distribution of sample DOL-1, the high dose values will be given a large weight in the average calculation and therefore they will bias the dose estimation towards high values deriving in an over-estimated burial dose. This effect can be clearly observed on Figure 4.25. Although these high D_e values do not have the behaviour of incomplete bleached aliquots, they present outlier value from the main peak and therefore the IEU approach is applied to exclude the high dose points from the calculation.

Although the remaining samples (DOL-2 to DOL-5) show a very symmetric dose distribution and CAM estimates are consistent with the main peak, IEU has been applied to all five samples in order to analyze its performance in each case.

For the four samples, DOL-2 to DOL-5, the IEU includes in the estimation ~90 to 100% of the aliquots, indicating that this is the percentage considered to be well-bleached. In contrast, from the dose distribution of DOL-1, only 65% of the aliquots measured are considered to have a dose corresponding to the event to be dated. Dose estimates with each approach and the involved percentage of aliquots involved in each one are summarized in Table 4.8.

Sample	Simple average		Robust average		CAM	IEU	
	D_e (Gy)	n	D_e (Gy)	n (%)	D_e (Gy)	D_e (Gy)	n (%)
DOL-1	2.4 ± 0.4	75	1.80 ± 0.10	92	2.3 ± 0.3	1.33 ± 0.05	64
DOL-2	2.0 ± 0.2	69	1.73 ± 0.07	84	1.85 ± 0.09	1.64 ± 0.06	84
DOL-3	3.0 ± 0.3	50	2.72 ± 0.09	86	3.1 ± 0.3	2.72 ± 0.09	90
DOL-4	2.9 ± 0.2	46	2.67 ± 0.09	91	2.71 ± 0.09	2.67 ± 0.10	97
DOL-5	3.5 ± 0.2	85	3.18 ± 0.08	89	3.27 ± 0.11	3.25 ± 0.08	94

Table 4.8. Dose estimates with each approach as well as the total number of aliquots measured (n) and the percentage of them involved in each calculation.

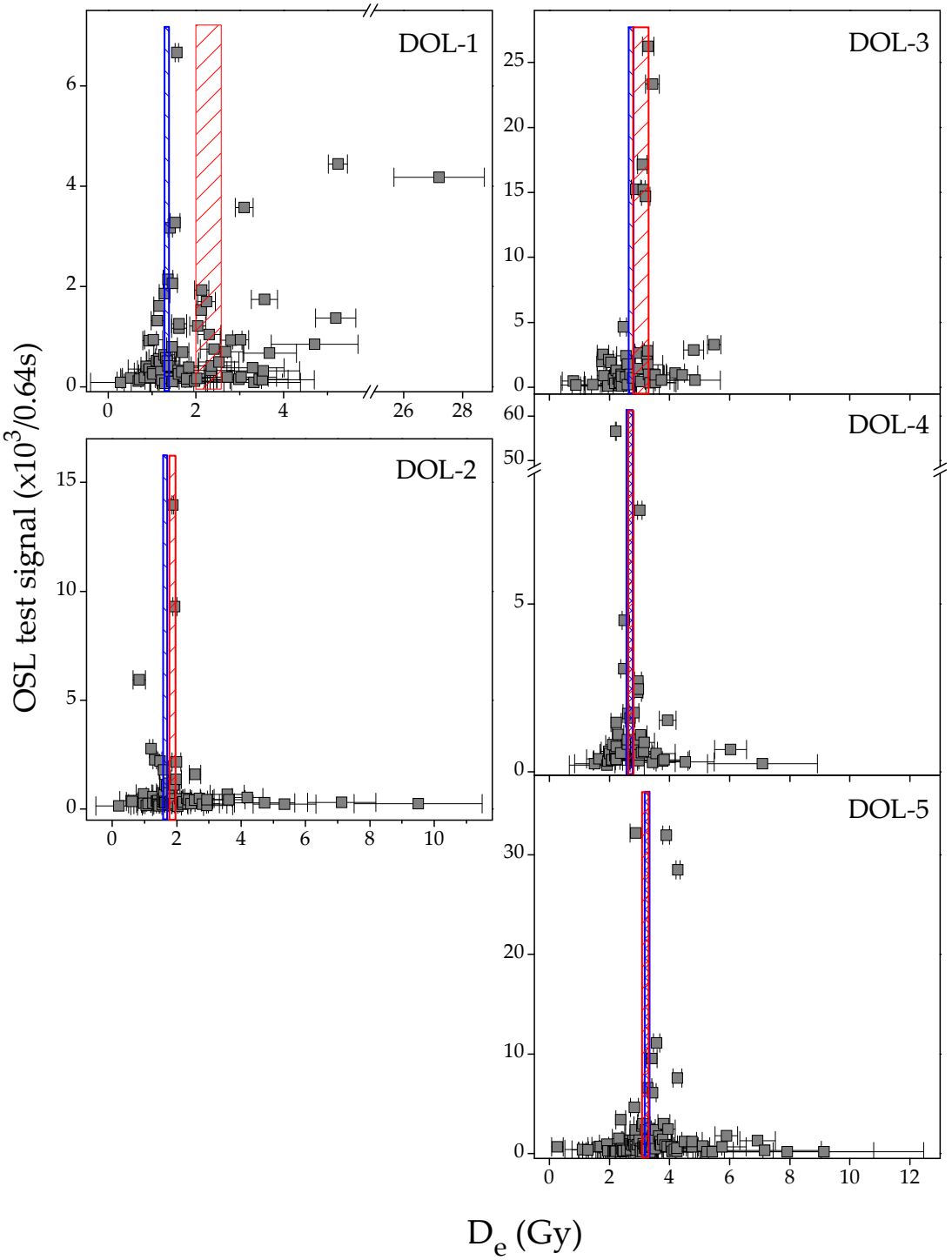

Figure 4.25. Dose distributions of Duero samples. CAM averages (red bars) and IEU dose estimates (blue bars) are shown.

4.7.5. Discussion

The slow decay curve shown when measuring blue-OSL signal of the quartz fraction extracted is not characteristic of pure quartz (Stokes, 1992). From the observations on the samples from Huebra River it can be assumed that this slow decay is cause by the presence of feldspar in the quartz separates (e.g. Godfrey-Smith *et al*., 1988; Thomsen *et al*., 2008; Buylaert *et al*., 2011). The use of IR stimulation prior to blue-OSL measurement, i.e. post IR OSL, succeeds in depleting the feldspar signal to negligible levels. Double SAR (Banerjee *et al*., 2001) has been used in all measurements as the post IR OSL signal can be assumed to be dominated by the quartz signal and thus the D_e determined can be rely as indicators of the dose the samples have been exposed to Roberts and Wintle, 2003.

If based on the observation a complete bleaching is assumed for all five samples and CAM model is applied, the dose estimates show an age inversion between samples DOL-1 and DOL-2, resulting in stratigraphic incoherence (Table 4.9). Visual observation of dose distributions in DOL-1 (Figure 4.25) shows a number of high D_e values out of the main peak centred at the lower doses, suggesting the contribution of grains with residual dose. Careful understanding of the behaviour of the dose distributions indicates that those high D_e values in DOL-1 sample have to be identified and excluded from the estimation of the burial dose. The IEU (Thomsen *et al*., 2003; 2007) approach was therefore applied. It identified 36% of the aliquots to have higher doses than those corresponding to the event depositing the sediment. Despite the presence of these high doses it would not be appropriate to identify sample DOL-1 as incompletely bleached. This contribution is likely to be a consequence of surface rework for farming purposes rather than incomplete bleaching of the samples during transport. Currently, the upper bench surface contains an olive tree field and it is expected that the uppermost surface was used for agricultural purposes favouring reworking of the subsurface.

The analysis of samples for Duero River suggest that the appropriated ages should be calculated based on the CAM model estimates for samples DOL-2 to DOL-5 and based on the IEU approach for sample DOL-1. The calculated ages derived from both, CAM and IEU dose estimates are summarized in Table 4.9.

Sample	Age (ka)	
	CAM	IEU
DOL-1	0.55 ± 0.08	0.32 ± 0.02
DOL-2	0.43 ± 0.03	0.38 ± 0.02
DOL-3	0.78 ± 0.08	0.69 ± 0.04
DOL-4	0.84 ± 0.05	0.82 ± 0.05
DOL-5	0.96 ± 0.06	0.95 ± 0.05

Table 4.9. Estimated ages using CAM model and IEU approach and the percentage of aliquots included by the latest for calculations are summarized. Also depth of each sample is indicated in the table. CAM estimates show an age inversion between samples DOL-1 and DOL-2, resulting in a stratigraphic incoherence. Applying the IEU approach indicates the contribution of high doses apparently out of the main peak centred at the lowest doses in sample DOL-1. For this specific site, CAM estimates are considered appropriate for samples of units located deeper than 50 cm.

4.8. **Conclusions**

The study of samples from Rambla de la Viuda, Huebra and Duero rivers shows that OSL dating can be applied for the accurate dating of sediments from different lithological environments and different age range. Regarding luminescence results each site present specific characteristics and thus, the analysis of the data cannot be done following an established protocol but special attention has to be put in each case to apply the measuring and analysing methods that most suitable.

On well bleached samples, a robust average or weighted mean (CAM) are sufficient to approach accurately the true burial dose values.

Samples from Rambla de la Viuda show dose distributions with a peak centred at the lower doses and a tail of higher values indicating the contribution of grains with

residual dose. In these cases the measurement of single grains and use of a minimum age model seems appropriate. It has also been shown that due to the small proportion of grains contributing to the total light detected, small multi-grain aliquots (~30 grains) can also behave as single grains thus, making it possible to differentiate the doses corresponding to the well-bleached fraction of the sample. The use of multi-grain aliquots instead of single grains reduces significantly the measuring (mainly the loading of samples) and the data analyzing time. If uncertainties are properly assigned based on a dose recovery test, the use of small multi-grain aliquots in combination with IEU approach can be widely used as its performance adapts to the bleaching degree of the sample. No previous identification of the bleaching degree of the sample is required since the IEU approach identifies it, including a larger proportion of D_e values for better bleached populations.

From the study of these various samples it can be concluded that IEU approach can also be applied to date sample with dose distribution containing different population of dose values. It has shown to be suitable for dating buried soils (sample B6-B from Huebra River). The contribution of post-depositional grains with lower doses than those expected for the burial time can be successfully identified. Also the IEU approach has succeeded identifying the mixture of grains with different doses due to rework of the land for agricultural purposes (sample DOL-1 from Duero River).

In contrast, MAM model shows problems in converging to results when applied to well-bleached samples as seen on those from Huebra River.

Samples from the Atlantic basins present feldspar contamination in the prepared quartz fraction, even after HF treatment. If feldspar contributes to the blue-OSL signal it would lead to a wrong dose estimate. Double SAR procedure has been used for samples from Huebra and Duero rivers. This procedure includes IR stimulation prior to blue-OSL measurement to deplete the feldspar contribution and maximize quartz contribution to the signal. The resulting blue-OSL signal is clearly dominated by the

fast component therefore confirming that feldspar signal has been successfully depleted.

Based on cumulative light sum it can be confirmed that for all samples, a small percentage of grains (less than 10%) contribute to the total light detected. This makes it possible to identify well bleached proportion when measuring small multi-grain aliquots since, due to the small percentage of grains giving light, some of this small multi-grain aliquots behave like single grains.

From the detailed study carried out on Chapter 4 on the analysis of samples from different lithological and geographical origin, each showing different characteristics it can be concluded that OSL technique is not only suitable for dating accurately them all but also for providing further information like soil formation and land use.

5.

Final Conclusions and future research

5.1. **Specific conclusions achieved**

The investigation of this thesis has result in a number of conclusions which will be of great help in further studies providing detailed analysis and a series of guidelines for the OSL dating of sediments from different environments. These conclusions can be summarized in the following:

1. OSL dating can be successfully applied to a wide type of sediments achieving reliable results even in case of dim signal or grains with residual dose.
2. The use of small multi-grain aliquots is appropriated not only for well-bleached grains but also to estimate precisely the burial dose of samples containing a large contribution (up to 60%) of incompletely bleached grains.
3. The limitation of CAM and MAM models when applied to young samples can be avoided using a exponential transformation.
4. Thermal transfer could only be significant for the burial dose estimation of young samples; for the young samples studied here it could be considered negligible.
5. Independently of the origin of the sediments, 80 to 90% do not contribute to the luminescence detected.
6. Decay curves of the different environments show that from the Mediterranean rivers, deposits from Guadalentin do not contain feldspar and those from Rambla de la Viuda show a small contribution with negligible effect on the

OSL. In contrast, all the deposits studied from Huebra and Duero (Atlantic) have a significant contribution of feldspar even after chemical treatment. Its effect on the OSL signal can be successfully minimized using a double SAR protocol.

7. Due to their lithology, deposits from Atlantic rivers can be OSL dated basing the burial dose estimates on both, quartz and feldspar; this latest making it possible to widen the age range.
8. The IEU approach identifies successfully the well-bleach aliquots not only when applied to single grains dose distributions but also on dose distributions of small multi-grain aliquots. Although IEU has been presented as a minimum age model it can be applied to deposits with all degrees of bleaching and wide age range. Its use is not limited to date incompletely bleached samples but it can also applied to
9. The suitability of IEU approach is not limited to dating deposits but it can also for provide further information on soil formation and land use.

5.2. Conclusiones y futuras líneas de investigación

El uso de la datación mediante luminiscencia ópticamente estimulada se está extendiendo entre los expertos sobre el Cuaternario, y en gran medida los avances de la técnica tienen relación con los retos específicos que se plantean desde las diferentes necesidades de datación. En este sentido, la técnica ha desarrollando herramientas y procedimientos para abordar el estudio de muestras muy antiguas o muy recientes, y en ambientes sedimentarios donde se presentan problemas de blanqueamiento y reinicio del reloj geológico. Esta Tesis Doctoral tiene como objetivo general determinar los procedimientos de medida de señal de luminiscencia y los métodos estadísticos de procesado de datos para la determinación de dosis de enterramiento de sedimentos de crecidas fluviales (paleocrecidas) de diferentes rangos de edad (con énfasis en muestras recientes) y en cuencas fluviales con distintas características litológicas, fisiográficas e hidroclimáticas dentro del ámbito de la Península Ibérica.

A menudo, la datación de sedimentos fluviales, en especial aquellos que han recibido dosis de radiación bajas (e.g. sedimentos jóvenes) puede resultar complicada. La exposición de los sedimentos a la luz solar antes de quedar enterrados se puede ver limitada por la turbiedad del agua o la breve duración del transporte. En esos casos, el sedimento estará compuesto por material que ha sido expuesto a la luz solar en distintos grados. La parte del sedimento que no haya sufrido un blanqueamiento total durante su transporte arrastrará una dosis residual correspondiente a eventos anteriores. Este trabajo explora las opciones para el estudio de este tipo de muestras desde la correcta identificación de sus características específicas en el laboratorio hasta la aplicación de las medidas y análisis adecuados en cada caso de cara a su precisa datación.

Por un lado, el desarrollo instrumental alcanzado en las últimas décadas permite la estimación de dosis acumulada en granos individual frente a la utilización de alícuotas compuestas por varios granos. Sin embargo, numerosos autores cuestionan la eficiencia de los procedimientos basados en el estudio de granos individuales debido a las fuentes de error que pueden afectar la estimación de la edad y al elevado tiempo requerido para el análisis de los resultados. Otras problemáticas que se plantean dentro del ámbito experimental es la influencia de los procedimientos de laboratorio en la lectura final de la luminiscencia, y concretamente en relación con la transferencia térmica (termal transfer), los protocolos de medida empleados incluyendo diversas fuentes de estimulación y el efecto de la reproducibilidad instrumental.

Por otro lado, y dentro del ámbito del análisis de resultados se han desarrollado diferentes procedimientos matemáticos y estadísticos que permiten fraccionar la contribución de las dosis medidas en granos con diferente blanqueamiento y dosis heredadas, de tal forma que se puede combinar, separar o eliminar la contribución de estas dosis en función del tipo de muestra. Los procedimientos experimentales y de análisis de dosis de enterramiento están en gran medida condicionadas por las características de los sedimentos (eólicos, fluviales), edad (jóvenes o antiguas), y características litológicas del área fuente.

En el capítulo 1 de esta Tesis Doctoral se han presentado los objetivos e hipótesis de trabajo. El capítulo 2 describe la instrumentación y metodología empleada. En el capítulo 3 se aborda la datación de muestras fluviales recientes realizando un detallado análisis del comportamiento de distintos procedimientos matemáticos aplicados a la determinación de la dosis acumulada por las muestras. El capítulo 4 analiza el efecto de los distintos condicionantes litológicos, fisiográficos e hidroclimáticos. En este último capítulo se exponen las conclusiones finales de la Tesis Doctoral y las futuras líneas de investigación que quedan abiertas.

Para llevar a cabo este detallado estudio se han seleccionado dos ríos de la cuenca Mediterránea (Guadalentín y Rambla de la Viuda) y dos de la cuenca atlántica (Huebra y Duero) de los cuales se han tomado un total de 29 muestras. En estos ríos, se han realizado ocho secciones estratigráficas detalladas de los depósitos de inundación en zonas de remanso, donde se han realizado los muestreos para OSL usando tubos opacos de PVC. Las medidas de OSL se han realizado en un lector de luminiscencia automática TL/OSL DA-20 (Bøtter-Jensen et al., 2010) en el Laboratorio Nórdico de datación por luminiscencia (Aarhus University, Dinamarca), usando el protocolo SAR (Capítulo 2).

La mejora de los protocolos de medida de la señal de luminiscencia y la identificación de los granos y fracciones con blanqueo parcial en muestras jóvenes (menos de 500 años) se ha abordado en el capítulo 3. Los registros de paleocrecidas del río Guadalentín presentan la ventaja de disponer de control cronológico preciso obtenido de registros documentales (Archivo Municipal de Lorca) y dataciones de radiocarbono, lo que ha permitido contrastar los resultados de la luminiscencia con la información histórica. En el Guadalentín, las 8 muestras analizadas (Capítulos 3) se han utilizado para hacer un exhaustivo estudio sobre la respuesta luminiscente de sedimentos que sufren blanqueamiento parcial y el comportamiento de distintos modelos estadísticos en la estimación de la edad de los depósitos.

Las medidas se han centrado en la fracción de cuarzo de tamaños 180-250 μm, previamente separada de la muestra original. Las muestras se han medido utilizando tanto granos individuales como alícuotas pequeñas (~30 granos). Las dosis acumuladas por los sedimentos durante el periodo que han permanecido enterrados así como su error asociado se han obtenido en base al análisis de los datos empleando modelos puramente estadísticos (media aritmética, media ponderada y modelo CAM) y modelos de edad mínima, "minimum age models" (MAM e IEU). Se ha establecido la incertidumbre asociada a una distribución afectada únicamente por factores intrínsecos, como la mínima incertidumbre que puede tener la distribución de dosis equivalentes de una muestra natural. De esta forma, la incertidumbre que exceda la mínima incertidumbre calculada será debida a factores extrínsecos como el blanqueamiento parcial. Basándonos en ese supuesto y aplicándolo sobre las medidas de granos individuales, el modelo MAM obtiene edades consistentes con las edades conocidas para las tres muestras más antiguas (<350 años). IEU obtiene valores consistentes para 7 de las 8 muestras. Las medidas sobre alícuotas pequeñas también dan resultados consistentes cuando se combinan con el modelo IEU.

En este estudio, el análisis de la suma total de la luz detectada en función del porcentaje de granos contribuyendo (cumulative light sum) muestra que solo un pequeño porcentaje de los granos medidos emite señal detectable, con menos del 10% de los granos aportando más del 80% de la luz total detectada. Estos valores sugieren que varias de las alícuotas (~30 granos) medidas, se comportarán como granos individuales permitiendo así la identificación de aquellos bien blanqueados. Esta conclusión supone que incluso en sedimentos con blanqueamiento parcial, el uso de alícuotas pequeñas para las medidas permite obtener edades precisas sin necesidad de recurrir a la medida de granos individuales, con la consiguiente implicación de tiempo y esfuerzo. El posible efecto de la transferencia térmica (generando señal luminiscente a causa del tratamiento térmico en el laboratorio) se ha estudiado en estas muestras ya que potencialmente podría ser significativo al tratarse de muestras jóvenes (con dosis bajas). Sobre una muestra blanqueada de forma artificial se ha medido 15±6 mGy. Este

valor es comparable a los ~ 35 mGy correspondientes a la muestra más joven, T-39, sin embargo entra dentro de valores que se pueden considerar prácticamente indetectables. Por tanto, este efecto no se ha restado de las dosis estimadas. Un efecto de esa magnitud se puede considerar despreciable en el caso de estudiar muestras más antiguas (i.e. con dosis ~1 Gy).

Otra parte importante de esta Tesis ha consistido en determinar los condicionantes hidro-sedimentarios (ambientes sedimentarios de los depósitos de remanso), las características de la cuenca (tamaño y distancia de transporte de los sedimentos, litología del sustrato), pueden introducir errores en la datación óptica de los depósitos de paleocrecidas en ríos Ibéricos (Capítulo 4). Las conclusiones obtenidas en el estudio de las muestras del Guadalentín se han aplicado a las 10 muestras de Rambla de la Viuda. Se han obtenido resultados coherentes con la estratigrafía y con las limitadas dataciones de ^{14}C por lo que podemos confirmar que el comportamiento observado no es exclusivo de muestras del Guadalentín.

El estudio de las muestras de los ríos Huebra y Duero (régimen hidroclimático Atlántico y litología dominante granítica) muestra que prácticamente todas ellas han sufrido un blanqueamiento completo. En este caso la dificultad está en la contaminación de feldespato en la fracción de cuarzo. La señal de OSL con estimulación azul del feldespato se superpone a la de cuarzo impidiendo obtener resultados precisos. Se ha empleado el protocolo conocido como Doble-SAR que incluye estimulación con IR, antes de la medida con estimulación azul, para reducir la señal del feldespato presente en la muestra y maximizar la contribución del cuarzo al medir con luz azul. Se han analizado la curva de decaimiento tras este protocolo para confirmar que la señal medida está dominada por la contribución del cuarzo.

En estas muestras con escaso o nulo blanqueamiento parcial y rangos de edades hasta 5 ka se ha comprobado que el modelo MAM no es apropiado. Sin embargo el modelo IEU es indiferente del grado de blanqueamiento y muestra resultados coherentes en todos los caso. La aplicación de este modelo para el estudio de las muestras del Huebra

ha permitido encontrar su utilidad en la datación de suelos desarrollados sobre los depósitos. IEU permite discernir entre los granos medidos, aquellos pertenecientes al sedimento sobre el que descansan y el sedimento que se ha depositado sobre el suelo desarrollado. Esta conclusión abre nuevas vías de investigación permitiendo la datación de varios eventos partiendo de la muestra de un único suelo.

Las muestras tomadas del río Duero también están bien blanqueadas. Ante esta situación cabría pensar que la determinación de la edad utilizando una simple media ponderada puede aportar estimaciones de edad precisas. Sin embargo, al aplicar el IEU se ha podido detectar que la muestra más reciente de entre las 5 muestras tomadas, situada a 45 cm de la superficie, se encuentra mezclada con granos de cuarzo aparentemente transportados en distintos eventos. En este caso no se trata de granos con dosis más altas, como las que se encuentran cuando la muestra ha sufrido un blanqueamiento parcial, sino que los granos "intrusos" no tienen dosis alguna, indicando que han sido expuestos a la luz recientemente. Esto sugiere un retrabajamiento del suelo, posiblemente debido a volcado de sedimento durante tareas agrícolas.

5.2.1. Conclusiones finales

De esta Tesis Doctoral se han obtenido las siguientes conclusiones:

1. La datación por OSL puede ser empleada para un amplio tipo de depósitos obteniendo resultados precisos incluso en el caso de señal luminiscente débil o intrusión de granos con dosis residual.
2. El uso de alícuotas multi-grano es apropiado para la datación de depósitos de crecidas fluviales, incluso en aquellos casos en los que hay una alta contribución (hasta el 60%) de granos con blanqueamiento parcial.
3. La limitación de los modelos CAM y MAM en la estimación de la dosis acumulada para muestras jóvenes se puede evitar aplicando una transformación exponencial a los datos.

4. El efecto de la transferencia térmica en las muestras estudiadas se puede considerar despreciable incluso para los sedimentos más recientes.
5. Independientemente del origen de la muestra, un pequeño porcentaje de los granos medidos (80-90%) no contribuye a la señal detectada.
6. Las curvas de decaimiento indican que en las muestras del río Guadalentín la contribución de feldespato es nula y por tanto para este entorno, las medidas de OSL deberán basarse siempre en la estimulación del cuarzo. Las muestras de la Rambla de la Viuda muestran una pequeña cantidad de feldespato cuya presencia no tiene efecto alguno en la medida de OSL sobre cuarzo. Las muestras de los ríos atlánticos (Huebra y Duero) presentan una alta concentración de feldespato siendo necesaria la eliminación de su contribución durante el proceso de medida aplicando el protocolo doble-SAR.
7. La datación de los sedimentos de los ríos atlánticos se pueden basar tanto en las medidas sobre cuarzo como en las medidas de feldespato; permitiendo éstos últimos la datación de un rango de edad más amplio.
8. El uso del modelo IEU permite identificar la fracción bien blanqueada de las distribuciones de dosis, tanto de granos individuales como de alícuotas multi-grano.
9. El modelo IEU aplicado al estudio de suelos permite determinar la edad los depósitos inmediatamente superiores e inferiores así como la contribución de cada uno de ellos al suelo desarrollado.

5.2.2. Futuras líneas de investigación

La investigación llevada a cabo en esta Tesis Doctoral abre nuevas líneas de investigación para el futuro. Las dataciones basadas en la medida de feldespato ofrecen la posibilidad de ampliar el rango de edad de las muestras, resultando especialmente prometedor en el campo de la arqueología.

Por otro lado la estimulación mediante luz pulsada, no empleada en este trabajo, tiene un gran potencial en la identificación de señales de luminiscencia puras. El estudio del decaimiento de la señal luminiscente puede aportar información sobre la contribución de las distintas trampas a la señal de luminiscencia, permitiendo así la datación comparada basada en la medida de distintas señales simultáneas.

Por último, las conclusiones de esta Tesis se pueden aplicar a la datación de numerosas muestras fluviales que no han sido datadas de forma precisa hasta este momento debido a su complejidad (blanqueamiento parcial, dosis bajas en muestras recientes, señal luminiscente débil). Esta posibilidad de datar de forma precisa sedimentos con esta problemática permite abordar nuevos proyectos en el tema de la erosión de suelos aportando información precisa sobre tasas de transporte de sedimentos, tasas de soterramiento en embalses, datación de deslizamientos en laderas y caída de bloques.

Las conclusiones obtenidas en esta Tesis Doctoral sobre el comportamiento de la datación por OSL permiten considerarla como una técnica precisa para la cuantificación de las tasas de actividad de procesos geodinámicos con aplicaciones al campo de la ingeniería civil.

References

Aitken, M.J., 1985. Thermoluminescence Dating. Academic. Press, London. 359 pp.

Aitken, M.J., 1998. An Introduction to Optical Dating. Oxford University Press, Oxford. 267 pp.

Ankjærgaard, C., Murray, A.S. and Denby, P.M., 2006. Thermal pre-treatment (preheat) in the OSL dating of quartz: is it necessary? *Radiation Protection Dosimetry* 119: 470-473.

Arnold, L.J. and Roberts, R.G., 2009. Stochastic modelling of multi-grain equivalent dose (D_e) distributions: Implications for OSL dating of sediment mixtures. Quaternary *Geochronology* 4: 204-230.

Arnold, L.J., Bailey, R.M. and Tucker, G.E., 2007. Statistical treatment of fluvial dose distributions from southern Colorado arroyo deposits. Quaternary Geochronology 2, 1-4: 162-167.

Arnold, L.J., Roberts, R.G., Galbraith, R.F. and DeLong, S.B., 2009. A revised burial dose estimation procedure for optical dating of young and modern-age sediments. *Quaternary Geochronology* 4: 306-325.

Bailey, R. M., Smith, B.W. and Rhodes, E.J., 1997. Partial bleaching and the decay form characteristics of quartz OSL. *Radiation Measurements* 27(2): 123-136.

Bailiff, I.K, Bøtter-Jensen, L., Correcher, V., Delgado, A., Göksu, H.Y., Jungner, H. and Petrov, S.A., 2000. Absorbed dose evaluations in retrospective dosimetry: methodological developments using quartz. Radiation Measurements 32, 5-6: 609-613.

Baker, V.R., Webb, R.H., House, P.K., 2002. The Scientific and societal value of paleoflood hydrology. In: House, P.K., Webb, R.H., Baker, V.R., Levish, D.R. (Eds.), Ancient Floods, Modern Hazards: Principles and Applications of Paleoflood Hydrology, Water Science and Application Series 5, pp. 127-146.

Baker, V.R., 1973. Paleohydrology, and sedimentology of Lake Missoula flooding in eastern Washington. *Geol. Soc. Am., Spec. Pap*. 144, 79 pp.

Baker, V.R., Kochel, R.C., Patton, P.C. and Pickup, G., 1983. Paleohydrologic analysis of Holocene flood slack-water sediments. *Internat. Assoc. of Sedimentologists Special Publication* 6: 229-239.

Baker, V.R., Pickup, G. and Polach H.A., 1985. Radiocarbon dating of flood events, Katherine Gorge, Northern Territory, Australia. *Geology* 13: 344-347.

Ballarini, M., Wintle, A.G. and Walinga, J., 2006. The spatial variation of dose rate beta as measured using single grains. *Ancient TL* 24: 1-8.

Ballarini, M., Wallinga, J., Murray, A.S., van Heteren, S., Oost, A.P., Bos, A.J.J., van Eijk, C.W.E., 2003. Optical dating of young coastal dunes on a decadal time scale, *Quaternary Science Reviews* 22, 10-13: 1011-1017.

Ballarini, M., Wallinga, J., Wintle, A.G. and Bos, A.J.J., 2007. Analysis of equivalent-dose distributions for single grains of quartz from modern deposits, Quaternary Geochronology 2, 1-4: 77-82.

Banerjee, D., Murray, A.S., Bøtter-Jensen, L. and Lang, A., 2001. Equivalent dose estimation using single aliquot of polymineral fine grains. *Radiation Measurements* 33: 73-93.

Bárcena, J.L., Urbina, M., Rowlands, A.P., Beneitez, P., Millán, A. and Calderón, T., 1999. Basic Thermoluminescence Properties of Micas: Muscovite, Sericite and Phlogopite. *Radiation Protection Dosimetry* 84: 289-292.

Baril, M.R., 2004. Emission and excitation spectra of feldspar inclusions within quartz. *Radiation Measurement* 38: 87-90.

Barriendos, M. and Coeur, D., 2004. Flood data reconstruction in historical times from non-instrumental sources in Spain and France. Systematic, palaeoflood and historical data for the improvement of flood risk estimation (G. Benito & V.R. Thorndycraft, eds.). Methodological Guidelines. European Commission. 29-42.

Benito, G., Machado, M.J. and Pérez-González, A., 1996. Climate change and flood sensitivity in Spain, In: J. Branson, A. G. Brown and K. J. Gregory (eds), *Global Continental Changes: The context of Palaeohydrology*, Geological Society of London Special Publication. 115: 85-98.

Benito, G., Sopeña, A., Sánchez-Moya Y., Machado, M.J. and Pérez-González, A., 2003. Palaeoflood record of the Tagus River (Central Spain) during the Late Pleistocene and Holocene. *Quaternary Science Reviews* 22 (15-17): 1737-1756.

Benito, G., Thorndycraft, V.R, Rico, M., Sánchez-Moya, Y. and Sopeña, A., 2008. Palaeoflood and floodplain records from Spain: Evidence for long-term climate variability and environmental changes. *Geomorphology* 101 (1–2): 68-77.

Benito, G., Rico M., Sánchez-Moya Y. Sopeña, Thorndycraft V. R and Barriendos, M., 2010. The impact of late Holocene climatic variability and land use change on the flood hydrology of the Guadalentín River, southeast Spain. *Global and Planetary Change* 70: 53-63.

Berger, G.W., 1995. Progress in luminescence dating methods for Quaternary sediments. In: Rutter, N.W., Catto, N. (Eds.), Dating Methods for Quaternary Deposits, Geological Association of Canada, GEOtext, 2: 81-103.

Blong, R.J and Gillespie,R., 1978. Fluvially transported charcoal gives erroneous ^{14}C ages for recent deposits. Nature 271, 739-741.

Bøtter-Jensen, L., Bulur, E., Duller, G.A.T. and Murray, A.S., 2000. Advances in luminescence instrument systems. *Radiation Measurements* 32 (5-6): 523-528.

Bøtter-Jensen, L., Thomsen, K.J. and Jain, M., 2010. Review of optically stimulated luminescence (OSL) instrumental developments for retrospective dosimetry. *Radiation Measurements* 45 (3–6): 253-257.

Buylaert, J.P., Jain, M., Thomsen, K.J., Murray, A.S., Thiel, C. and Sohabati, R., 2012. A robust feldspar luminescence dating method for Middle and Late Pleistocene sediments. *Boreas* 41, 3: 435-451.

Buylaert, J.P., Thiel, C., Murray, A.S., Vandenberghe, D.A.G., Yi, S. and Lu, H., 2011. IRSL and post-IR IRSL residual doses recorded in modern dust samples from the Chinese Loess Plateau. *Geochronometria* 38: 432-440.

Calderón, T., Khanlary, M.-R. Rendell, H.M. and Townsend, P.D., 1992. Luminescence from natural fluorite crystals, International Journal of Radiation Applications and Instrumentation. Part D. *Nuclear Tracks and Radiation Measurements* 20, 3: 475-485.

Camarasa, A., Segura, F., 2001. Flood events in Mediterranean ephemeral streams (ramblas) in Valencia region, Spain. *CATENA* 45, 3: 229-249

Capel, J., 1981. *Los Climas de España*. Col. Ciencias Geográficas Oikos-Tau, Barcelona, 429 pp.

Cherkinsky, A.E. and Brovkin, V.A., 1991. A model of humua formation in soils based on radiocarbon data of natural ecosystems. In ''International Radiocarbon conference, Tucson, Arizona.'' *Radiocarbon* 33, 186-187.

Choi, J.H., Murray, A.S., Cheong, C.S., Hong, D.G. and Chang, H.W., 2003. The resolution of stratigraphic inconsistency in the luminescence ages of marine terracesediments from Korea. *Quaternary Science Reviews* 22: 1201-1206.

Chougaonkar, M.P. and Bhatt B. C., 2004. Blue light stimulated luminescence in calcium fluoride, its characteristics and implications in radiation dosimetry. *Radiation Protection Dosimetry* 112, 2: 311-321.

Cunningham, A. and Wallinga, J., 2010. Selection of integration time intervals for quartz OSLdecay curves. *Quaternary Geochronology* 5: 657-666.

Denby, P.M., Bøtter-Jensen, L., Murray, A.S., Thomsen, K.J. and Moska, P., 2006. Application of pulsed OSL to the separation of the luminescence components from a mixed quartz/feldspar sample. *Radiation Measurement* 41: 774-779.

Duller, G.A.T., 1996. Recent developments in luminescence dating of Quaternary sediments. *Progress in Physical Geography* 20: 127-145.

Duller, G.A.T., 2003. Distinguishing quartz and feldspar in single grain luminescence measurements. Radiation Measurements 37, 2: 161-165

Duller, G.A.T., 2004. Luminescence dating of quaternary sediments: recent advances. Journal of Quaternary Science 19, 2 183-192.

Duller, G.A.T., 2007. Assessing the error on equivalent dose estimates derived from single aliquot regenerative dose measurements. *Ancient TL* 25: 1: 15-24.

Duller, G.A.T., 2008. Single-grain optical dating of Quaternary sediments: why aliquot size matters in luminescence dating. Boreas 37, 4: 589–612.

Duller, G.A.T. and Bøtter-Jensen, L., 1993. Luminescence from potassium feldspars stimulated by infrared and green light. *Radiation Protection Dosimetry* 47: 683-688.

Duller, G.A.T. and Murray, A.S, 2000. Luminescence dating of sediments using individual mineral grains. *Geologos* 5: 87-106.

Duller, G.A.T., Bøtter-Jensen, L., Murray, A.S. and Truscott, A.J. 1999. Single grain laser luminescence (SGLL) measurements using a novel automated reader. *Nuclear Instruments and Methods in Physics Research Section B: Beam Interactions with Materials and Atoms* 155 (4): 506-514.

Duller, G.A.T., Bøtter-Jensen, L. and Murray, A.S., 2000: Optical dating of single sand-sized grains of quartz: Sources of variability. *Radiation Measurements* 32: 453-457.

Galbraith, R.F., 2002. A note on the variance of a background corrected OSL count. *Ancient TL* 20 (2): 49-51.

Galbraith, R.F., Roberts, R.G., Laslett, G.M., Yoshida, H. and Olley, J.M., 1999. Optical dating of single and multiple grains of quartz from Jinmium rock shelter, Northern Australia: Part 1, experimental design and statistical models. *Archaeometry* 41: 339-364.

Godfrey-Smith, D.L., Huntley, D.J. and Chen, W.H., 1988. Optically dating studies of quartz and feldspar sediment extracts. *Quaternary Science Reviews* 7: 373-380.

Grodek, T., Benito, G., Botero, B.A., Jacoby, Y., Porat, N., Haviv, I., Cloete, G. and Enzel, Y. (*submitted in 2012*). The last millennium largest floods along the hyperarid Kuiseb River Canyon, Namibia. Submitted to *Journal of Quaternary Science*.

Hu, G., J-F. Zhang, Qiu, W-L. and Zhou, L-P., 2010. Residual OSL signals in modern fluvial sediments from the Yellow River (HuangHe) and the implications for dating young sediments. *Quaternary Geochronology* 5 (2-3): 187-193.

Huntley, D.J., Hutton, J.T. and Prescot, J.R., 1993. Optical dating using inclusions within quartz. *Geology* 21: 1087-1090.

Jacobson RB, O'Connor J, Oguchi T., 2003. Surficial geologic tools in fluvial geomorphology. In Tools in Fluvial Geomorphology, Kondolf M, Piegay H (eds). Wiley: New York; 25–57.

Jacobs, Z., Duller, G.A.T. and Wintle, A.G., 2003. Optical dating of dune sand from Blombos Cave, South Africa: II – Single grain data. *Journal of Human Evolution* 44: 613-625.

Jain, M., Murray, A.S. and Bøtter-Jensen, L., 2003. Characterisation of blue-light stimulated luminescence components in different quartz samples: implications for dose measurement. *Radiation Measurements* 37: 441-449.

Jain, M., Murray, A.S. and Bøtter-Jensen, L, Wintle, A.G., 2005. A single-aliquot regenerative-dose method based on IR bleaching of the fast OSL component in quartz. *Radiation Measurements* 39, 3: 309-318.

Jain, M., Murray, A.S. and Bøtter-Jensen, L., 2004. Optically stimulated luminescence dating: how significant is incomplete light exposure in fluvial environments? *Quaternaire* 15, 1-2: 143-157.

Jia, Y., Huang, C., Pang, J. and Niu J., 2008. Chronology of the Holocene loess-paleosol section and its deposition and pedogenesis on the south of Chinese Loess Plateau. *Journal of Geographical Sciences* 18, 4: 425-442.

Kochel, R.C. and Baker, V.R., 1988. Paleoflood analysis using slackwater deposits. P.C. Patton (Eds.), Flood Geomorphology, Wiley, NY, pp: 357-376.

Kortekaas, M. and Murray, A.M., 2005. A method for the removal of mica from quartz separates. *Ancient TL* 23, 2: 43-46.

Lamothe, M., Balescu, S. and Auclair, M., 1994. Natural IRSL intensities and apparent luminescence ages of single feldspar grains extracted from partially bleached sediments. *Radiation Measurements* 23: 555-562.

Lancaster, N. 2008: Desert dune dynamics and development: insights from luminescence dating. *Boreas* 37: 559-573.

Lapp, T., Jain, M., Thomsen, K.J., Murray, A.S. and Buylaert, J.P., 2012. New luminescence measurement facilities in retrospective dosimetry. *Radiation Measurements* 47 (9): 803-808.

Llasat, M.C. and Puigcerver, M., 1990. Cold air pools over Europe. *Meteorology and Atmospheric Physics* 42: 171-177.

Lepper, K. and McKeever, S. W. S.,2002. An Objective Methodology for Dose Distribution Analysis. *Radiation Protection Dosimetry* 101, 1-4, 349-352.

Machado, M.J., Benito, G., Barriendos, M. and Rodrigo, F.S., 2011. 500 years of rainfall variability and extreme hydrological events in Southeastern Spain drylands. *Journal of Arid Environments* 75: 1244-1253.

Madsen, A.T. and Murray, A. S., 2009. Optically stimulated luminescence dationg of young sediments: A review. *Geomorphology* 109: 3-16.

Madsen, A.T., Murray, A.S., Andersen, T.J. and Pejrup, M., 2007. Optical dating of young tidal sediments in the Danish Wadden Sea. *Quaternary Geochronology* 2, 1-4: 89-94.

Masachs, V., 1948. *El régimen de los ríos Peninsulares*. CSIC. Barcelona. 511 pp.

Masachs, V., 1950. Aportación al conocimiento del régimen fluvial mediterráneo. Comptes Rendus du Congrès International de Géographie, vol. II, UGI, Lisbonne pp: 358-390.

Mateu, J.F.,1974. La Rambla de la Viuda: Clima e hidrología. Cuadernos de geografía, 48-68.

Mayya, Y.S., Morthekai, P., Murari, M. and Singhvi, A.K., 2006. Towards quantifying beta microdosimetric effects in single-grain quartz dose distribution. *Radiation Measurements* 41: 1032-1039.

McKee, E.D., 1938. Original Structures in Colorado River Flood Deposits of Grand Canyon. *Journal of Sedimentary Petrology* 8 (3): 77-83.

Medialdea, A., Porat, N., Benito, G., 2011. Optically Stimulated Luminescence Characteristics of Modern Flash-Flood Deposits in Small Mountain Catchments. Spectroscopy Letters 44, 7-8: 530-534.

Murray, A.S., Roberts, R.G., 1997. Determining the burial time of single grains of quartz using optically stimulated luminescence. Earth and Planetary Science Letters 152, 1-4: 163-180.

Murray, A.S., Wintle, A.G., 1998. Factors controlling the shape of the OSL decay curve in quartz. Radiation Measurement 29: 65–79.

Murray, A.S. and Olley, J.M., 2002. Precision and accuracy in the optically stimulated luminescence dating of sedimentary quartz: a status review. *Geochronometria* 21: 1-16.

Murray, A.S. and Wintle, A.G., 2000. Luminescence dating of quartz using an improved single-aliquot regenerative-dose protocol. *Radiation Measurements* 32: 57-73.

Murray, A.S. and Wintle, A.G., 2003. The single aliquot regenerative dose protocol: potential for improvements in reliability. Radiation Measurements 37, 4–5: 377-381.

Murray, A.S., Marten, R., Johnston, A. and Martin, P., 1987. Analysis for naturally occurring radionuclides at environmental concentration by gamma spectrometry. *Journal of Radioanalytical and Nuclear Chemistry* 115 (2): 263-288.

Murray, A.S., Thomsen, K.J., Masuda, N., Buylaert, J.P. and Jain, M., 2012. Identifying well-bleached quartz using the different bleaching rates of quartz and feldspar luminescence signals. *Radiation Measurements* 47 (9): 688-695.

O'Connor, J.E., 1993. Hydrology, hydraulics, and geomorphology of the Bonneville flood. *Geological Society of America, Special Paper* 274, 83 pp.

O'Connor, J.E. and Webb, R.H., 1988. *Hydraulic Modeling for Paleoflood Analysis. Flood Geomorphology*. John Wiley & Sons New York, pp: 393-402.

Olley, J.M., Caitcheon, G. and Murray, A.S., 1998. The distribution of apparent dose as determined by optically stimulated luminescence in small aliquots of fluvial quartz: implications for dating young sediments. *Quaternary Science Review* 17: 1033-1040.

Olley, J.M., Caitcheon, G.G. and Roberts, R.G., 1999: The origin of dose distributions in fluvial sediments, and the prospect of dating single grains from fluvial deposits using optically stimulated luminescence. *Radiation Measurements* 30: 207-217.

Olley, J.M., Pietsch, T., Roberts, R.G., 2004. Optical dating of Holocene sediments from a variety of geomorphic settings using single grains of quartz. *Geomorphology*, 60, 3-4: 337-358.

Pagonis, V., Chen, R. and Wintle, A.G., 2007. Modelling thermal transfer in optically stimulated luminescence of quartz. *Journal of Physics D: Applied Physics* 40, 4: 998-1006.

Pardé, M., 1949. Le regime des cours d'eau ibériques. *Pirineos* V: 575-655.

Patton, P.C., Baker, V.R. and Kochel, R.C., 1979. Slackwater deposits: A geomorphic technique for the interpretation of fluvial paleohydrology. In: D.D. Rhodes and G. Williams (Eds) Adjustments of the Fluvial System, Kendall-Hunt, Dubuque, Iowa. pp: 225-252.

Porat, N., 2006. Use of magnetic separation for purifying quartz for luminescence dating. *Ancient TL* 24, 2: 33-36.

Prescott, J.R. and Hutton, J.T., 1994. Cosmic ray contributions to dose rates for luminescence and ESR: large depths and long-term time variations. *Radiation Measurements* 23: 497-500.

Reimann, T., Lindhorst, S., Thomsen, K.J., Murray, A.S. and Frechen, M., 2012. OSL dating of mixed coastal sediment (Sylt, German Bight, North Sea). *Quaternary Geochronology* 11: 52-67.

Roberts, H.M., 2007. Assessing the effectiveness of the double-SAR protocol in isolating a luminescence signal dominated by quartz. *Radiation Measurements* 42: 1627-1636.

Roberts, H.M., 2008. The development and application of luminescence dating to loess deposits: a perspective on the past, present, and future. *Boreas* 37: 483-507.

Roberts, H.M. and Wintle, A.G., 2003. Luminescence sensitivity changes of polymineral fine grains during IRSL and [post-IR] OSL measurements. *Radiation Measurements* 37: 661-671.

Rhodes, E., 2000. Observations of thermal transfer OSL signals in glacigenic quartz. *Radiation Measurements* 32 (5-6): 595-602.

Rhodes, E., 2007. Quartz single grain OSL sensitivity distributions: implications for multiple grain single aliquot dating. *Geochronometria* 26: 19-29.

Rhodes, E.J. and Pownall, L., 1994. Zeroing of the OSL signal in quartz from young glacio-fluvial sediments. *Radiation Measurements* 23: 581-586.

Rodrigo, F.S., Esteban-Parra, M.J., Pozo-Vázquez, D. and Castro-Díez, Y., 1999. A 500-year precipitation record in southern Spain. *International Journal of Climatology* 19: 1233-1253.

Rubin, D.M., Schmidt, J.C. and Moore, J.N., 1990. Origin, Structure, and Evolution of a Reattachment Bar, Colorado River, Grand Canyon, Arizona. *Journal of Sedimentary Petrology* 60 (6): 982-991.

Schmidt, J.C., 1990. Recirculating flow and sedimentation in the Colorado River in Grand Canyon, Arizona. *The Journal of Geology* 98 (5): 709-724.

Segura, F., 2001. Evolución urbana e inundaciones en Castelló. *Cuadernos de Geografía* 69/70: 253-278.

Sim, A.K., Thomsen, K.J., Murray, A.S., Jacobsen, G., Drysdale, R. and Erskine, W. (*submitted in 2012*). Dating recent floodplain sediments in the Hawkesbury-nepean river system using single grain quartz OSL. *Submitted to Boreas*.

Singarayer, J.S., Bailey, R.M., 2003. Further investigations of the quartz optically stimulated luminescence components using linear modulation. *Radiation Measurements* 37, 4-5: 451-458

Smith, B.W., Rhodes, E.J., 1994. Charge movements in quartz and their relevance to optical dating. *Radiation Measurements* 23, 2-3: 329-333.

Spooner, N.A. and Allsop, A., 2000. The spatial variation of dose rate from $^{90}Sr/^{90}Y$ beta sources for use in luminescence dating. *Radiation Measurements* 32: 97-102.

Stokes, S., 1992. Optical dating of young (modern) sediments using quartz: results from a selection of depositional environments. *Quaternary Science Review* 11: 153-159.

Stokes, S. and Rhodes, E.J., 1989. Limiting factors in the optical dating of quartz from young sediments. In: Long and Short Range Limits in Luminescence Dating. Research Laboratory for Archaeology and the History of Art, Oxford, Occasional Publication 9, Research Laboratory for Archaeology and the History of Art, Oxford, pp: 105-110.

Sweeney, M.R., Mcdonald, E., Hanson, P.R., Young, A.R., 2010. Using luminescence dating to decipher timing and origin of eolian AV soil horizons, southwest US. Geological Society of America Abstracts with Programs, Vol. 42, No. 5, p. 416.

Thomas, P.J., Jain, M., Juyal, N., Singhvi, A.K., 2005. Comparison of single-grain and small-aliquot OSL dose estimates in years old river sediments from South India. *Radiation Measurements* 39, 5: 457-469.

Thomsen, K.J., 2004. *Optically Stimulated Luminescence Techniques in Retrospective Dosimetry using Single Grains of Quartz extracted from Unheated Materials*. PhD Thesis, Risø National Laboratory, Denmark. 176 pp.

Thomsen, K.J., Jain, M., Bøtter-Jensen, L., Murray, A.S. and Jungner, H., 2003. Variation with depth of dose distributions in single grains of quartz extracted from an irridatiated concrete block. *Radiation Measurements* 37: 315-321.

Thomsen, K.J., Murray, A.S. and Bøtter-Jensen, L., 2005. Sources of variability in OSL dose measurements using single grains of quartz. *Radiation Measurements* 39: 47-61.

Thomsen, K.J., Murray, A.S., Bøtter-Jensen, L. and Kinahan, J., 2007. Determination of burial dose in incompletely bleached fluvial samples using single grains of quartz. *Radiation Measurements* 42 (3): 370-379.

Thomsen, K.J., Murray, A.S., Jain, M. and Bøtter-Jensen, L., 2008. Laboratory fading rates of various luminescence signals from feldspar-rich sediment extracts. *Radiation Measurements* 43: 1474-1486.

Thomsen, K.J., Murray, A.S. and Jain, M., 2012. The dose dependency of the over-dispersion of quartz OSL single grain dose distributions. *Radiation Measurements* 47 (9): 732-739.

Tooth, S., Rodnight, H., Duller, G.A.T., McCarthy, T.S., Marren, P.M. and Brandt, D., 2007. Chronology and controls of avulsion along a mixed bedrock-alluvial river. *Geological Society of America Bulletin* 119: 452-461.

Topping, J., 1955. Errors of Observation and their Treatment. Chapman and Hall, London.

Truelsen, J.L. and Wallinga, J, 2003. Zeroing of the OSL signal as a function of grain size: investigating bleaching and thermal transfer for a young fluvial sample. *Geochronometria* 22: 1-8.

Tukey, J.W, 1977. *Exploratory Data Analysis*. Reading, Mass.: Addison Wesley. 688 pp.

Wallinga, J., 2002. Optically stimulated luminescence dating of fluvial deposits: a review. *Boreas* 31: 303-322.

Wang, Y., Amundson R. and Trumbore, S., 1996. Radiocarbon dating of soil organic matter. *Quaternary Research* 45: 282-288.

Wintle, A.G. and Murray, A.S., 2006. A review of quartz optically stimulated luminescence characteristics and their relevance in single-aliquot regeneration dating protocols. *Radiation Measurements* 41 (4): 369-391.

Zander, A., Degering, D., Preusser, F., Kasper, H.U. and Brückner, H., 2007. Optically stimulated luminescence dating of sublittoral and intertidal sediments from Dubai, UAE: Radioactive desequilibria in the uranium decay series. *Quaternary Geochronology* 2: 123-128.

List of Figures

List of Tables

Annex: Summary dose rate and ages

Sample	Depth (cm)	Total dose rate (Gy/ka)	Age (ka)
T-39	59	0.82 ± 0.04	0.07 ± 0.02
T-37	95	0.90 ± 0.05	0.08 ± 0.02
T-36	122	0.91 ± 0.05	0.11 ± 0.01
T-31	216	0.85 ± 0.05	0.16 ± 0.02
T-30	259	1.00 ± 0.06	0.20 ± 0.02
T-26	351	0.91 ± 0.05	0.31 ± 0.03
T-23	367	0.84 ± 0.05	0.40 ± 0.03
T-17	478	1.13 ± 0.05	0.96 ± 0.06
RVD2-1	20	2.05 ± 0.09	0.28 ± 0.02
RVD2-3	100	1.59 ± 0.07	0.38 ± 0.02
RVD2-5	135	1.63 ± 0.08	0.61 ± 0.02
RVD5-2	50	1.79 ± 0.08	0.19 ± 0.01
RVD5-3	90	2.00 ± 0.09	0.19 ± 0.01
RVD5-5A	123	1.79 ± 0.08	0.22 ± 0.01
RVD5-5B	167	1.88 ± 0.08	0.16 ± 0.01
RVD8-8	82	1.85 ± 0.08	0.94 ± 0.03
RVD8-5	150	1.99 ± 0.09	7.7 ± 0.2
RVD8-3C	332	1.98 ± 0.09	8.5 ± 0.2
B6-1	22	4.1 ± 0.2	1.30 ± 0.07
B6-B	47	4.4 ± 0.2	2.00 ± 0.12
B6-2	63	4.1 ± 0.2	2.8 ± 0.2
B6-3	104	4.2 ± 0.2	6.0 ± 0.3
R5-1	20	4.4 ± 0.2	0.65 ± 0.06
R5-3	75	4.5 ± 0.2	4.8 ± 0.3
DOL-1	45	4.2 ± 0.4	0.32 ± 0.02
DOL-2	55	4.3 ± 0.2	0.43 ± 0.03
DOL-3	122	3.9 ± 0.2	0.78 ± 0.08
DOL-4	149	3.2 ± 0.1	0.84 ± 0.05
DOL-5	174	3.4 ± 0.2	0.96 ± 0.06